ฤทธิ์ยับยั้งไลพ็อกซีจีเนสของสทิลบีนอยด์จากรากพลวง *Dipterocarpus tuberculatus*

นายเสริม สุรพินิจ

วิทยานิพนธ์นี้เป็นส่วนหนึ่งของการศึกษาตามหลักสูตรปริญญาวิทยาศาสตรดุษฎีบัณฑิต
สาขาวิชาเทคโนโลยีชีวภาพ
คณะวิทยาศาสตร์ จุฬาลงกรณ์มหาวิทยาลัย
ปีการศึกษา 2556

LIPOXYGENASE INHIBITORY ACTIVITIES OF STILBENOIDS FROM ROOTS OF *Dipterocarpus tuberculatus*

Mr. Serm Surapinit

A Dissertation Submitted in Partial Fulfillment of the Requirements
for the Degree of Doctor of Philosophy Program in Biotechnology
Faculty of Science
Chulalongkorn University
Academic Year 2013

Thesis Title	LIPOXYGENASE INHIBITORY ACTIVITIES OF STILBENOIDS FROM ROOTS OF *Dipterocarpus tuberculatus*
By	Mr. Serm Surapinit
Field of Study	Biotechnology
Thesis Advisor	Associate Professor Santi Tip-pyang, Ph.D.

Accepted by the Faculty of Science, Chulalongkorn University in Partial Fulfillment of the Requirements for the Doctoral Degree

.....Dean of the Faculty of Science

(Professor Supot Hannongbua, Dr.rer.nat.)

THESIS COMMITTEE

.....Chairman

(Assistant Professor Varawut Tangpasuthadol, Ph.D.)

.....Thesis Advisor

(Associate Professor Santi Tip-pyang, Ph.D.)

.....Examiner

(Assistant Professor Aroonsiri Shitangkoon, Ph.D.)

.....Examiner

(Associate Professor Chanpen Chanchao, Ph.D.)

.....External Examiner

(Assistant Professor Jongkolnee Jongaramruong, Ph.D.)

เสริม สุรพินิจ : ฤทธิ์ยับยั้งไลพ็อกซีจีเนสของสทิลบีนอยด์จากรากพลวง *Dipterocarpus tuberculatus*. (LIPOXYGENASE INHIBITORY ACTIVITIES OF STILBENOIDS FROM ROOTS OF *Dipterocarpus tuberculatus*) อ.ที่ปรึกษาวิทยานิพนธ์หลัก: รศ. ดร.สันติ ทิพยางค์ , 99 หน้า.

ในการศึกษาสารที่มีฤทธิ์ยับยั้งไลพ็อกซีจีเนสจากพืชสมุนไพรไทยในวงศ์ Dipterocarpaceae ได้เลือกสิ่งสกัดอะซิโตนของรากพลวง (*Dipterocarpus tuberculatus*) มาแยก ทำให้บริสุทธ์ และหาสูตรโครงสร้าง จากการแยกสารจากสิ่งสกัดนี้โดยวิธีทางโครมาโทรกราฟี ได้โอลิโกสทิลบีนอยด์ใหม่ 4 ชนิดคือ dipterostilbenes A-D (1-4) และสทิลบีนอยด์ไกโคไซด์ชนิดใหม่ 2 ชนิดคือ dipterostilbenosides A และ B (14-15) พร้อมกับสทิลบีนอยด์ที่มีรายงานมาแล้วจำนวน 9 ชนิด ได้แก่ diptoindonesin E (5), vaticanol B (6), trans-resveratrol (7), trans-**ε**-(-)-viniferin (8), cis-**ε**-(-)-viniferin (9), pallidol (10), **α**-viniferin (11), gnetin H (12) และ (-)-hopeaphenol (13) โดยพิสูจน์สูตรโครงสร้างสารและโครงสร้างสัมพัทธ์ของสารที่แยกได้ด้วยวิธีทางสเปกโตรสโกปี และเปรียบเทียบกับข้อมูลที่มีรายงานแล้ว ในการศึกษาความสัมพันธ์ระหว่างฤทธิ์ยับยั้งและโครงสร้างของสทิลบีนอยด์ จึงนำสทิลบีนนอยด์จากมะเมื่อย (*Gnetum macrostachyum*) จำนวน 11 ชนิด (16-26) และจากพะยอม (*Shorea roxburghii*) จำนวน 2 ชนิด (27-28) มาร่วมทดสอบด้วย ผลการทดสอบเบื้องต้นของการยับยั้งเอ็นไซม์ไลพ็อกซีจีเนสจากถั่วเหลือง (sbLOX-1) ด้วยวิธีคัลเลอริเมทริก พบว่าสาร 1, 3, 21, 24, 25 และ 26 มีฤทธิ์การยับยั้งที่ดีที่สุด และยังพบว่าฤทธิ์ยับยั้งของสทิลบีนอยด์จากรากมะเมื่อยจะเพิ่มขึ้นตามจำนวนหน่อยย่อยสทิลบีนอยด์ที่เพิ่มขึ้น แต่ฤทธิ์ยับยั้งของสทิลบีนอยด์จากรากพะยอมและพลวงกลับขึ้นอยู่กับชนิดของสทิลบีนอยด์เป็นหลัก จากการศึกษาจลนศาสตร์เอนไซม์เพื่อหากลไกการยับยั้ง พบว่าสาร 1 และ 26 มีกลไกการยับยั้งเป็นแบบไม่แข่งขัน สาร 3, 21 และ 25 มีกลไกการยับยั้งแบบไม่สามารถแข่งขันได้โดยตรง และสาร 24 มีกลไกการยังยั้งแบบผสม โดยกลไกการยับยั้งเอ็นไซม์ไลพ็อกซีจีเนสจากไม่สัมพันธ์กับโครงสร้างของสทิลบีนอยด์ นอกจากนี้ยังพบว่าการยับยั้งเอ็นไซม์ไลพ็อกซีจีเนสของสาร 1, 3, 21, 24, 25 และ 26 ไม่ได้มาจากฤทธิ์ต้านอนุมูลอิสระจากการศึกษาฤทธิ์ต้านอนุมูลอิสระ DPPH และ 13-HPOD และความสามรถรีดิวซ์เฟอร์ริกไอออน ซึ่งยืนยันผลด้วยเทคนิคยูวีสเปกโทรโฟโตเมตรีและเซอร์คิวลาร์ไดโครอิสมสเปกโตรสโกปี ดังนั้นจึงสรุปได้ว่าโอลิโกสทิลบีนอยด์ออกฤทธิ์โดยตรงที่เอ็นไซม์ไลพ็อกซีจีเนส ซึ่งไม่เกี่ยวข้องกับการรบกวนปฏิกิริยารีดอกซ์ของเหล็กที่เป็นองค์ประกอบของเอ็นไซม์ไลพ็อกซีจีเนส หรือการเปลี่ยนแปลงโครงสร้างของเอ็นไซม์ไลพ็อกซีจีเนสแต่อย่างใด

สาขาวิชา เทคโนโลยีชีวภาพ ลายมือชื่อนิสิต .....

ปีการศึกษา 2556 ลายมือชื่อ อ.ที่ปรึกษาวิทยานิพนธ์หลัก .....

5373834823 : MAJOR BIOTECHNOLOGY
KEYWORDS: DIPTEROCARPUS TUBERCULATUS / LIPOXYGENASE INHIBITORS / OLIGOSTILBENES

SERM SURAPINIT: LIPOXYGENASE INHIBITORY ACTIVITIES OF STILBENOIDS FROM ROOTS OF *Dipterocarpus tuberculatus*. ADVISOR: ASSOC. PROF. SANTI TIP-PYANG, Ph.D., 99 pp.

In phytochemical investigation for lipoxygenase inhibitory activity from Thai medicinal plants in the family of Dipterocarpaceae, acetone crude extract from the roots of *Dipterocarpus tuberculatus* was selected for isolation, purification and structure elucidation. The chromatographic separation of this crude extract led to the isolation of four new oligostilbenoids, dipterostilbenes A-D (1-4) and two stilbenoid glycosides, dipterostilbenosides A and B (14-15), were isolated together with nine known stilbenoids, diptoindonesin E (5), vaticanol B (6), trans-resveratrol (7), trans-**ε**-(-)-viniferin (8), cis-**ε**-(-)-viniferin (9), pallidol (10), **α**-viniferin (11), gnetin H (12) and (-)-hopeaphenol (13). The structures and relative configuration were determined on the basis of spectroscopic data as well as comparison with the previous literature data. For the structure-activity relationship study, eleven stilbenes (16-26) from *Gnetum macrostachyum* and two stilbenes (27-28) from *Shorea roxburghii* were also selected for evaluation of sbLOX-1 inhibitory activity. The results of colorimetric sbLOX-1 screening assay showed that 1, 3, 21, 24, 25 and 26 were the most active oligostilbenes. It was also found that the inhibitory activities of stilbenoids from *G. macrostachyum* were enhanced by the increasing number of stilbenoid monomer. However, the potency of Shorea- and Dipterocarpus-derived stilbenoids correlated with the type of oligostilbenes. The enzyme kinetic study of the inhibitory mechanisms revealed that compounds 1 and 26 were uncompetitive inhibitors, compounds 3, 21 and 25 were non-competitive inhibitor, and compound 24 were a mixed-competitive inhibitor. The inhibitory activity of 1, 3, 21, 24, 25 and 26 was not resulted from the antioxidant property and iron redox interferences as demonstrated by DPPH and 13-HPOD scavenging assays, and UV spectrophotometric and circular dichroism spectroscopic studies. Thus, the inhibitory mechanisms of these active oligostilbenoids were resulted from the enzyme inhibition without iron redox interferences or alteration of the active enzyme structure.

Field of Study: Biotechnology Student's Signature .....

Academic Year: 2013 Advisor's Signature .....

ACKNOWLEDGEMENTS

This study was carried out during the past four years at the Program in Biotechnology, Natural Product Research Unit and Department of Chemistry, Faculty of Science, Chulalongkorn University. I am grateful to the University of Phayao for doctoral scholarship. Financial support from the Graduate School of Chulalongkorn University, the Higher Education Research Promotion and National Research University Project of Thailand, the Office of the Higher Education Commission and the Ratchadaphiseksomphot Endowment Fund (FW645A) are gratefully acknowledged.

I would like to express my deepest gratitude to my supervisor, Associate Professor Santi Tip-pyang, for his excellent guidance, enthusiasm, instruction and support from the very beginning to the very end of my Ph.D. thesis. I am grateful to my chair committee, Asst. Prof. Varawut Tangpasuthadol, and my thesis committee, Asst. Prof. Aroonsiri Shitangkoon, Assoc. Prof. Chanpen Chanchao and Asst. Prof. Jonkolnee Jong-aramruang.

Sincere thanks are also extended to all member and friends, for lending a helping hand whenever needed, sharing the great time in laboratory, their warm assistance and friendship, at Program in Biotechnology and Natural Product Research Unit, Chulalongkorn University; Wisuttaya Worawalai, Dr. Thanakorn Damsud and Vassana Musa.

Last, but not least, I wish to thank my parents and family for keeping my feet tightly on the ground and my mind away from science when I was at home. They are the best family one could wish for.

CONTENTS

Page

THAI ABSTRACT iv
ENGLISH ABSTRACT v
ACKNOWLEDGEMENTS vi
CONTENTS vii
LIST OF FIGURE ix
LIST OF TABLES xiii
LIST OF ABBREVIATION xiv
Chapter I Introduction 1
1.1. Lipoxygenase 1
1.1.1. Lipoxygenase biochemistry 1
1.1.2. Lipoxygenase in AA metabolism 4
1.1.3. Lipoxygenase in diseases 5
1.2. Soybean lipoxygenase-1 (sbLOX-1) as an experimental enzyme 8
1.3. Lipoxygenase inhibitors 11
1.4. Stilbenoids and biological activity reports from Dipterocarpus species 12
1.5. Objectives 17
Chapter II Experimental 18
2.1. Instruments and chemical 18
2.2. Plant material 18
2.4. Acidic hydrolysis 20
2.5. Colorimetric lipoxygenase inhibitory assay 20
2.6. 2,2-Diphenyl-1-picrylhydrazyl 1,1-diphenyl-2-picrylhydrazyl radical (DPPH) scavenging assay 21
2.7. Hydroperoxide scavenging assay 21
2.8. Enzyme kinetic study 21
2.9. Iron redox interference 23
2.10. Colorimetric total iron determination 23

Page

2.11. Spectroscopic studies 24
2.11.1. UV-vis spectrophotometry 24
2.11.2. Visible circular dichroism (CD) spectroscopy 24
2.12. Statistical analysis 25
Chapter III Results and Discussion 26
3.1. Structure elucidation of the isolated compounds 26
3.1.1. Dipterostilbene A (1) 26
3.1.2. Dipterostilbene B (2) 32
3.1.3. Dipterostilbene C (3) 36
3.1.4. Dipterostilbene D (4) 38
3.1.5. Dipterostilbenoside A (14) 42
3.1.6. Dipterostilbenoside B (15) 47
3.2. Chemical taxonomy significances 50
3.3. Lipoxygenase inhibitory activity 51
3.4. Antioxidant activities of stilbenoids 54
3.5. Enzyme kinetic studies of selected active stilbenes 56
3.6. Iron redox interferences 59
Chapter IV Conclusion 63
REFERENCES 70
APPENDIX 78
VITA 99

LIST OF FIGURE

PAGE

Figure **1** AA metabolism catalyzed by 5-lipoxygenase (Sala, Folco et al. 2010). 2
Figure **2** AA metabolism catalyzed by 12-lipoxygenase (Sala, Folco et al. 2010). 3
Figure **3** AA metabolism catalyzed by 15-lipoxygenase (Sala, Folco et al. 2010). 3
Figure **4** Conversion of 5-EETE to 15-HPETE by 12/15-LOX (Sala, Folco et al. 2010). . 4
Figure **5** Biochemical pathways of the formation and action of the leukotrienes in asthma and sites of action of leukotriene-modifying drugs (Drazen, Israel et al. 1999).5
Figure **6** Main putative roles of 5-lipoxygenase in atherosclerosis (Berliner and Watson 2005). 7
Figure **7** Three dimensional structure of lipoxygenases. Schematic diagram of the 3D structure of soybean (Glycine max) lipoxygenase-1, showing the small N-terminal domain I and the large C-terminal domain II. The iron-containing active site is located in domain II, and can be reached by molecular oxygen through cavity I and by linolelic acid through cavity II (Maccarrone, Melino et al. 2001). 9
Figure **8** Comparison between three different lipoxygenases. Conserved aromatic amino acids (Phe169 and Trp201) that flank the region are in stick rendering. Phe177 and Tyr181, which make up the cork that helps define the active site, are in stick. The catalytic iron is an orange sphere. (B) A full overlay of the three structures in which it is apparent thst, with the exception of a2, the secondary structural element in the enzymes are conserved (Gilbert, Bartlett et al. 2011). 10
Figure **9** Multiple alignment of SLO (green), 15-HLOa (blue), and 15-HLOb (red). The amino acids in the active site pocket within 8 A° are highlighted by yellow background (Sadeghian, Seyedi et al. 2008). 10
Figure **10** Lipoxygenase inhibitor reported from natural origins (Adams, Pacher *et al*. 2005, Deschamps, Kenyon *et al*. 2006)..... 11
Figure **11** Lipoxygenase inhibitor oligostilbenes from *Vitis amurensis* (Ha do, Kim *et al*. 2009). 13
Figure **12** Oligostilbenes from *D. grandiflorus* (Ito, Tanaka et al. 2004, Ito, Abe et al. 2009). 15
Figure **13** Oligostilbenes from *D. grandiflorus* (Cont.) (Ito, Tanaka et al. 2004, Ito, Abe et al. 2009). 16
Figure **14** Oligostilbenes from *D. hasseltii (Muhtadi, Hakim et al. 2006)*..... 16

Figure **15** Extraction, isolation and purification of stilbenoids from the acetone extract. 20
Figure **16** Extraction, isolation and purification of stilbenoids from the methanol extract. 20
Figure **17** Typical double-reciprocal plot or Lineweaver-Burk plot. K_m and V_{max} value are calculated as shown (Lehninger, Nelson et al. 2013). 22
Figure **18** Double-reciprocal plots of enzyme inhibition mechanisms. Inhibition constants were calculated according to their type of inhibition as shown (Lehninger, Nelson et al. 2013). 23
Figure **19** Position assignment of 1. 27
Figure **20** Selected HMBC (arrow curves) and COSY (bold lines) correlations of **1**.... 28
Figure **21** Comparison between planar structure of 1 and relative structure of 5.... 29
Figure **22** Key NOESY correlations for **1**. 30
Figure **23** Position assignment of 2. 33
Figure **24** Selected HMBC (arrow curves) and COSY (bold lines) correlations of **2**.... 33
Figure **25** CD spectra of **2** and diptoindonesin E (**5**) in methanol. 34
Figure **26** Key NOESY correlations for **2**. 34
Figure **27** Position assignment of 3. 37
Figure **28** Selected HMBC (arrow curves) and COSY (bold lines) correlations of **3**.... 37
Figure **29** Key NOESY correlations for **3**. 38
Figure **30** Position assignment of 4. 40
Figure **31** Selected HMBC (arrow curves) and COSY (bold lines) correlations of **4**.... 40
Figure **32** Comparison between Planar structure of 4 and pallidol (10). 41
Figure **33** Selected NOESY correlations of **4**. 41
Figure **34** Position assignment of 14. 44
Figure **35** Selected HMBC (arrow curves) and COSY (bold lines) correlations of **14**. 44
Figure **36** Key NOESY correlations for **14**. 45
Figure **37** Position assignment of 15. 48
Figure **38** Selected HMBC (arrow curves) and COSY (bold lines) correlations of **15.** 48
Figure **39** CD spectra of aglycone **15** and (-)-***ε***-viniferin in methanol..... 49
Figure **40** Structures of known stilbenoids from the roots of *D. tuberculatus*..... 50
Figure **41** Structures of known stilbenoids from the roots of *D. tuberculatus* (Cont.). 51

Figure **42** Structure of stilbenoids from *G. macrostachyum*. 52
Figure **43** Structure of stilbenoids from *G. macrostachyum* (Cont.). 53
Figure **44** Structure of stilbenoids from *G. macrostachyum* and *S. roxburghii*. 54
Figure **45** Lineweaver-Burk plot of **1** and **26**. 57
Figure **46** Lineweaver-Burk plot of **3**, **21** and **25**. 58
Figure **47** Lineweaver-Burk plot of **24**. 59
Figure **48** The UV-vis spectra of ferric reduction activities of oligostilbenes on Fe^{3+}-sbLOX-1. 62
Figure **49** Visible CD spectra of the effect of oligostilbenes on Fe^{3+}-sbLOX-1. 62
Figure **50** ^{1}H-NMR spectrum of **1** in CD_3COCD_3. 78
Figure **51** ^{13}C-NMR spectrum of **1** in CD_3COCD_3. 78
Figure **52** COSY spectrum of **1** in CD_3COCD_3. 79
Figure **53** HSQC spectrum of **1** in CD_3COCD_3. 79
Figure **54** MHBC spectrum of **1** in CD_3COCD_3. 80
Figure **55** NOESY spectrum of **1** in CD_3COCD_3. 80
Figure **56** HRESIMS spectrum of **1**. 81
Figure **57** ^{1}H-NMR spectrum of **2** in CD_3COCD_3. 81
Figure **58** ^{13}C-NMR spectrum of 2 in CD_3COCD_3. 82
Figure **59** COSY spectrum of **2** in CD_3COCD_3. 82
Figure **60** MHBC spectrum of **2** in CD_3COCD_3. 83
Figure **61** MHBC spectrum of **2** in CD_3COCD_3. 83
Figure **62** NOESY spectrum of **2** in CD_3COCD_3. 84
Figure **63** HRESIMS spectrum of **2**. 84
Figure **64** ^{1}H-NMR spectrum of **3** in CD_3COCD_3. 85
Figure **65** ^{13}C-NMR spectrum of **3** in CD_3COCD_3. 85
Figure **66** COSY spectrum of **3** in CD_3COCD_3. 86
Figure **67** HSQC spectrum of **3** in CD_3COCD_3. 86
Figure **68** HMBC spectrum of **3** in CD_3COCD_3. 87
Figure **69** NOESY spectrum of **3** in CD_3COCD_3. 87
Figure **70** HRESIMS spectrum of **3**. 88
Figure **71** ^{1}H-NMR spectrum of **4** in CD_3COCD_3. 88
Figure **72** ^{13}C-NMR spectrum of **4** in CD_3COCD_3. 89
Figure **73** COSY spectrum of **4** in CD_3COCD_3. 89

Figure **74** HSQC spectrum of **4** in CD_3COCD_3. 90
Figure **75** HMBC spectrum of **4** in CD_3COCD_3. 90
Figure **76** NOESY spectrum of **4** in CD_3COCD_3. 91
Figure **77** HRESIMS spectrum of **4**. 91
Figure **78** ^{1}H-NMR spectrum of **14** in CD_3OD. 92
Figure **79** ^{13}C-NMR spectrum of **14** in CD_3OD. 92
Figure **80** COSY spectrum of **14** in CD_3OD. 93
Figure **81** HSQC spectrum of **14** in CD_3OD. 93
Figure **82** HMBC spectrum of **14** in CD_3OD. 94
Figure **83** NOESY spectrum of **14** in CD_3OD. 94
Figure **84** HRESIMS spectrum of **14**. 95
Figure **85** ^{1}H-NMR spectrum of **15** in CD_3OD. 95
Figure **86** ^{13}C-NMR spectrum of **15** in CD_3OD. 96
Figure **87** COSY spectrum of **15** in CD_3OD. 96
Figure **88** HSQC spectrum of **15** in CD_3OD. 97
Figure **89** HMBC spectrum of **15** in CD_3OD. 97
Figure **90** HRESIMS spectrum of **15**. 98

LIST OF TABLES

PAGE

Table **1** ^{1}H and ^{13}C Spectroscopic data of compound **1**. 31
Table **2** ^{1}H and ^{13}C Spectroscopic data of compound **2**. 35
Table **3** ^{1}H and ^{13}C Spectroscopic data of compound **3**. 39
Table **4** ^{1}H and ^{13}C Spectroscopic data of compound **4**. 42
Table **5** ^{1}H and ^{13}C Spectroscopic data of compound **14**. 46
Table **6** ^{1}H and ^{13}C Spectroscopic data of compound **15**. 49
Table **7** Lipoxygenase inhibitory activity of the oligostilbenes from *D. tuberculatus*, *G. macrostachyum* and *S. roxburghii*. 55
Table **8** Fe^{3+} and Fe^{3+}-sbLOX-1 reduction activity of the active oligostilbenes. 61

LIST OF ABBREVIATION

12(*S*)-HETE	12(*S*)-Hydroxyeicosatetraenoic acid
12(*S*)-HPETE	12(*S*)-Hydroperoxyeicosatetraenoic acid
13(*S*)-HODE	13(*S*)-Hydroxyoctadecadienoic
^{13}C NMR	Carbon-13 Nuclear Magnetic Resonance
15(*S*)-HETE	15(*S*)-Hydroxyeicosatetraenoic acid
15(*S*)-HPETE	15(*S*)-Hydroperoxyeicosatetraenoic acid
^{1}H NMR	Hydrogen-1 Nuclear Magnetic Resonance
5(*S*)-HETE	5(*S*)-Hydroxyeicosatetraenoic acid
5(*S*)-HPETE	5(*S*)-Hydroperoxyeicosatetraenoic acid
AA	Arachidomnic acid
ANOVA	Analysis of Variance
CD Spectroscopy	Circular Dichrosim Spectroscopy
CD_3COCD_3	Deuterated acetone
CD_3OD	Deuterated methanol
CH_2Cl_2	Dichloromethane
CHD	Coronary Heart Disease
COSY	Correlation Spectroscopy
CysLTs	Cysteinyl leukotrienes
DC	Dendritic cell
DMSO	Dimethyl sulfoxide
DPPH	1,1-Diphenyl-2-picrylhydrazyl radical
EGF	Epidermal growth factor
EtOAc	Ethyl acetate
FCC	Flash column chromatography
FLAPs	5-Lipoxygenase activating proteins
FOX reagent	Ferric Oxidation-Xylenol orange reagent
FT-IR Spectroscopy	Fourier Transform Infrared Spectroscopy
HMBC	Heteronuclear Multiple Bond Correlation
HRESIMS	High-Resolution Electrospray Ionisation Mass Spectrometry
HSQC	Heteronuclear Single Quantum Coherence

IC_{50}	Half inhibition
K_i	Inhibition constant
K_m	Michaelis constant
LDL	Low Density Lipoprotein
LOXs	Lipoxygenases
LTA4	Leukotriene A4
LTB4	Leukotriene B4
LTC4	Leukotriene C4
LTD4	Leukotriene D4
LTD4	Leukotriene E4
MeOH	Mehtnaol
NDGA	Nordihydroguaiaretic acid
NOESY	Nuclear Overhauser Effect Spectroscopy
OCC	Open column chromatography
sbLOX-1	Soybean lipoxygenase-1
SD	Standard deviation
SEC	Size-exclusion chromatography
VCC	Vacuum column chromatography
V_{max}	Maximum velocity

Chapter I

Introduction

1.1. Lipoxygenase

1.1.1. Lipoxygenase biochemistry

Lipoxygenases (LOXs), non-heme iron dioxygenases, catalyze the regio- and stereospecific peroxidation of polyunsaturated fatty acid containing a 1,4-*cis*,*cis*-pentadiene system to conjugated hydroperoxide derivatives. On the basis of its regiospecificity, human lipoxygenases have been designated as arachidonate 5-, 12-, 15-lipoxygenase (5-LOX, 12-LOX, and 15-LOX). The three distinct enzymes insert molecular oxygen at carbons 5, 12 or 15 of arachidonic acid (AA). The primary products are 5*S*-, 12*S*-, or 15*S*-hydroperoxyeicosatetraenoic acid (5(*S*)-, 12(*S*)-, or 15(*S*)-HPETE), which can be further reduced by glutathione peroxidase to the hydroxy forms (5(*S*)-, 12(*S*)-, 15(*S*)-HETE), respectively (Ivanov, Heydeck *et al*. 2010).

Lipoxygenases are selectively distributed in different cell types. Thus, lipoxygenases can produce various types of the eicosanoids. In myeloid cells (neutrophils, monocyte or macrophage), the 5-lipoxygenase pathway of AA metabolism leads to the formation of the biologically active leukotrienes through enzymes that control the formation and metabolism of several products. 5-LOX is inducible enzyme that require 5-lipoxygenase activating proteins (FLAPs) for the activation of enzymatic activity. After binding to FLAPs, 5-LOX primarily oxygenates AAs into 5(*S*)-HPETE. 12-lipoxygenase have been identified into three isoenzymes including the leukocyte-type, platelet-type and an epidermal-type 12-LOX. The classification is based on the enzyme localization, substrate specificities, immunogenic properties and amino acid sequence homology. The platelet 12-LOX produces 12-(*S*)-HETE from AA while the leukocyte 12-LOX produces either 12(*S*)-HETE or 15(*S*)-HETE from AA or linoleic acid. Arachidonate 15-lipoxygenase (15-LOX) can be subclassified according to specificity of tissue distribution and enzymatic characteristics into 15-LOX-1 and 15-LOX-2. 15-LOX-1 is expressed in reticulocytes, eosinophils, macrophages, tracheobronchial epithelial cells, skin, and colon. This isoenzyme converts linoleic acid and AA to their metabolites, 13(*S*)-hydroxyoctadecadienoic acid (13(*S*)-HODE) and 15(*S*)-

hydroxyeicosatetraenoic acid (15(*S*)-HETE), respectively. By contrast, 15-LOX-2 is expressed in prostate, lung, skin, and cornea but not in colon, and it converts AA to 15(*S*)-HETE but metabolizes linoleic acid poorly (Buczynski, Dumlao *et al*. 2009).

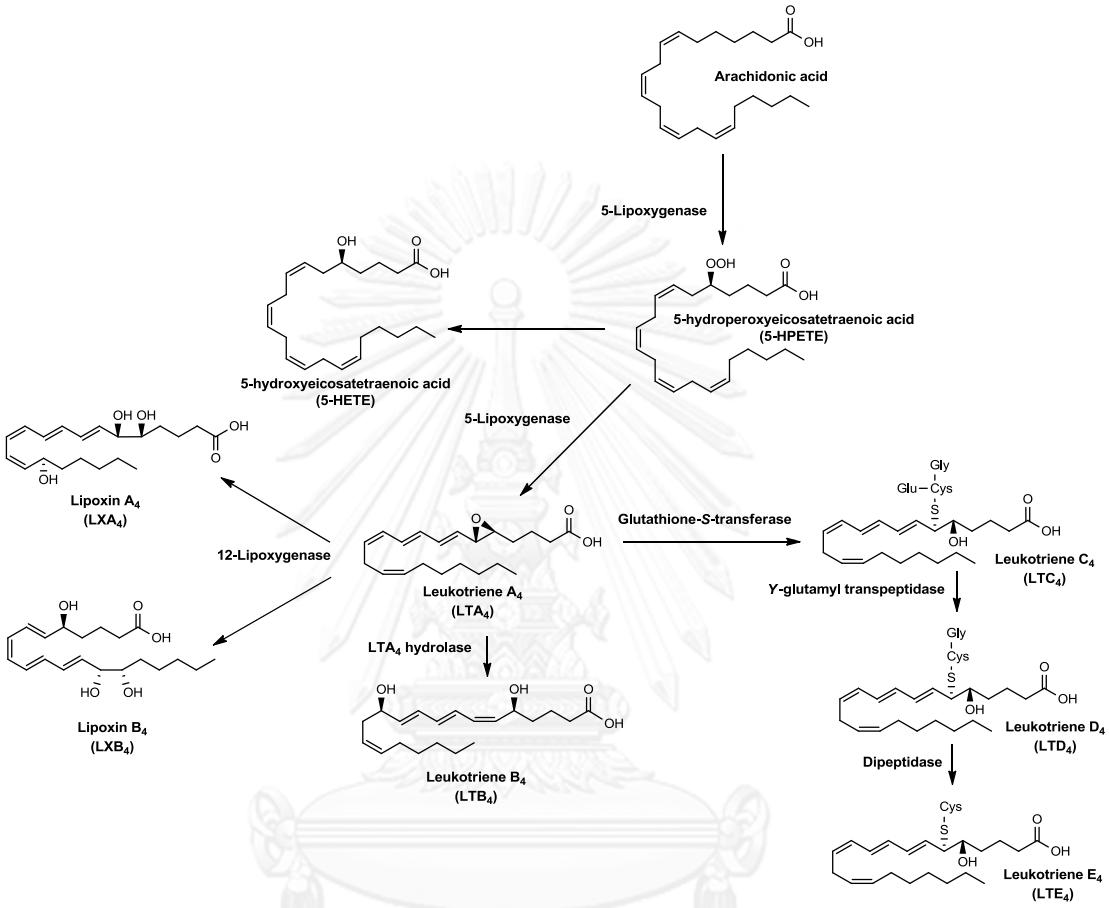

Figure **1 AA** metabolism catalyzed by 5-lipoxygenase (Sala, Folco et al. 2010).

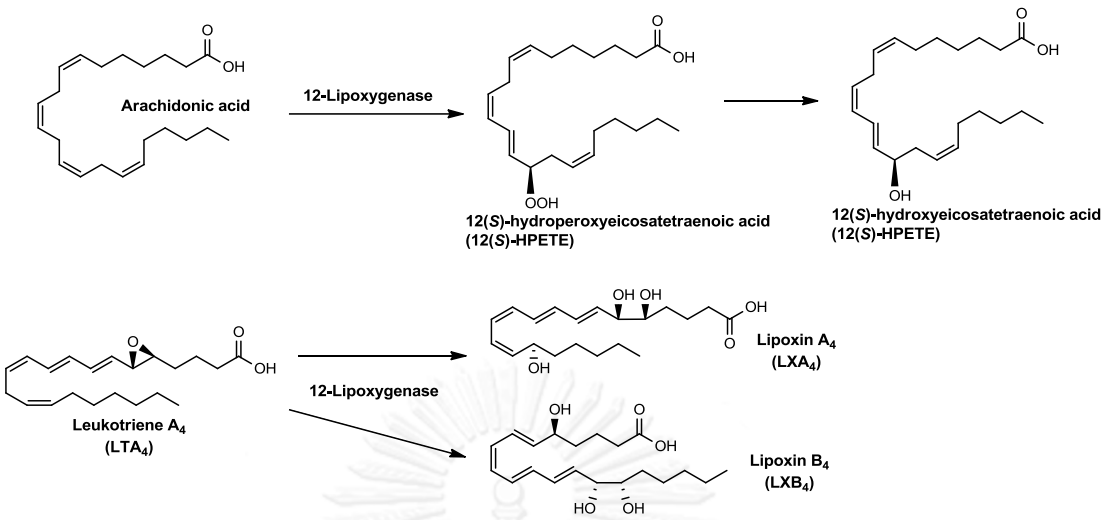

Figure **2** AA metabolism catalyzed by 12-lipoxygenase (Sala, Folco et al. 2010).

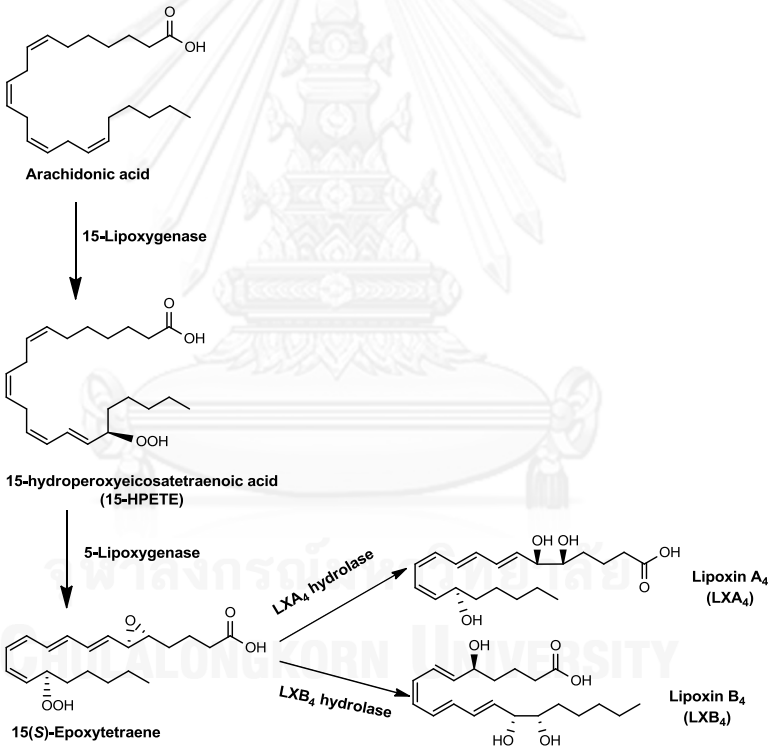

Figure **3** AA metabolism catalyzed by 15-lipoxygenase (Sala, Folco et al. 2010).

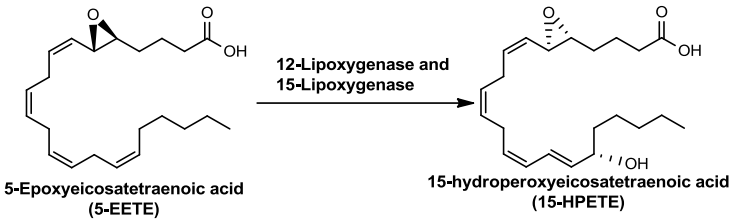

Figure **4** Conversion of 5-EETE to 15-HPETE by 12/15-LOX (Sala, Folco et al. 2010).

1.1.2. Lipoxygenase in AA metabolism

The catalytic action of 5-LOX possess two enzymatic activities, dioxygenase and LTA4 synthase activities. The first step of reaction initiate by incorporation of molecular oxygen into AA to produce unstable 5(S)-hydroperoxyeicosatetraenoic acid (5(*S*)-HPETE). The LTA4 synthase activity of 5-LOX subsequently converts to an unstable epoxide derivative, leukotriene A4 (LTA4), which is further hydrolyzed by LTA4 hydrolase to form leukotriene B4 (LTB4).

The term cysteinyl leukotrienes (CysLTs) is refered to the leukotriene conjugated with a small amino acid residue, including LTC4, LTD4 and LTE4. 15-HPETE is also used as the precursor of CysLT biosynthesis. Initially, glutathione-*S*-transferase converts LTA4 to LTC4 which is further cut glutaryl residue by gamma-glutamyl transpeptidase to form LTD4. Dipeptidase subsequently catalyzes the transformation of LTD4 to LTE4 (Gilbert, Bartlett *et al*. 2011).

Another AA metabolism is lipoxin (LX) pathway. AA is undergone dioxygenation reaction at the C-15 to form 15(*S*)-HPETE. In addition, 15(*S*)-HPETE is also formed by the conversion from 5(*S*)-HPETE with the catalysis of 12-LOX and 15-LOX. An intermediate 15(*S*)-HPETE is catalyzed by 5-LOX to form 15(*S*)-epoxytetraene which is further hydrolyzed by LXA4 hydrolase or LXB4 hydrolase to the LXA4 or LXB4. The formation of LXs is also found in the leukotriene pathway by the transformation of LTA4 to LXA4 or LXB4 (Burrall, Cheung *et al*. 1988).

1.1.3. Lipoxygenase in diseases

1.1.3.1. Asthma

LTB4 is a potent chemotactic and chemokinetic mediator and acts as leukocyte activator by stimulating migration and activation of granulocytes and T cells, leading to adherence of granulocytes to vessel walls and degranulation. It is also potent to enhance the phagocytic activity of neutrophils and macrophages and to stimulate secretion of immunoglobulins by lymphocytes. The CysLTs induce smooth muscle contraction, mucus secretion, plasma extravasation, vasoconstriction, eosinophils recruitment and fibrocyte proliferation. Thus, CysLTs are the important mediator of bronchoconstriction and hypersensitivity reactions such as asthma and allergic rhinitis. However, they also play important roles in chronic inflammation and in regulation of the adaptive immune response (Drazen, Israel *et al*. 1999).

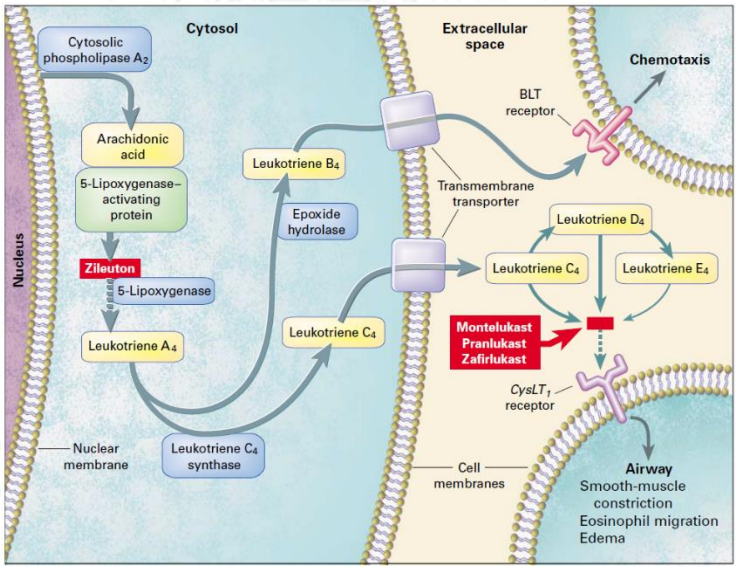

Figure **5** Biochemical pathways of the formation and action of the leukotrienes in asthma and sites of action of leukotriene-modifying drugs (Drazen, Israel et al. 1999).

1.1.3.2. Atherosclerosis

There are many researches demonstrate that lipoxygenases involve the pathogenesis of atherosclerosis. A role for 15-LOX in mediating pathogenic lipid

peroxidation associated with inflammatory vascular disease has been discussed for many years. The first report on the role of 15-LOX on lipid peroxidation demonstrated that soybean 15-LOX incubation with LDL and phospholipase A2 led to formation of oxidized fatty acids. This work was later confirmed by the experiment that utilized either purified or intracellular 15-LOX. It was found that both of enzyme sources could oxidize extracellular LDL forming specific 15-LOX-derived free and esterified products (Sparrow, Parthasarathy *et al*. 1989). At that time, lipid peroxidation to form oxidized LDL was considered to be a major mechanism of pro-atherogenesis. These observations indicated a vascular damaging role for 15-LOX and guide for in vivo and ex vivo studies to test this hypothesis. However, overexpression of 15-LOX in macrophages was found to lower intracellular lipid deposition. It was resulted from decreased uptake of modified LDL via impaired scavenger receptor A expression and accelerated intracellular lipid metabolism. These reports indicated that the roles of 15-LOX in atherogenesis was likely to be more complex than simply oxidizing LDL and might involve alterations in lipid uptake and turnover (Berliner and Watson 2005). Moreover, 5-LOX also play an important role in atherogenesis as key enzyme in the inflammation. Recently, the expression of 5-LOX was found in human atherosclerotic lesions such as aorta, coronary arteries and carotid arteries. This report clearly demonstrated the role of 5-LOX in the pathogenesis of atherosclerosis. Most of the 5-LOX was in CD68+ macrophages, many of these also carried the dendritic cell (DC) marker CD1a. Moreover, most 5LOX+ cells contained lipid particles. In view of these findings, cells containing 5-LOX and lipid were designated 5-LOX+ macrophage foam cells, and 5-LOX+ DC foam cells. The number of 5-LOX+ cells in vessel wall was higher in samples from more advanced coronary heart disease and increased in all vascular layers (laminae adventitia, media, and intima). Several proteins involved leukotriene synthesis were also found, including 5-LOX activating protein (FLAP), LTA4 hydrolase, and LTC4 synthase (De Caterina and Zampolli 2004, Cipollone, Mezzetti *et al*. 2005).

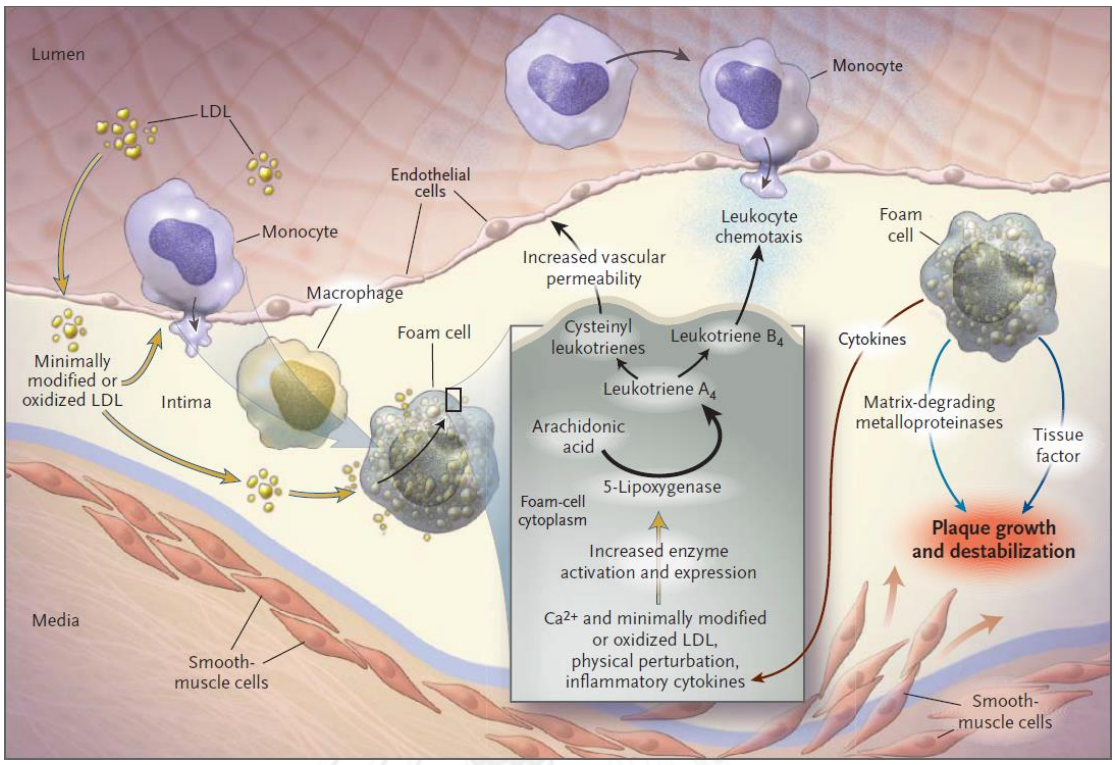

Figure **6** Main putative roles of 5-lipoxygenase in atherosclerosis (Berliner and Watson 2005).

1.1.3.3. Cancers

Lipoxygenases also have important roles in carcinogenesis. Accumulating evidences suggests that the 5-LOX pathway probably associate with the development and progression of human cancers (Catalano and Procopio 2005). The 5-LOX pathway interacts with multiple intracellular signaling pathways that control cancer cell proliferation. The 5-LOX inhibitors have chemopreventive effects in animal lung carcinogenesis (Avis, Jett *et al*. 1996). Blockade of 5-LOX inhibits prostate cancer cell proliferation (Ghosh and Myers 1998) while the 5-LOX metabolite, 5-HETE stimulates prostate cancer cell growth (Ghosh and Myers 1997).

Both the platelet and leukocyte 12-LOX have been found in different cancer tissues, including melanoma, prostate and epidermal cancers (Funk, Chen *et al*. 2002). These evidences indicate that 12-LOX is involved in both cancer cell proliferation and survival. Inhibition of 12-LOX with either 12-LOX inhibitors or a 12-LOX antisense oligonucleotide inhibits proliferation and induces apoptosis in carcinosarcoma cells,

while adding back 12(S)-HETE prevents 12-LOX inhibitor-induced apoptosis. The overexpression of 12-LOX is also correlated with tumor cell metastasis. 12(S)-HETE directly stimulates prostate cancer cell migration (Timar, Raso *et al*. 2000). Clinically, the degree of 12-LOX expression in human prostate cancer positively correlates with the tumor grade and stage and 12-LOX expression level is higher in metastatic prostate cancers than in non-metastatic ones (Gao, Grignon *et al*. 1995).

15-Lipoxygenase converts AA to 15(S)-HPETE which is then reduced by glutathione peroxidase to 15(S)-HETE. There are two 15-LOX isoenzymes, 15-LOX-1 and 15-LOX-2. Linoleic acid is preferred as substrate for 15-LOX-1, while AA is preferred as substrate for 15-LOX-2. The 15-LOX-1 produce 13-S-HODE whereas 15-LOX-2 produce 15-HETE (Kuhn and Thiele 1999). The roles of 15-LOX in cancer development have not been clear. A series of studies from one group suggest that 13-S-HODE enhances colonic tumorigenesis. 13-S-HODE also enhances cell proliferation and potentiates the mitogenic response to epidermal growth factor (EGF) in different cell types. These proposed effects were not consistent with other reports that 13(S)-HODE did not enhance EGF-dependent DNA synthesis. Another report showed that 13(S)-HODE induced apoptosis and cell cycle arrest in colorectal cancer cells. It also indicated that 15(S)-HETE probably has anti-tumorigenic effects through the other LOX product antagonism. Therefore, extensive studies are needed to clarify the roles of 15-LOX in tumorigenesis and cancer growth (Shureiqi and Lippman 2001).

1.2. Soybean lipoxygenase-1 (sbLOX-1) as an experimental enzyme

Plant secondary metabolites was extensively studied on the inhibitory action on lipoxygenase to discover new inhibitor. The discovery of LOXs inhibitor from the mammalian LOX model, especially human LOX, is limited by the enzyme complexity, instability and availability. Soybean lipoxygenase-1 (sbLOX-1) has been used as an experimental enzyme for the drug discovery, which was well studied. This plant LOX is globular protein composing of domain I and II which domain II is active portion with Fe2+ as a cofactor in the resting form. Oxygen and linoleic acid enter to the active domain via cavity I and II, respectively (Maccarrone, Melino *et al*. 2001). As compared to human 5-LOX and rabbit 8-LOX, sbLOX has similar active site to those of mammalian

LOX. Amino acid sequence comparison between sbLOX-1, human 15-LOXa and 15-LOXb also confirmed the similarity of these three enzymes (Sadeghian, Seyedi *et al*. 2008). Moreover, enzyme kinetic behavior of sbLOX-1 was similar to those of mammalian LOX, especially human lipoxygenases (Berry, Debat *et al*. 1998). Therefore, sLOX-1 is a good model for the enzyme studies and the results could be extendable to human lipoxygenase.

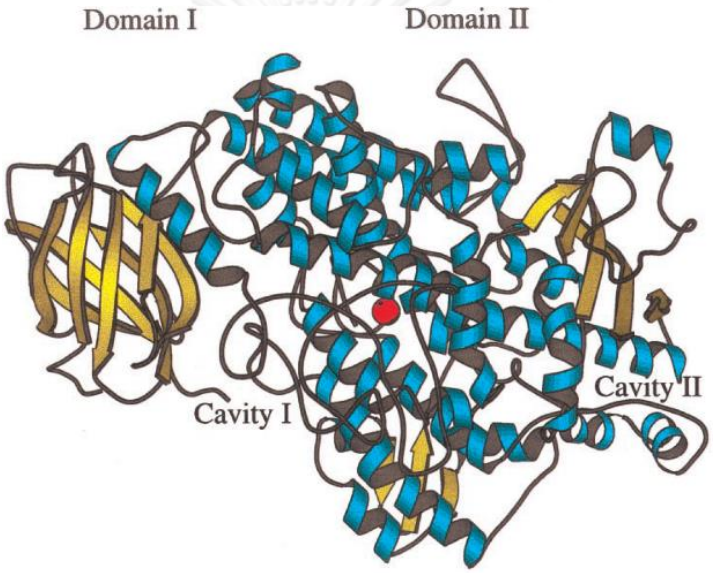

Figure **7** Three dimensional structure of lipoxygenases. Schematic diagram of the 3D structure of soybean (Glycine max) lipoxygenase-1, showing the small N-terminal domain I and the large C-terminal domain II. The iron-containing active site is located in domain II, and can be reached by molecular oxygen through cavity I and by linolelic acid through cavity II (Maccarrone, Melino et al. 2001).

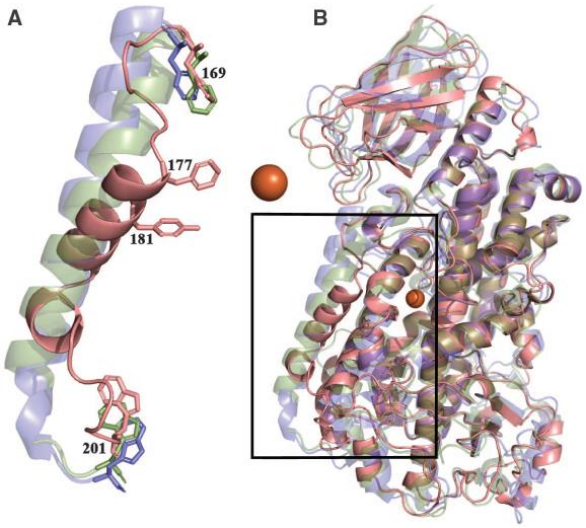

Figure **8** Comparison between three different lipoxygenases. Conserved aromatic amino acids (Phe169 and Trp201) that flank the region are in stick rendering. Phe177 and Tyr181, which make up the cork that helps define the active site, are in stick. The catalytic iron is an orange sphere. (B) A full overlay of the three structures in which it is apparent thst, with the exception of a2, the secondary structural element in the enzymes are conserved (Gilbert, Bartlett et al. 2011).

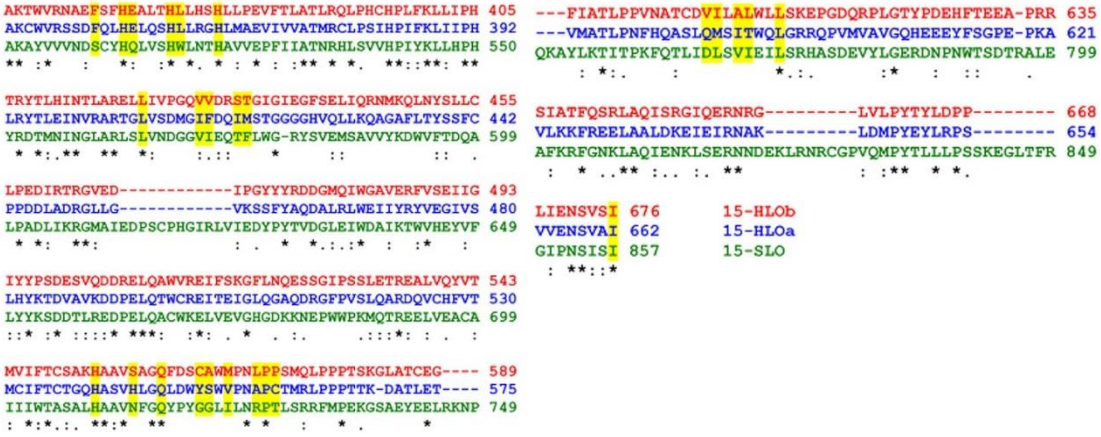

Figure **9** Multiple alignment of SLO (green), 15-HLOa (blue), and 15-HLOb (red). The amino acids in the active site pocket within 8 A˚ are highlighted by yellow background (Sadeghian, Seyedi et al. 2008).

1.3. Lipoxygenase inhibitors

According the roles of LOXs in the clinical pathogenesis, LOX inhibitors may be beneficial for the preventive and therapeutic application of these diseases. The searches for novel synthetic as well as natural origin-derived LOX inhibitors pose a challenge. Several series of secondary metabolites exert excellently inhibitory activity, for example quinones, anthraquinones, flavonoids, and stilbenoids (Odukoya, Houghton *et al*. 1999, Adams, Pacher *et al*. 2005, Deschamps, Kenyon *et al*. 2006, Landa, Kutil *et al*. 2013).

Resveratrol, the common stilbenoid derivative, is known as lipoxygenase inhibitor, which acts as both an enzyme inhibitor and ferric ion reducer. Recently, oligostilbenes from Vitis amurensis displayed potent lipoxygenase inhibitory activity (Ha do, Kim *et al*. 2009). This report showed that trans-amurensin B, trans-**ε**-viniferin, (+)-ampelopsin A and r-2-viniferin were more potent that the referent compound, baicalein. Moreover, (+)-Ampelopsin A, trans-resveratrol and amurensin G also exhibited the same level of inhibitory activity as baicalein. This report revealed an important clue for the possibility of medicinal plant-derived oligostilbenoids as an lipoxygenase inhibitor.

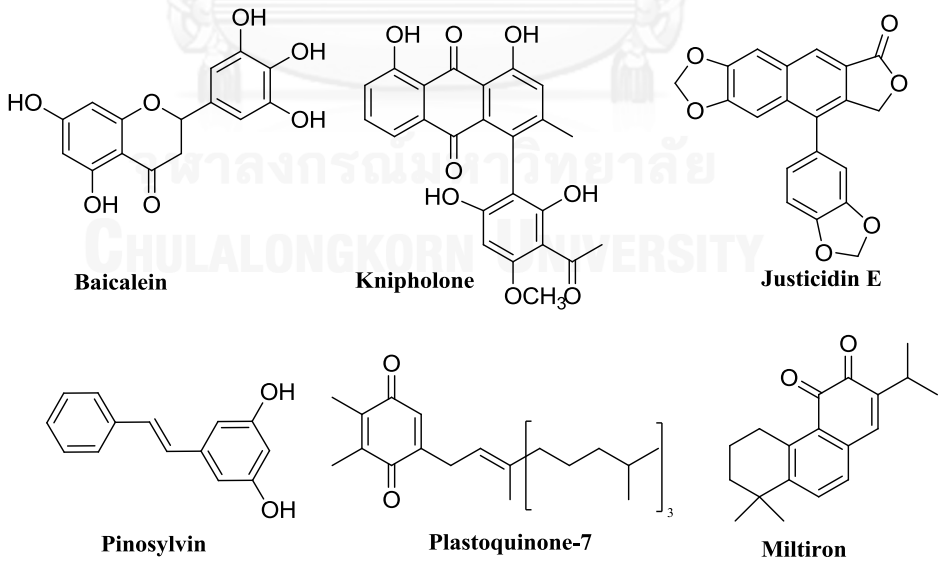

Figure **10** Lipoxygenase inhibitor reported from natural origins (Adams, Pacher *et al*. 2005, Deschamps, Kenyon *et al*. 2006).

1.4. Stilbenoids and biological activity reports from Dipterocarpus species

Resveratrol, a common secondary metabolite categorized in stilbenoid class, is biogenetically synthesized through phenylpropanoid pathway (Choi, Wu *et al*. 2011). Resveratrol has been attracted considerable interest in the area of natural product research, since they exhibit wide range of biological activities. The well-known health beneficial effect of resveratrol was described as "French Paradox", a phenomenon of low coronary heart disease (CHD) death rates in wine consumption people despite high intake of dietary cholesterol and saturated fat (Wu and Hsieh 2011). The extensive researches also reveal other health-promoting effects of resveratrol such as chemotherapeutic potential against several types of cancers, prevention and improvement of diabetic-related complications, prevention and reduction of oxidative stress and so on (Tome-Carneiro, Larrosa *et al*. 2013). Interestingly, resveratrol is able to undergo either homogeneous or heterogeneous coupling of monomeric stilbenoids to produce high complexity in chemical structure (Lin and Yao 2006). Resveratrol oligomers are presented in unrelated plant families, namely Vitaceae, Gnetaceae, Cyperaceae, Leguminosae and Dipterocarpaceae (Sotheeswaran and Pasupathy 1993, Chong, Poutaraud *et al*. 2009). The continuous studies on resveratrol oligomers also demonstrate a wide range of pharmacological and biological activities as their precursor do.

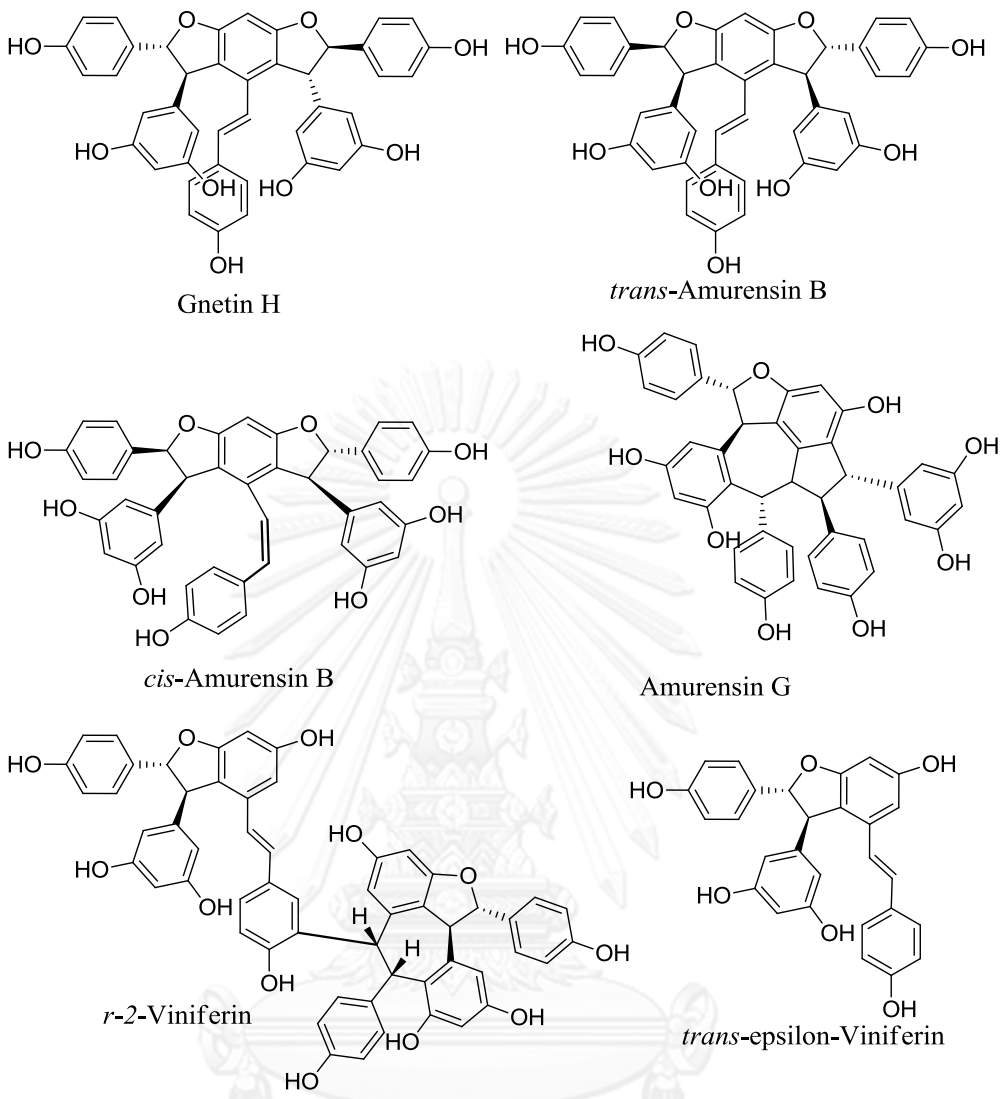

Figure 11 Lipoxygenase inhibitor oligostilbenes from *Vitis amurensis* (Ha do, Kim *et al*. 2009).

The extensively phytochemical investigations of the plants from the family Dipterocarpaceae have been clearly revealed that resveratrol oligomers are the principal natural products (Tanaka, Ito *et al*. 2000, Ito, Tanaka *et al*. 2001, Morikawa, Chaipech *et al*. 2012). Thus, the author is interested in the phytochemical and biological investigation of Thai medicinal plant in this plant family, especially the genus Dipterocarpus. In the search of resveratrol oligomers possessed lipoxygenase inhibitory activity, *D. tuberculatus* was collected for further study. To date, there is no lipoxygenase inhibitory activity and phytochemical reports from this plant. Two species

from this genus had been studied for the biological activity and chemical constituents, including *D. grandiflorus* and *D. hasseltii*.

Oligostilbenes were isolated from the stem of *D. grandiflorus* (Ito, Tanaka *et al*. 2004, Ito, Abe *et al*. 2009), namely grandiphenols A-D, vaticanols B-C, hemsleyanol D, (-)-hopeaphenol, (+)-***α***-viniferin, miyabenol C, (-)-***ε***-viniferin, (-)-ampelopsin A, (-)-ampelopsin F, isoampelopsin F, and shorealactone (13). However, there was no biological activity reported from this plant.

Biphenyl-type stilbenoid tetramer, diptoindonesin E, was isolated from the bark of *D. hasseltii* together with (–)-***ε***-viniferin, laevifonol, (–)-***α***-viniferin, vaticanol B and (–)-hopeaphenol (Muhtadi, Hakim *et al*. 2006). The isolated constituents were evaluated for cytotoxic activity against murine leukemia P-388 cells. It was showed that diptoindonesin E was more potent than (–)-***ε***-viniferin and (–)-***α***-viniferin. Other constituents were inactive.

Dipterocarpus tuberculatus is medium to large size tree which widely distributed in Bangladesh, Myanmar, Thailand, Cambodia, Laos and Vietnam. In Thailand, certain parts of the plant were used as a traditional medicine such as leaf gum as anti-envonomization and roots as ectopic anti-inflammation and anti-dysentery (ผู้พัฒนพงศ์ and วงศ์ประเสริฐ์ 2530). To our best knowledge, the present research is the first phytochemical report from this species.

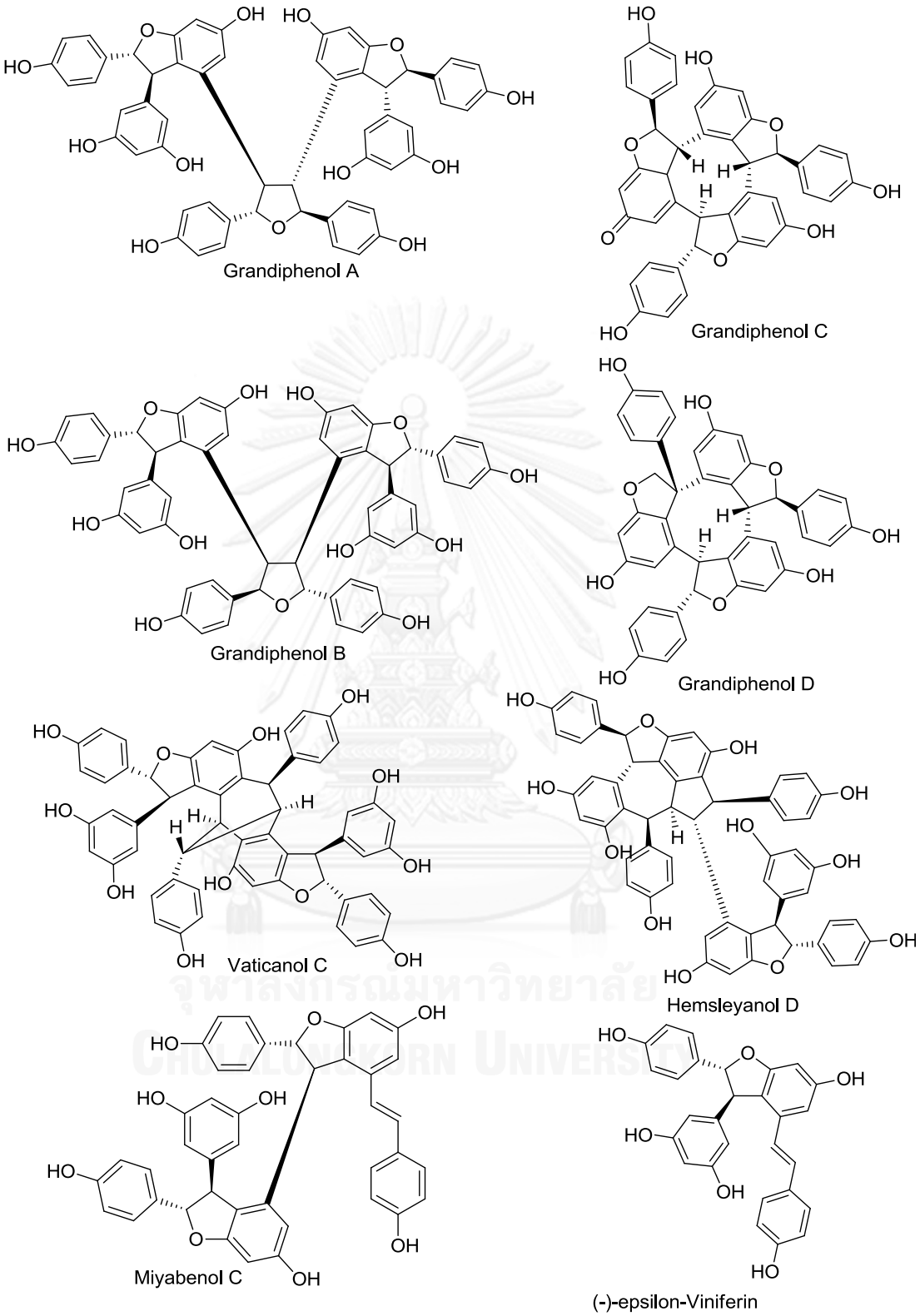

Figure **12** Oligostilbenes from *D. grandiflorus* (Ito, Tanaka et al. 2004, Ito, Abe et al. 2009).

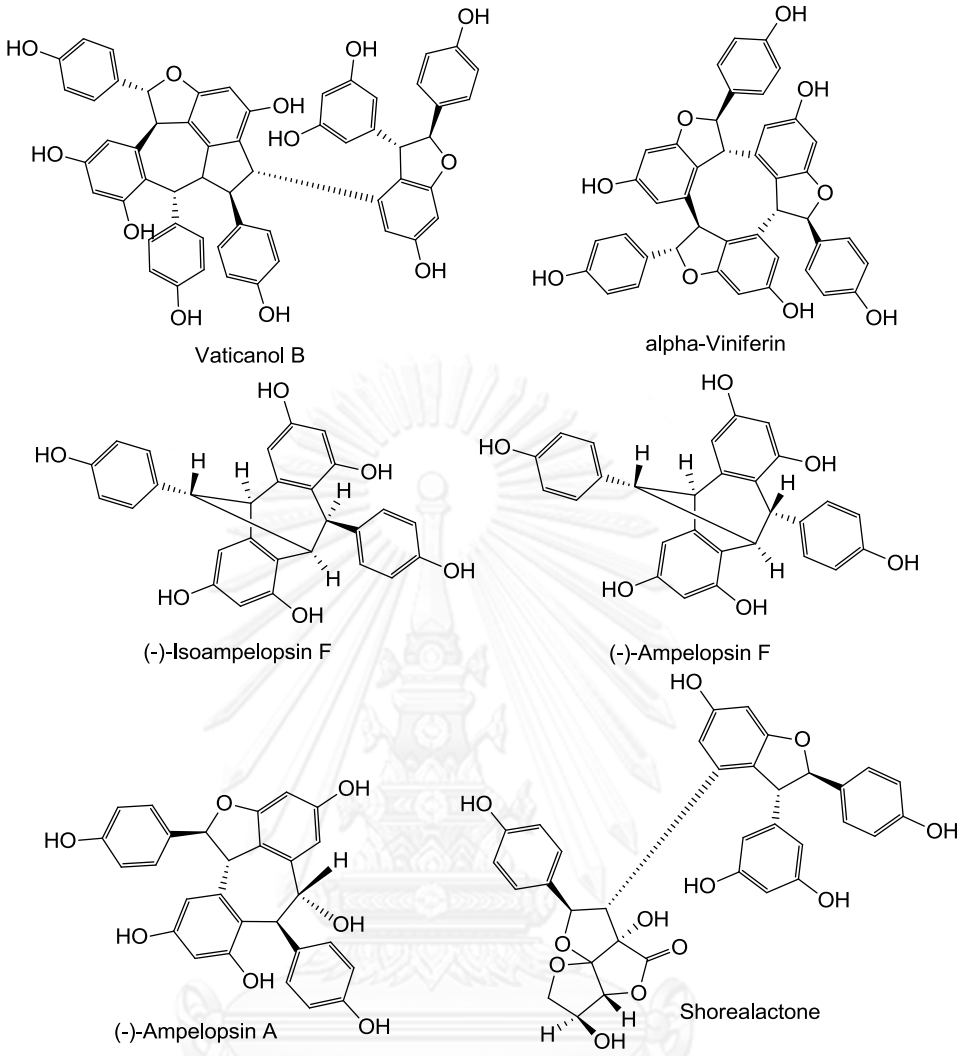

Figure **13** Oligostilbenes from *D. grandiflorus* (Cont.) (Ito, Tanaka et al. 2004, Ito, Abe et al. 2009).

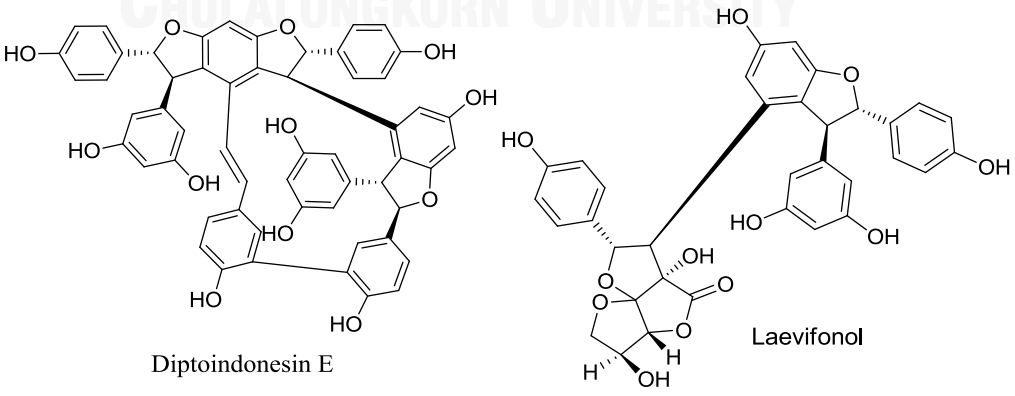

Figure **14** Oligostilbenes from *D. hasseltii (Muhtadi, Hakim et al. 2006).*

1.5. Objectives

The objectives of this research can be summarized as followed:

1.5.1. To extract and isolate compounds from the roots of *D. tuberculatus.*

1.5.2. To elucidate the structures of all isolated compounds.

1.5.3. To evaluate lipoxygenase inhibitory activity of the isolated compounds.

1.5.4. To investigate the inhibitory mechanism of selected active compounds.

Chapter II

Experimental

2.1. Instruments and chemical

Optical rotation and Circular Dichroism (CD) spectra were measured on a Jasco P-1010 polarimeter and Jasco J-815 CD spectrometer (Jasco Cooperation, Tokyo, Japan). UV spectra were run on a Shimadsu UV-2550 spectrophotometer (Shimadsu, Kyoto, Japan). IR spectra were obtained on a Thermo Scientific Nicolet 6700 FT-IR spectrometer (Thermo Scientific, MA, USA). NMR spectroscopic data were recorded at room temperature on Bruker Avance DRX-400 spectrometers (Bruker, MA, USA), Varian Mercury 400 and 500 spectrometers (Varian Inc., CA, USA). Chemical shifts were reported in ppm (δ) referenced to solvent residues. High-resolution electrospray ionization mass spectra (HRESIMS) were performed on a Bruker Microflex™ (Bruker, MA, USA) mass spectrometer operated in the positive-ion mode, with NaI being used for mass calibration for a calibration range of m/z 100–2000. Column chromatography was carried out with silica gel (Arch. No. 7729, 7734 and 8795, Merck, USA). Size-exclusion chromatography was performed over Sephadex™ LH-20 lipophilic resin (GE Healthcare Life Sciences, Freiburg, Germany). Analytical TLC was conducted on pre-coated 250 μm thick silica gel UV254 aluminum-backed plates (Merck, NJ, USA). Soybean lipoxygenase-1 was purchased as liquid form (Cayman Chemical Company, MI, USA).

2.2. Plant material

The roots of *D. tuberculatus* were collected from Mahasarakham Province, Thailand in July 2011. A voucher specimen (khomkratok No 1-22) has been deposited in the herbarium of Walai Rukhavej Botanical Research Institute, Mhasarakham University, Mahasarakham Province, Thailand.

2.3. Extraction and isolation

The air-dried and finely ground roots of *D. tuberculatus* (5 kg) were sequentially extracted with CH_2Cl_2, acetone and methanol by a soxhlet extractor at 80°C for 12 hr. The acetone portion was evaporated under reduced pressure to yield 157 g of a crude extract. The extract was separated by a vacuum column chromatography (VCC) over

Si gel using a CH_2Cl_2–EtOAc gradient solvent system (10:1 to pure EtOAc) to obtain four subtractions. The CH_2Cl_2 soluble fractions, F1 and F2, were excluded from the study. The CH_2Cl_2 insoluble fraction F3 (500 mg) was separated over an open column chromatography (OCC, Si gel Arch. No. 7734) using gradient CH_2Cl_2–EtOAc gradient (5-25%, 1 L each) to obtain pure *trans*-resveratrol (**7**, 13 mg), *trans*-***ε***-(-)-viniferin (**8**, 126 mg) and *cis*-***ε***-(-)-viniferin (**9**, 8 mg). The fraction F4 (20 g) was separated over OCC (Si gel Arch. No. 7734) using CH_2Cl_2–EtOAc gradient solvent system (10:1 to pure EtOAc) to obtain three subtractions, F4A (2 g), F4B (7 g) and F4C (5 g), respectively. The fraction F4A was separated over a size-exclusion chromatography (SEC) using MeOH as mobile phase to obtain pure pallidol (**10**, 20 mg), ***α***-viniferin (**11**, 14 mg) and gnetin H (**12**, 8 mg). The fraction F4B was separated over SEC using MeOH as mobile phase to obtain pure dipterostilbene A (**1**, 15 mg) and subfraction F4B2 (3 g). The fraction F4B2 was separated over flash column chromatography (FCC, Si gel Arch. No. 8795) using gradient MeOH-CH_2Cl_2 solvent system (2, 5, 7%, 250 mL each) to yield pure diptoindonesin E (**5**, 22 mg), dipterostilbene C (**3**, 53 mg) and vaticanol B (**6**, 31 mg). The fraction F4C was separated over FCC using gradient MeOH-CH_2Cl_2 solvent system (5, 10, 15, 20%, 500 mL each) to yield pure dipterostilbene B (**2**, 114 mg), D (**4**, 17 mg) and (-)-hopeaphenol (**13**, 10 mg).

The methanol portion was evaporated and subjected to separate by VCC over Si gel using a CH_2Cl_2–MeOH gradient solvent system (10:1 to 1:1) to obtain four subfractions (M1-4). Fraction M4 was separated over FCC (Si gel Arch. No. 8795) using gradient MeOH-CH_2Cl_2 solvent (20-35% MeOH/ CH2Cl2) to obtain pure form of dipterostilbenoside A (**14**, 45 mg) and dipterostilbwnoside B (**15**, 20 mg). Fraction M3 and M2 were purified over OCC (Si gel Arch. No. 7734) using isocratic 20% and 15% MeOH/ CH_2Cl_2 solvent to obtained a pure form of (-)-hopeaphenol (7 mg) and ***α***-viniferin (5 mg). Fraction M1 was separated over FCC with gradient MeOH-CH_2Cl_2 solvent (5-10% MeOH/ CH_2Cl_2) to obtain a pure pallidol (12 mg) and *trans*-***ε***-viniferin (75 mg).

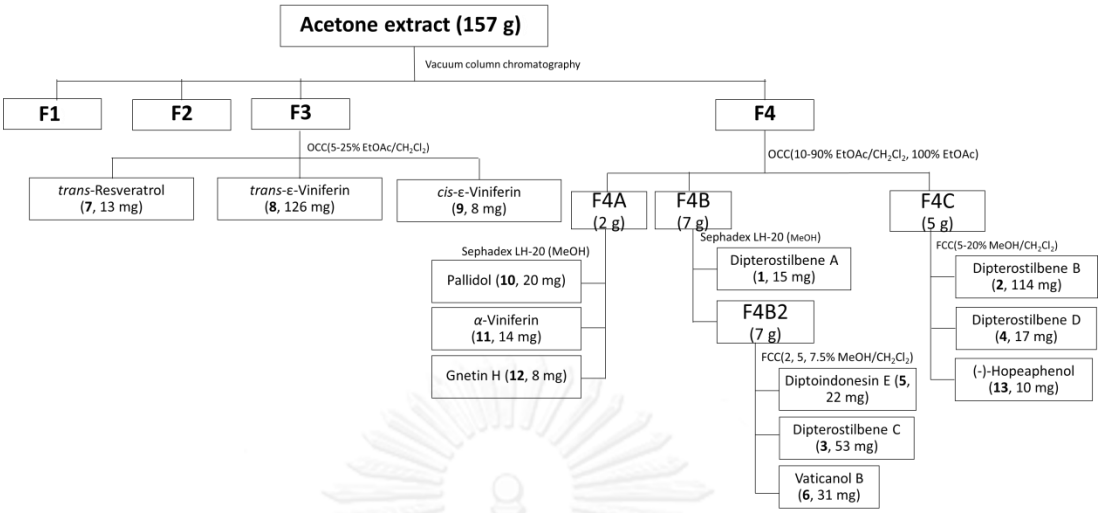

Figure **15** **Extraction, isolation and purification of stilbenoids from the acetone extract.**

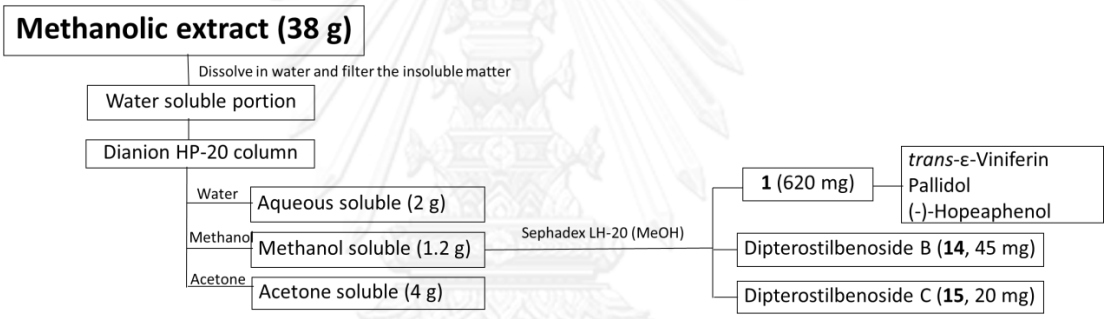

Figure **16** Extraction, isolation and purification of stilbenoids from the methanol extract.

2.4. Acidic hydrolysis

A solution of the dipterostilbenosides A (1 mg) in 1% H_2SO_4 (0.05 mL) was refluxed for an hour. The reaction mixture was neutralized with equal volume of 1% Na_2SO_4 and extracted with 10% MeOH/CH_2Cl_2 (2 × 0.5 mL). Glucose was identified as the sugar moiety by co-TLC (MeOH-EtOAc-H_2O 8:1:1) of the aqueous solution compared with an authentic glucose sample.

2.5. Colorimetric lipoxygenase inhibitory assay

The colorimetric screening assay was applied from the earlier method using ferric oxidation-xylenol orange (FOX) reagent for the detection of 13-HPOD (Sircar,

Schwender *et al*. 1983, Waslidge and Hayes 1995). Briefly, the reaction mixture consisted of 200 unit/ml of sbLOX-1 and the sample (dissolved in 50% DMSO/H_2O). The reaction was started by adding 30 μM linoleic acid, and then further incubated for 5 min. Then, the reaction was stopped by adding freshly prepared FOX reagent (100 μM xylenol orange, 100 μM $FeSO_4$ and 25 mM H_2SO_4 dissolved in 10% water/methanol) and the color was developed for 30 min prior to measuring the absorbance at 585 nm. The inhibitory activity was presented as the IC_{50} value, the concentration required for half inhibition. The data was obtained from seven independent experiments, each conducted in duplicate.

2.6. 2,2-Diphenyl-1-picrylhydrazyl 1,1-diphenyl-2-picrylhydrazyl radical (DPPH) scavenging assay

Free radical scavenging activity was performed in 96-well microplate format (Udomchotphruet, Phuwapraisirisan *et al*. 2012). Briefly, reaction mixture was consisted of 30 μM sample and 60 μM DPPH solution with total volume of 250 μL. The optical density of reaction mixture was measured at 517 nm against reagent blank. The inhibitory activity was presented as IC_{50}. All tests were run in triplicate and averaged.

2.7. Hydroperoxide scavenging assay

13(S)-HPOD scavenging activity was performed in the same manner as the colorimetric sbLOX-1 assay. Linoleic acid was incubated with sb-LOX-1 for 10 minutes prior to fully generating 13(S)-HPOD. An aliquot of reaction mixture was incubated in the presence of 30 μM of sample. The inhibitory activity was presented as the IC_{50} value, the concentration required for half inhibition. All tests were run in triplicate and averaged.

2.8. Enzyme kinetic study

Enzyme activity was determined by following the increase in absorbance at 234 nm due to the formation of 13-HPOD (ε = 25000 M-1cm-1) in the presence of 200 unit/ml sbLOX-1, and 30 μM linoleic acid in 0.1 M borate buffer pH 9.0 (Glickman and Klinman 1995). The initial rate was calculated during the first 15-45 sec after linoleic acid was added. The initial rate was obtained to construct the Lineweaver-Burk Plot

(1/v versus 1/[S]). One unit of enzyme caused an increase of 0.001 absorbance units per minute at 234 nm when incubated with 0.02% linoleate at 25°C in 0.1 M borate buffer, pH 9.0, at a total volume of 1.0 ml. Analysis of kinetic parameters was performed with GraphPad Prism 6.0 software.

Kinetic parameters (K_m, V_{max}) were obtained from the analysis of double-reciprocal plot or Lineweaver-Burk plot (Figure **17**). A double-reciprocal plot of enzyme kinetics is generated by plotting 1/V0 as a function 1/[S]. The slope is the K_m/V_{max}, the intercept on the vertical axis is $1/V_{max}$, and the intercept on the horizontal axis is -1/Km. To investigate inhibition mechanism of selected inhibitors, the double-reciprocal plot or Lineweaver-Burk plot at the various concentrations of inhibitor (Figure **18**). The inhibition constants (K_i or K_i') were calculated in the similar manner to K_m and V_{max}.

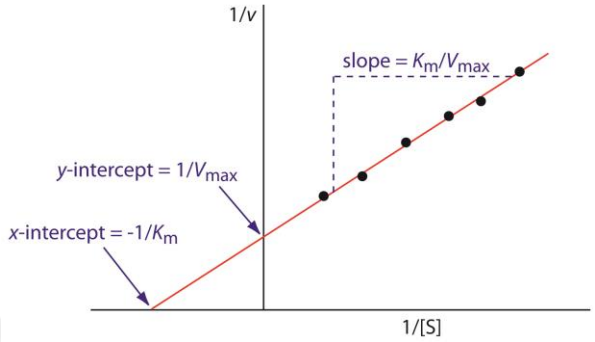

Figure **17** Typical double-reciprocal plot or Lineweaver-Burk plot. K_m and V_{max} value are calculated as shown (Lehninger, Nelson et al. 2013).

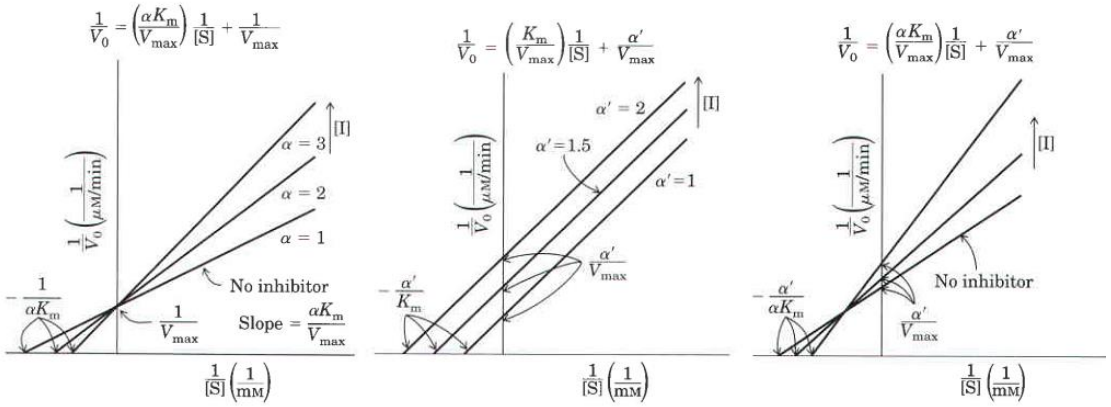

Figure **18** Double-reciprocal plots of enzyme inhibition mechanisms. Inhibition constants were calculated according to their type of inhibition as shown (Lehninger, Nelson et al. 2013).

2.9. Iron redox interference

To investigate iron redox interference, free Fe^{2+} oxidation and Fe^{3+} reduction models were utilized (Gay, Collins *et al*. 1999, Hayes, Mills *et al*. 2011). For the ferrous oxidation, a solution of 1 μM Fe^{2+} was incubated with active oligostilbenes (1 μM) with the total volume of 500 μL for 5 min at room temperature. The amount of formed Fe^{3+} was quantified by adding an equal volume of 100 μM acidified xylenol orange (100 μM xylenol orange and 25 mM H_2SO_4 dissolved in 10% water/methanol). The results were presented as the percentage of Fe^{2+} oxidation. The ferric reduction assay was performed in a similar way to the oxidation assay, except the quantification of formed Fe^{2+} was done using acidified 10% o-phenanthroline. The results were presented as the Fe^{3+} reduction percentage. All tests were run in triplicate and averaged.

2.10. Colorimetric total iron determination

Stock solution of soybean lipoxygenases (10 μL) was treated with 6 M Hydrochloric acid (100 μL) and placed in boiling bath for an hour. After cooling down in ice bath, 100 μL of 6 M sodium hydroxide was added and further treated with 90 μL of 1 M ascorbic acid. The total iron amount was quantified with 790 μL acidified 10% *o*-phenanthroline and optical density was monitored at 420 nm against reagent

blank (Braunschweig, Bosch *et al*. 2012). Calibration curve was set in the range of 0.01-50 μM.

2.11. Spectroscopic studies

2.11.1. UV-vis spectrophotometry

UV-vis spectrophotometric assay was utilized to investigate the effect of active oligostilbenes on the active enzyme, Fe^{3+}-sbLOX-1 (Spaapen, Veldink *et al*. 1979, Nelson, Seitz *et al*. 1990) To activate the enzyme, 180 μM of native sbLOX-1 was incubated with 180 μM 13-HPOD which was synthesized according to the method described earlier. After 10 min of incubation, an aliquot of active oligostilbenes was added (100 μM) and the mixture further incubated for 5 min prior to following with UV-vis spectrophotometry.

2.11.2. Visible circular dichroism (CD) spectroscopy

Circular Dichroism is an absorption spectroscopy method based on the differential absorption of left and right circularly polarized light. Optically active chiral molecules will preferentially absorb one direction of the circularly polarized light. The difference in absorption of the left and right circularly polarized light can be measured and quantified, which is so-called dichroic band or Cotton effect. The Cotton effect is the characteristic change in optical rotatory dispersion and/or circular dichroism in the vicinity of an absorption band of a substance. In a wavelength region where the light is absorbed, the absolute magnitude of the optical rotation at first varies rapidly with wavelength, crosses zero at absorption maxima and then again varies rapidly with wavelength but in opposite direction (Woody 1995). The Cotton effect is called positive if the optical rotation first increases as the wavelength decreases (as first observed by Cotton), and negative if the rotation first decreases (Eliel, Wilen *et al*. 1994).

Visible CD spectroscopic assay in the same manner to UV-vis spectrophotometric assay. The assays were carried out in the visible region of 350–550 nm in 0.1M borate buffer, pH 9.0 with scan speed of 200 nm/min. All scans were an average of four runs. Sample preparation was followed UV spectrophotometric

method. The Cotton effect of both Fe^{3+}-sbLOX-1 and oligostilbene-treated Fe^{3+}-sbLOX-1 was observed at 420 nm (Spaapen, Veldink *et al*. 1979).

2.12. Statistical analysis

Data was presented as mean ± standard error of mean (S.E.M). One-way ANOVA was used to test for overall differences. The significant ANOVA was followed by Duncan multiple comparison for pair-wised differences between the treatment groups. *P*-value of less than 0.05 was considered statistically significant.

Chapter III

Results and Discussion

3.1. Structure elucidation of the isolated compounds

3.1.1. Dipterostilbene A (**1**)

Compound **1** was obtained as pale yellow amorphous solid with a molecular ion at 1379.3672 m/z [M+Na^+] (calculated for 1379.3677) in HRESIMS, corresponding to a molecular formula of $C_{84}H_{60}O_{18}Na$. The ^1H NMR spectrum indicated the presence of four sets of *ortho*-coupled protons in the A_2B_2 system on the *p*-substituted phenyl moieties [δ_H 7.31/6.86, 6.47/6.54, 7.13/6.74 and 6.97/6.81], two sets of A_2X-type meta-coupled aromatic proton signals [δ_H 6.26/6.29 and 5.90/6.26], three sets of *meta*-coupled aromatic proton signals [δ_H 5.95/6.19; 6.19/6.48 and 6.14/6.33], two sets of ABX-type *ortho*-coupled aromatic proton signals [δ_H 6.47/6.54 and 6.79/7.26] and a single aromatic proton signal [δ_H 6.51], as well as five sets of mutually coupled aliphatic proton signals [δ_H 5.47/4.74, 5.05/4.84, 5.21/4.89, 5.46/4.43 and 5.18/3.59]. In addition, the ^1H NMR signal at δ_H 6.82 and 6.79 (1H each, d, J = 16.0 Hz) together with the UV (λ_{max} 324 nm) and IR (ν_{max} 998 cm^{-1}) spectra demonstrated the *trans*-olefinic protons present in the resveratrol unit.

The 2D NMR spectra of **1** including ^1H-^1H COSY, HSQC and HMBC allowed the assignment of all proton and carbon signals (Figure **19** and Table **1**). The analysis of the ^1H-^1H COSY experiment and the coupling value of proton revealed the presence of the three isolated spin systems, shown in bold in Figure **20**. The combination between the analysis of the HMBC and ^1H-^1H COSY spectra, a planar structure of **1** was revealed. The HMBC correlation of δ_H 5.47 (H-7a) and 4.74 (H-8a) with δ_C 117.4 (C-10b) and 163.3 (C-11b), δ_H 5.05 (H-7c) and 4.84 (H-8c) with δ_C 122.3 (C-13b) and 162.8 (C-14b), and δ_H 6.51 (H-12b) with C-10b/C11b/C-13b/C-14b demonstrated that the resveratrol moiety A was coupled with moiety C with aromatic ring B2 of resveratrol moiety B. The coupling between resveratrol moieties D and C was confirmed by the correlations of methine protons δ_H 5.21 (H-7d), 4.89 (H-8d) and 6.19 (H-12c) with δ_C 162.6 (C-13c) and 118.9 (C-14c). The presence of HMBC correlation of aromatic proton δ_H 7.56 (H-2b) with δ_C 124.7 (C-3d) and δ_H 7.64 (H-2d) with δ_C 120.2 (C-3b) indicated

the biphenyl linkage between two ABX spin systems of ring B1 and D1 in **1**. The biphenyl linkage presented in oligostilbene was first reported from *D. hasseltii*, however it was common in liverworts such as *Marchantia polymorpha*, *Ricciocarpos natans* and *Radula perrotteii* (Kunz and Becker 1994, Toyota, Kinugawa *et al*. 1994, Fang, Guo *et al*. 2007). The partially structural assignment of **1** was identical to **5**, the resveratrol tetramer earlier isolated from *D. hasseltii* (Figure **21**). The cross correlations between δ_H 4.43 (H-7e), 5.46 (H-8e) and 6.48 (H-12d) with δ_C 160.1 (C-13d) and 120.2 (C-14d), and δ_H 5.18 (H-7f), 3.59 (H-8f) and 6.33 (H-12e) with δ_C 162.3 (C-13e) and 120.3 (C-14e) indicated the additional coupling of two resveratrol units. These observation allowed us to propose structure of **1** was derived from the coupling of **5** with additional two units of resveratrol.

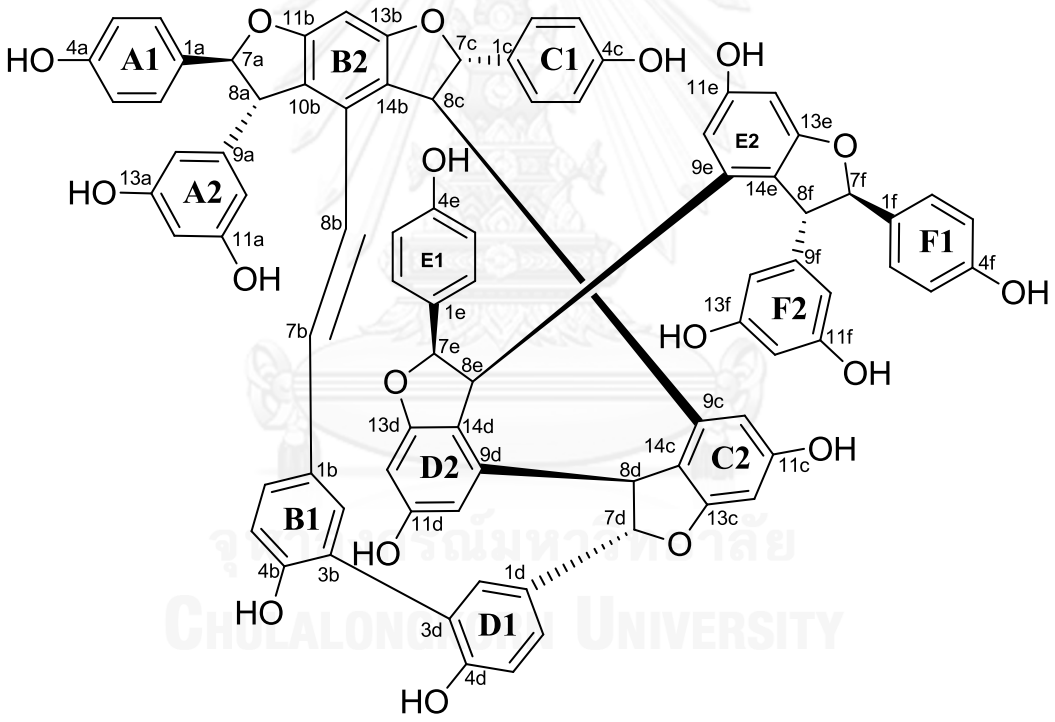

Dipterostilbene A (**1**)

Figure **19** Position assignment of **1.**

Most of the stilbenoids are not crystalline, which are unable to confirm the absolute configuration by X-ray crystallography. Until now, the spectroscopic data based on 2D NMR, especially NOESY experiment, are essential for the determination of resveratrol oligomer configuration. The *trans*-1,2-diaryl-dihydrobenzofuran

relationships were demonstrated by strong NOEs between H-7a/H-9a, H-8a/H-2a, H-7c/H-9c, H-8c/H-2c, H-7d/H-10d, H-8d/H2d, H-7f/H10f and H-8f/H-2f. The partial-

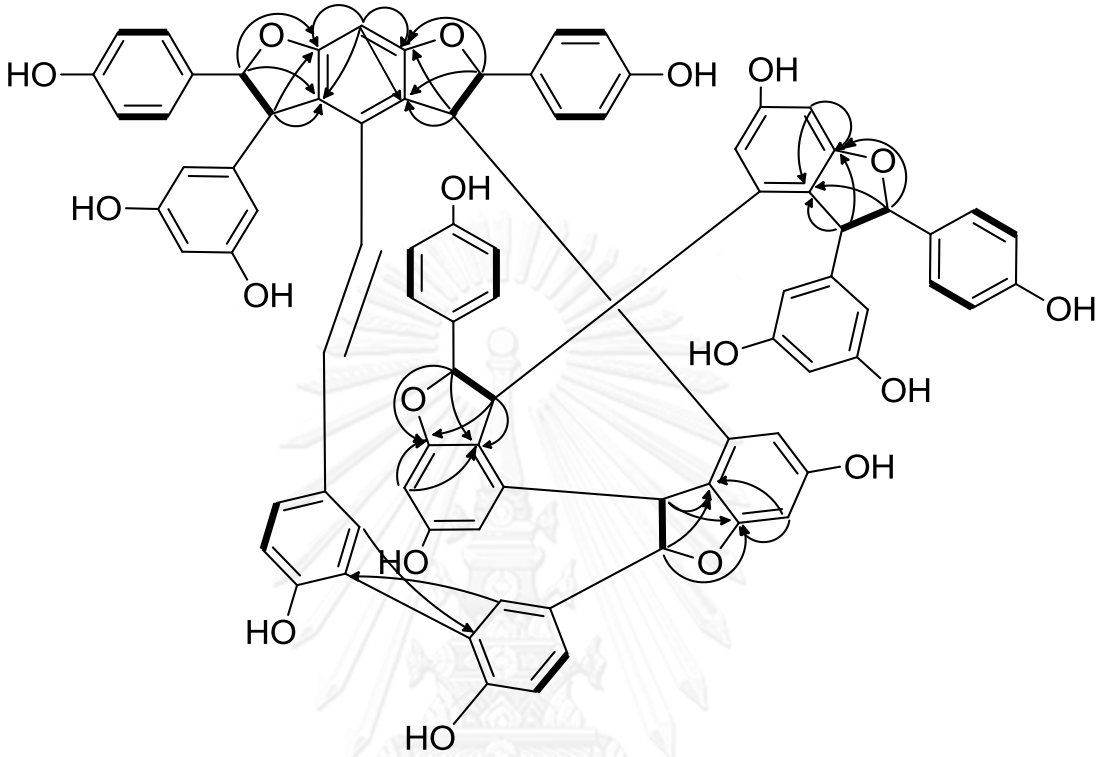

Figure **20** Selected HMBC (arrow curves) and COSY (bold lines) correlations of **1**.

configuration of **1** showed symmetric system and anisotropic effects of aromatic ring C1 as found in **12** (He, Peng *et al*. 2010), the possible intermediate for **5** biosynthesis. The additional NOEs of H-2b/H2d and H-7d/H-8f indicated the C1-D2 ring disclosed and spatial vicinity proton, respectively (Figure **22**). The presence of strong NOEs of H-7e/H-8e indicated cis-1,2-diaryl-dihydrobenzofuran. All spectroscopic data allowed to the structural assignment of **1** as dipterostilbene A.

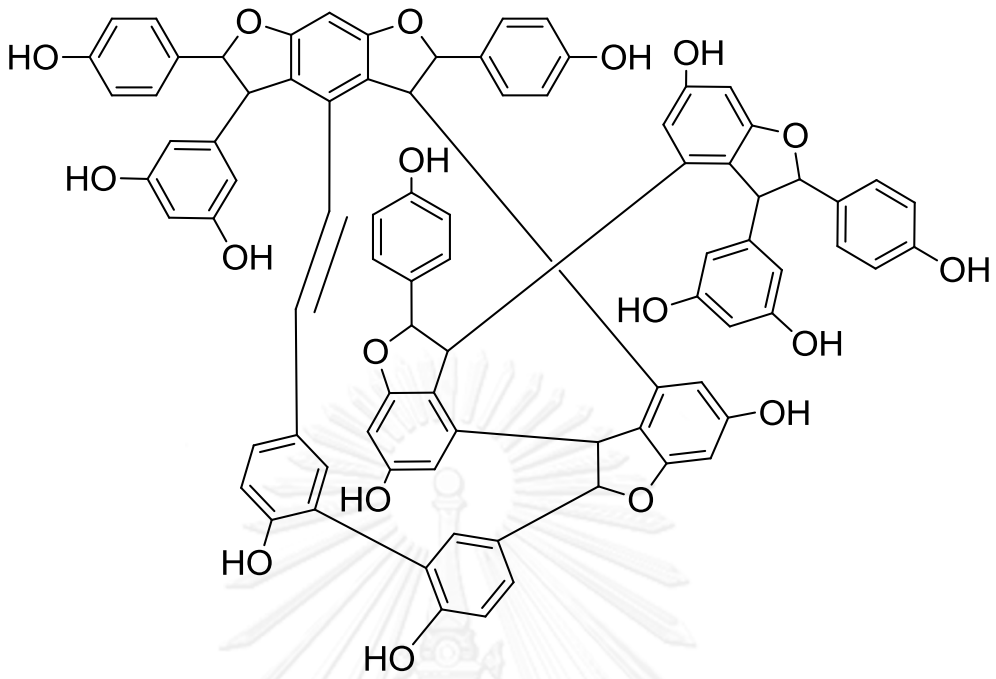

Dipterostilbene A (**1**)

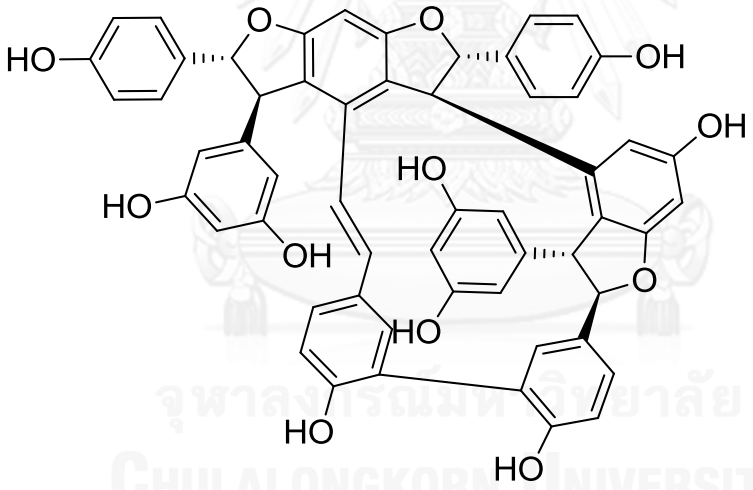

Diptoindonesin E (**5**)

Figure **21** Comparison between planar structure of 1 and relative structure of 5.

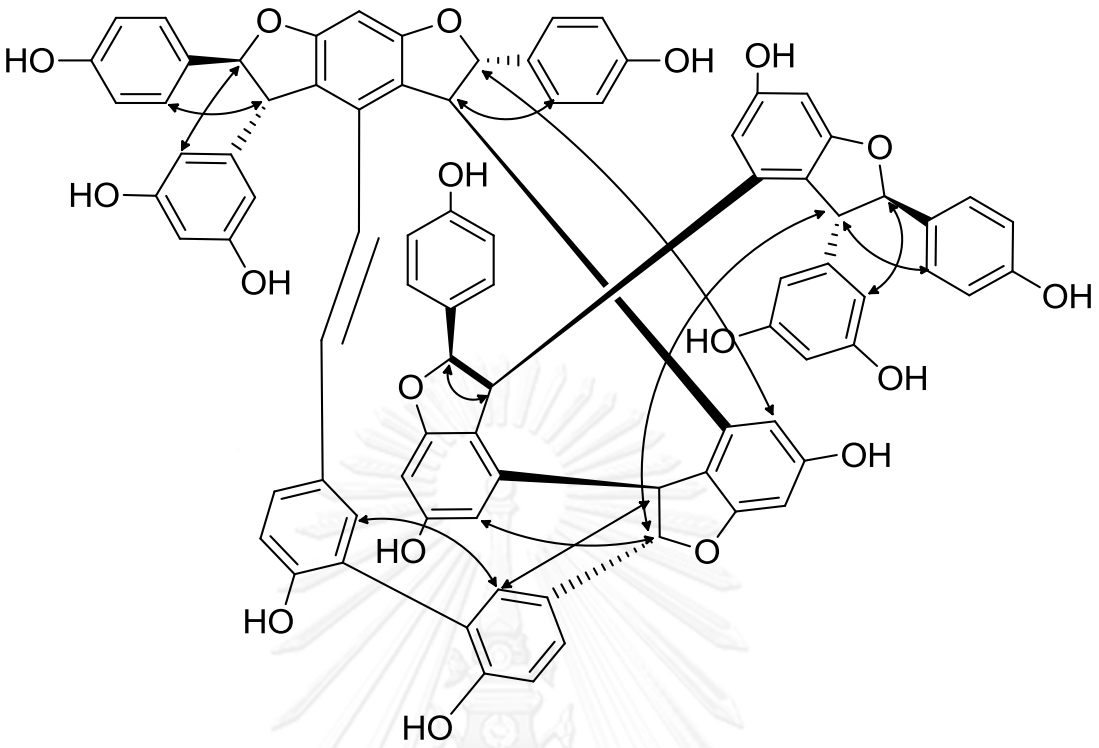

Figure 22 Key NOESY correlations for **1**.

Table **1** ^{1}H and ^{13}C Spectroscopic data of compound **1**.

Position	δ_C, type	δ_H (*J* in Hz)	Position	δ_C, type	δ_H (*J* in Hz)
1a	133.4, C		1d	134.5, C	
2a (6a)	127.5, CH	7.31, d (8.6)	2d	130.4, CH	7.64, d (1.6)
3a (5a)	115.5, CH	6.86, d (8.6)	3d	124.7, C	
4a	157.9, C		4d	155.3, C	
7a	93.3, C	5.47, d (3.6)	5d	116.9, CH	6.79, d (8.2)
8a	57.3, CH	4.74, d (3.6)	6d	128.9, CH	7.26, dd (1.9, 8.2)
9a	146.4, C		7d	92.4, CH	5.21, s
10a (14a)	106.3, CH	6.26, t (2.1)	8d	54.2, CH	4.89, s
11a (13a)	159.3, C		9d	147.7, C	
12a	101.2, CH	6.29, t (2.1)	10d	106.0, CH	6.19, br s
1b	130.2, C		11d	159.9, C	
2b	129.5, CH	7.56, s	12d	91.0, CH	6.48, br s
3b	120.2, C		13d	160.1, C	
4b	155.4, C		14d	120.2, C	
5b	114.8, CH	6.47, d (8.6)	1e	129.8, C	6.74, d (8.6)
6b	123.2, CH	6.54, d (8.6)	2e (6e)	128.1, CH	7.13, d (8.6)
7b	130.8, CH	6.82, d (16.0)	3e (5e)	115.7, CH	
8b	128.2, CH	6.79, d (16.0)	4e	159.2, C	
9b	138.9, C		7e	94.6, CH	5.46, d (9.4)
10b	117.4, C		8e	54.1, CH	4.43, d (9.4)
11b	163.3, C		9e	139.1, C	
12b	91.0, CH	6.51, s	10e	107.1, CH	6.14, d (2.0)
13b	162.8, C		11e	159.3, C	
14b	122.3, C		12e	96.1, CH	6.33 d (2.0)
1c	133.0, C		13e	162.3, C	
2c (6c)	127.0, CH	6.47, d (8.6)	14e	120.3, C	
3c (5c)	114.8, CH	6.54, d (8.6)	1f	132.6, C	
4c	157.5, C		2f (6f)	127.6, C	6.97, d (8.6)
7c	91.0, CH	5.05, d (1.0)	3f (5f)	115.3, C	6.81, d (8.6)
8c	52.4, CH	4.84, d (1.0)	4f	158.1, C	
9c	142.1, C		7f	93.3, CH	5.18, d (4.9)
10c	107.2, CH	5.95, d (2.0)	8f	55.7, CH	3.59, d (4.9)
11c	160.0, C		9f	146.3, C	
12c	96.4, CH	6.19, d (2.0)	10f (14f)	106.2, CH	5.90, d (2.1)
13c	162.6, C		11f (13f)	159.2, C	
14c	118.9, C		12f	101.6, CH	6.26, brs

^{1}H and ^{13}C NMR spectra were recorded at 500 and 150 MHz in CD3COCD3. Chemical shifts (δ) are in ppm, and coupling constants (*J* in Hz) are given in parentheses. The assignments were based on COSY, HSQC, HMBC and NOESY experiments.

3.1.2. Dipterostilbene B (**2**)

The molecular formula of compound **2** was determined as $C_{56}H_{40}O_{12}Na$ based on the ion peak at m/z 927.2413 [M+Na^+] (calcd 927.2417) in the HRESIMS. The ^{1}H NMR spectrum indicated the presence of two sets of *ortho*-coupled protons in the A_2B_2 system on the p-substituted phenyl moieties [δ_H 7.27/6.85 and 6.49/6.55], two sets of A_2X-type meta-coupled aromatic proton signals [δ_H 6.25/6.14 and 6.33/6.25], two sets of ABX-type *ortho*-coupled aromatic proton signals [δ_H 6.55/6.65 and 6.69/7.03] and a singlet aromatic proton signal [δ_H 6.40], as well as three sets of mutually coupled aliphatic proton signals [δ_H 5.43/4.66, 5.03/4.74 and 5.09/4.73]. In addition, the ^{1}H NMR spectrum also exhibited a signal at δ_H 6.70 and 6.72 (1H each, d, *J* = 16.0 Hz) for *trans*-olefinic protons in the resveratrol unit. The 2D NMR spectra of **2** including ^{1}H-^{1}H COSY, HSQC and HMBC allowed the assignment of all proton and carbon signals (Figure **23** and Table **2**). The HMBC correlation of δ_H 5.43 (H-7a) and 4.66 (H-8a) with δ_C 117.6 (C-10b) and 163.5 (C-11b), δ_H 5.03 (H-7c) and 4.74 (H-8c) with δ_C 162.7 (C-13b) and 122.6 (C-14b), and δ_H 6.40 (H-12b) with C-10b/C11b/C-13b/C-14b demonstrated that the resveratrol moiety A was coupled with moiety C with aromatic ring B2 of resveratrol moiety B. The coupling between resveratrol moieties D and C was confirmed by the correlation of methine protons δ_H 5.09 (H-7d), 4.73 (H-8d) and 6.17 (H-12c) with δ_C 163.4 (C-13c) and 120.1 (C-14c). The presence of HMBC correlation of aromatic proton δ_H 7.69 (H-2b) with δ_C 128.9 (C-3d) and δ_H 7.54 (H-2d) with δ_C 129.0 (C-3b) indicated the biphenyl linkage between two ABX spin systems of ring B1 and D1 in **2**. All these spectroscopic data indicated that the planar structure of **2** was substructure of **1** and similar to **5** (Figure **24**). The difference of optical rotation between **2** [$[\alpha]_D^{20}$ -30.2 (c 0.10, MeOH)] and **5** [$[\alpha]_D^{20}$ +100 (c 0.10, MeOH)] indicated that these two compounds were diastereomers. The CD spectra of **2** showed positive Cotton effect at 262 nm as found in **5**. Moreover, the additional negative Cotton effects at 315 and 385 nm also confirmed **2** was a diastereomer of **5** (Figure **25**). The relative configuration of **2** was deduced by NOESY experiment (Figure **26**). The *cis*-1,2-diaryl-dihydrobenzofuran relationships were demonstrated by the presence of strong NOEs between H-7a/H-8a, and H-7c/H-8c. The additional strong NOEs of H-7d/H-10d and H-8d/H-2d suggested

the *trans*-orientation. The NOEs of H-2b/H2d was absence for **2** as observed in **5**. The relative structure of **2** was assigned as dipterostilbene B.

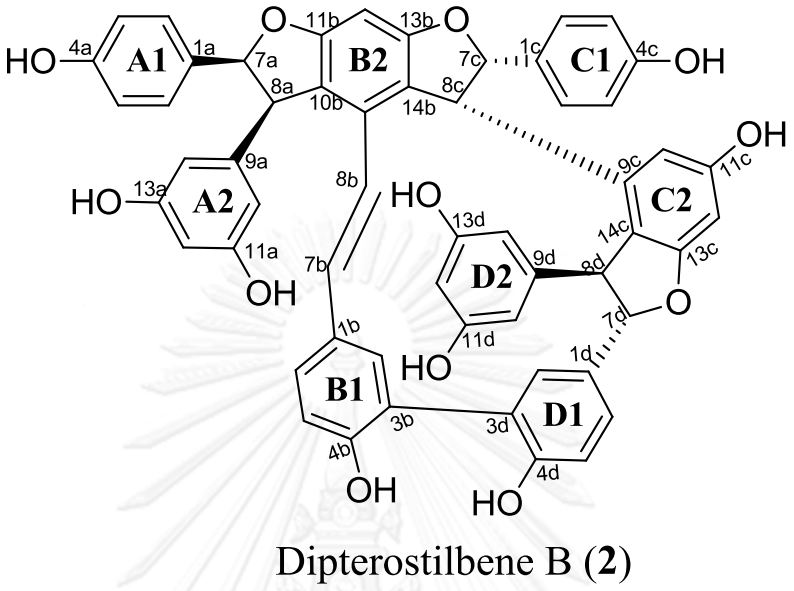

Dipterostilbene B (**2**)

Figure **23** Position assignment of **2.**

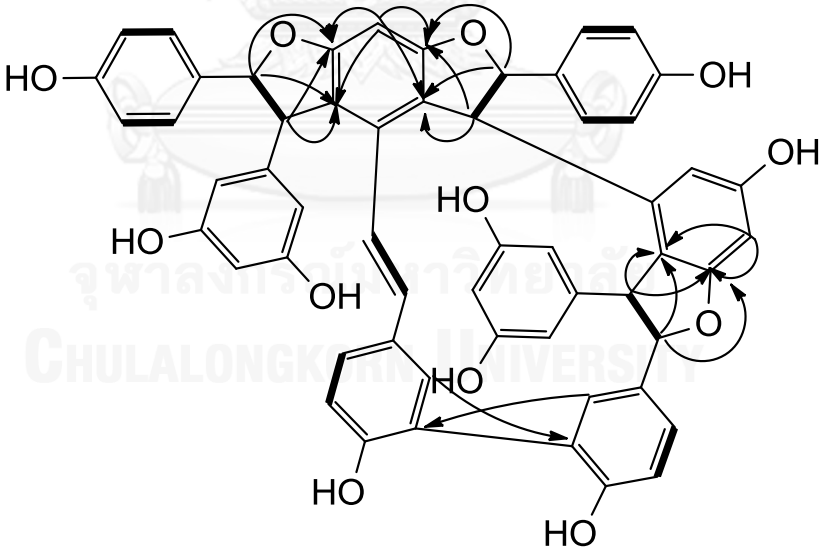

Figure **24** Selected HMBC (arrow curves) and COSY (bold lines) correlations of **2**.

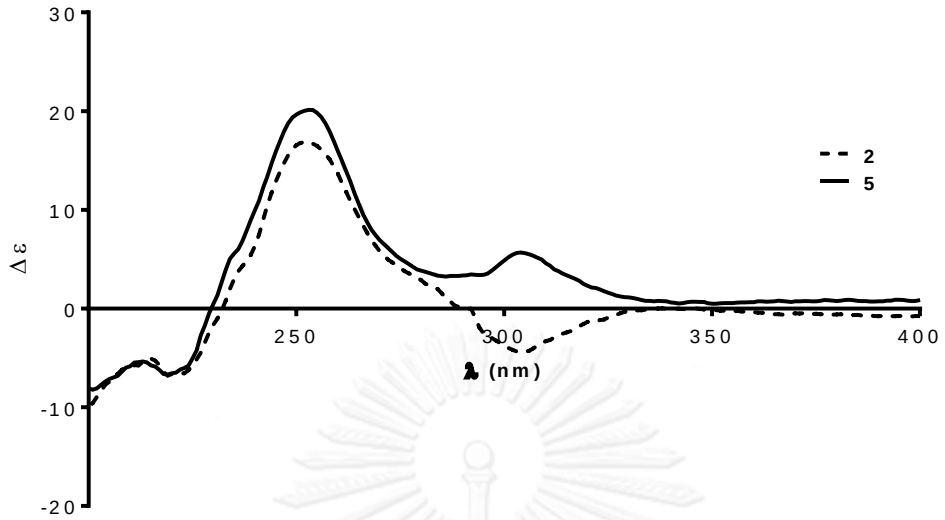

Figure **25** CD spectra of **2** and diptoindonesin E (**5**) in methanol.

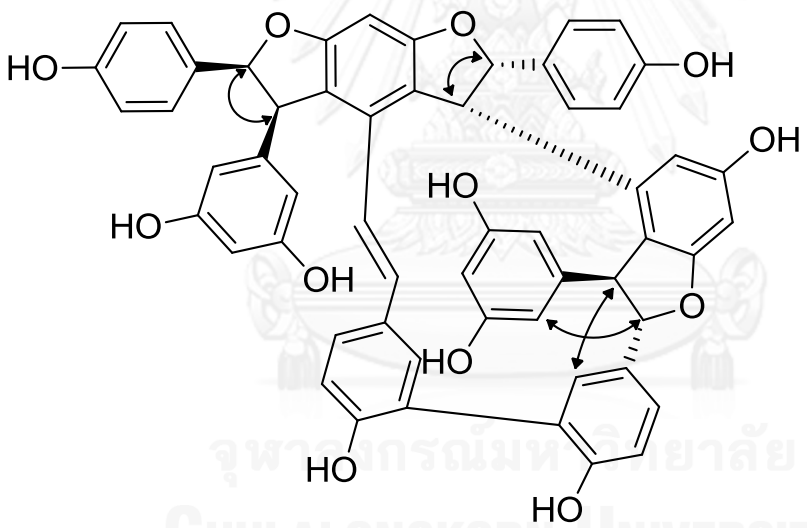

Figure **26** Key NOESY correlations for **2**.

Table **2** ^{1}H and ^{13}C Spectroscopic data of compound **2**.

Position	δ_C, type	δ_H (J in Hz)	Position	δ_C, type	δ_H (J in Hz)
1a	134.2, C		1c	133.8, C	
2a (6a)	127.9, CH	7.27, d (8.6)	2c (6c)	127.9, CH	6.49, d (8.6)
3a (5a)	116.3, CH	6.85, d (8.6)	3c (5c)	115.7, CH	6.55, d (8.6)
4a	158.2, C		4c	157.7, C	
7a	94.5, CH	5.43, d (4.2)	7c	91.1, CH	5.03, d (1.5)
8a	58.1, CH	4.66, d (4.2)	8c	52.7, CH	4.74, d, (1.5)
9a	146.7, C		9c	142.4, C	
10a (14a)	107.0, CH	6.25 d (2.0)	10c	107.9, CH	5.99, d (2.1)
11a (13a)	160.2, C		11c	159.3, C	
12a	102.2, CH	6.14, t (2.0)	12c	97.0, CH	6.17, d (2.1)
1b	132.3, C		13c	163.4, C	
2b	130.3, CH	7.69, s	14c	120.1, C	
3b	129.0, C		1d	132.7, C	
4b	160.3, C		2d	130.2, CH	7.54, d (2.0)
5b	117.9, CH	6.55, d (8.2)	3d	128.9, C	
6b	128.6, CH	6.65, dd (2.1, 8.2)	4d	160.1, C	
7b	128.1, CH	6.70, d (16.0)	5d	117.0, C	6.69, d (8.1)
8b	125.4, CH	6.72, d (16.0)	6d	127.2, CH	7.03, dd (2.0, 8.1)
9b	132.5, C		7d	94.3, CH	5.09, d (1.2)
10b	117.6, C		8d	56.4, CH	4.73, s
11b	163.5, C		9d	148.4, C	
12b	92.0, CH	6.40, s	10d (14d)	107.0, CH	6.25, br s
13b	162.7, C		11d (13d)	159.8, C	
14b	122.6, C		12d	102.1, CH	6.33,s

^{1}H and ^{13}C NMR spectra were recorded at 400 and 100 MHz in CD_3COCD_3. Chemical shifts (δ) are in ppm, and coupling constants (*J* in Hz) are given in parentheses. The assignments were based on COSY, HSQC, HMBC and NOESY experiments.

3.1.3. Dipterostilbene C (**3**)

Compound **3** was obtained as pale yellow amorphous solid with a molecular ion at 929.2572 m/z [M+Na^+] (calcd 929.2574) in HRESIMS, corresponding to a molecular formula of $C_{56}H_{42}O_{12}Na$. The ^1H NMR spectrum indicated the presence of four sets of *ortho*-coupled aromatic proton signals [δ_H 6.97/6.74, 6.64/6.53, 6.41/6.52 and 7.10/6.81], two sets of A_2X-type *meta*-coupled aromatic proton signals [δ_H 5.98/6.19 and 5.80/6.12] and one set of *meta*-coupled aromatic proton signals [δ_H 6.17/6.29] and a singlet aromatic proton signal [δ_H 6.40], as well as three sets of mutually coupled aliphatic proton signals [δ_H 5.28/3.83, 5.24/3.90 and 5.24/4.15]. In addition, the ^1H NMR spectrum also exhibited a signal at δ_H 5.61 and δ_H 5.36 (1H each, d, *J* = 12.2 Hz) for *cis*-olefinic protons in the resveratrol unit. The 2D NMR spectra of **3** including ^1H-^1H COSY, HSQC and HMBC allowed the assignment of all proton and carbon signals (Figure **27** Table **3**). The analysis of the ^1H-^1H COSY experiment and the coupling value of proton revealed the presence of the three isolated spin systems, shown in bold in Figure **28**. The combination between the analysis of the HMBC spectrum and COSY experiment, a planar structure of **3** was revealed. The sets of HMBC correlations of δ_H 5.28 (H-7a), 3.83 (H-8a) and 6.40 (H-12b) with δ_C 120.9 (C-10b) and 162.1 (C-11b), and δ_H 5.24 (H-7c), 3.90 (H-8c) and 6.40 (H-12b) with δ_C 161.6 (C-13b) and 123.9 (C-14b) indicated that resveratrol moieties A and C coupled with resveratrol moiety B at aromatic ring B2. The coupling between resveratrol moieties D and C was confirmed by the cross correlation of methine protons δ_H 5.24 (H-7d), 4.15 (H-8d) and 6.29 (H-12c) with δ_C 162.1 (C-13c) and 119.0 (C-14c). In addition, there was no HMBC correlation between aromatic ring B1 and D1 as found in **1**, **2** and **5**. According to these spectroscopic data, the planar structure of **3** was similar to flexuosol A and amurensin J which were *trans* olefinic resveratrol tetramers isolated from *Vitis flexuosa* and *Vitis amurensis* (Li, Li *et al*. 1998, Huang, Lin *et al*. 2001). The relative configuration of **3** was determined by NOESY experiment (Figure **29**). The presence of strong NOEs of H-7a/H8a and H-7c/H8c indicated *cis*-1,2-diaryl-dihydrobenzofuran. The *trans*-1,2-diaryl-dihydrobenzofuran relationships were demonstrated by strong NOEs between H-7d/H-9d and H-8d/H-2d. The optical activity differences between of flexuosol A [$[\alpha]_D^{20}$ -99.6° (c 0.15, MeOH)], amurensin J [$[\alpha]_D^{20}$ +174.9° (c 0.12, MeOH)] and 3 [$[\alpha]_D^{20}$

+84.1° (c 0.12, MeOH)] confirmed these three oligostilbenes were diastereomers. All spectroscopic data allowed to assign structure of **3** as dipterostilbene C.

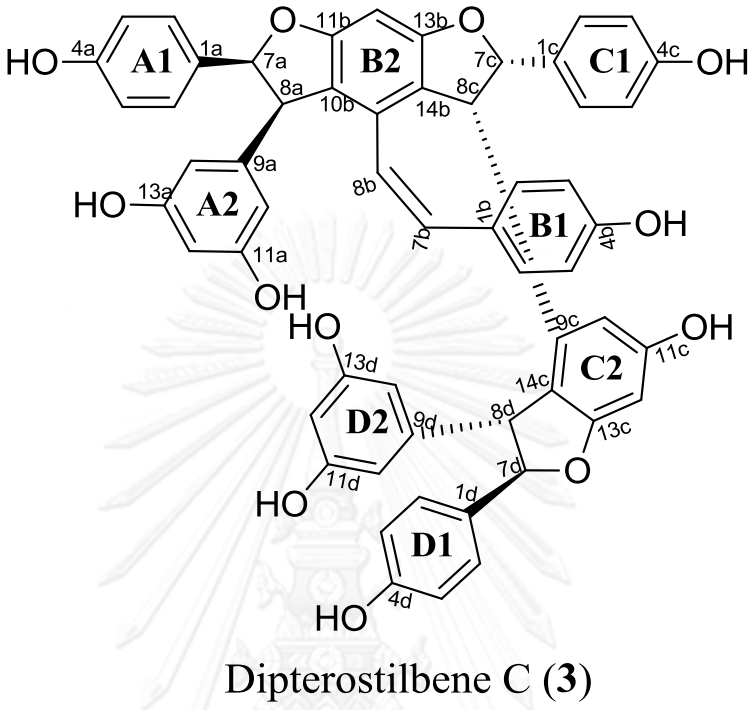

Dipterostilbene C (**3**)

Figure **27** Position assignment of **3.**

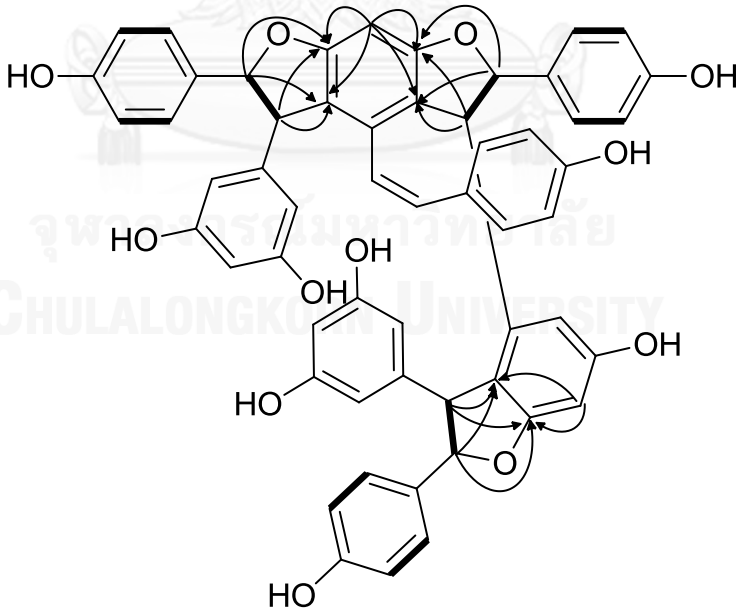

Figure **28** Selected HMBC (arrow curves) and COSY (bold lines) correlations of **3**.

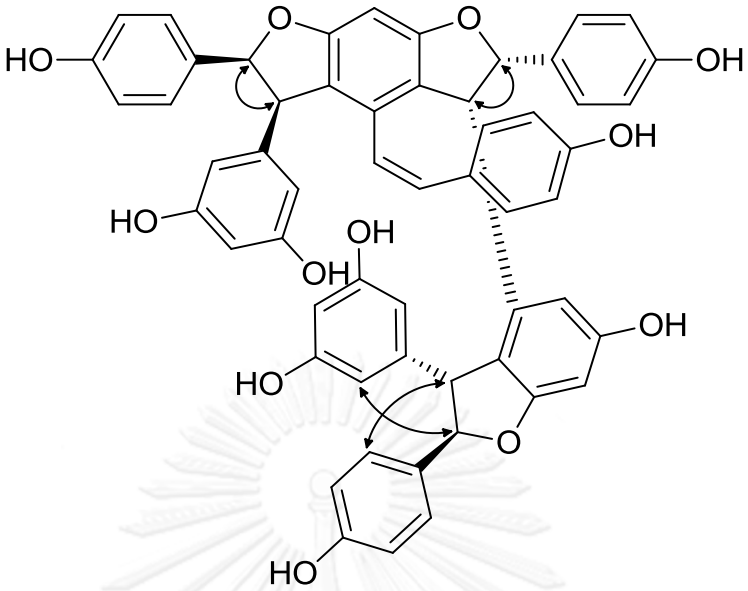

Figure **29** Key NOESY correlations for **3**.

3.1.4. Dipterostilbene D (**4**)

Compound **4** was obtained as pale yellow amorphous solid with a molecular ion at 929.2564 m/z [M+Na^+] (calculated for 929.2574) in HRESIMS, corresponding to a molecular formula of $C_{56}H_{42}O_{12}Na$. The ^1H NMR spectrum indicated the presence of four sets of *ortho*-coupled protons in the A_2B_2 system on the *p*-substituted phenyl moieties [δ_H 7.24/6.84, 7.01/6.68, 6.66/6.46 and 7.23/6.85], two sets of A_2X-type *meta*-coupled aromatic proton signals [δ_H 6.55/6.33 and 6.40/6.36], two singlet aromatic proton signals [δ_H 6.12 and 6.16], a sequence of four aliphatic methine protons coupled successively in the ^1H-^1H COSY spectrum in the order [δ_H 4.16, 3.38, 3.99 and 3.10] and two sets of mutually coupled aliphatic proton signals [δ_H 5.61/4.55 and 5.43/4.94]. The 2D NMR spectra of **4** including ^1H-^1H COSY, HSQC and HMBC allowed to the assignment of proton and carbon signals (Figure **30** and Table **4**). The sets of HMBC correlations of δ_H 3.38 (H-8b) and 3.99 (H-7c) with δ_C 143.0 (C-9c) and 127.2 (C-14b), δ_H 4.16 (H-7b) and 3.10 (H-8c) with δ_C 143.0 (C-9c) and 116.6 (C-14c), δ_H 4.16 (H-7b) with δ_C 137.2 (C-1b) and δ_H 3.99 (H-7c) with δ_C 133.3 (C-1c) illustrated that core structure of **4** was derived from **10** (Figure **31** and **32**). The coupling of resveratrol moiety A with resveratrol moiety B at aromatic ring B2 was illustrated by the HMBC correlations of δ_H 5.61 (H-7a), 4.55 (H-8a) and 6.12 (H-12b) with δ_C 117.6 (C-10b) and 159.8 (C-11b).

Table **3** ^{1}H and ^{13}C Spectroscopic data of compound **3**.

Position	δ_C, type	δ_H (*J* in Hz)	Position	δ_C, type	δ_H (*J* in Hz)
1a	133.6, C		14b	123.9, C	
2a (6a)	128.3, CH	6.97, d (8.5)	1c	133.3, C	
3a (5a)	116.1, CH	6.74, d (8.5)	2c (6c)	127.3, CH	6.41, d (8.5)
4a	158.0, C		3c (5c)	116.0, CH	6.52, d (8.5)
7a	94.6, CH	5.28, d (5.3)	4c	157.4, C	
8a	56.9, CH	3.83, d (5.3)	7c	93.0, CH	5.24, br s
9a	146.6, C		8c	52.3, CH	3.90, d (3.0)
10a	106.9, CH	5.98, d (2.0)	9c	143.1, C	
11a	159.4, C		10c	107.0, CH	6.17, d (2.0)
12a	102.2, CH	6.19, t (2.0)	11c	160.2, C	
13a	159.4, C		12c	96.1, CH	6.29, d (2.0)
14a	105.9, C	5.98, d (2.0)	13c	162.1, C	
1b	134.3, C		14c	119.0, C	
2b (6b)	130.5, CH	6.64, d (8.5)	1d	134.7, C	
3b (5b)	115.8, CH	6.53, d (8.5)	2d (6d)	127.3, CH	7.10, d (8.5)
4b	157.9, C		3d (5d)	116.0, CH	6.81, d (8.5)
7b	131.4, CH	5.61, d (12.2)	4d	158.2, C	
8b	123.1, CH	5.36, d (12.2)	7d	93.7, CH	5.24, br s
9b	129.1, C		8d	56.7, CH	4.15, d (3.0)
10b	120.9, C		9d	148.0, C	
11b	162.1, C		10d (14d)	106.5, CH	5.80, d (2.0)
12b	91.4, C	6.40, s	11d (13d)	159.9, C	
13b	161.6, C		12d	102.0, CH	6.12, t (2.0)

^{1}H and ^{13}C NMR spectra were recorded at 400 and 100 MHz in CD_3COCD_3. Chemical shifts (δ) are in ppm, and coupling constants (*J* in Hz) are given in parentheses. The assignments were based on COSY, HSQC, HMBC and NOESY experiments.

The cross correlations of δ_H 5.43 (H-7d), 4.94 (H-8d) and 6.16 (H-12c) with δ_C 113.6 (C-10c) and 156.7 (C-11c) indicated that resveratrol moiety D with resveratrol moiety C at aromatic ring C2. These data suggested that the planar structure of **4** was similar to ampelopsin H, stenophyllol C and nepalensinol B which were isolated from *Ampelopsis brevipedunculata* var. hancei, *Sophora stenophylla* and *Kobresia nepalensis* (Oshima and Ueno 1993, Ohyama, Tanaka *et al*. 1998, Yamada, Hayashi *et*

al. 2006). The relative configuration of **4** was determined by NOESY experiment (Figure **33**). The strong NOEs of H-7a/H8a and H-7d/H-8d indicated the *cis*-1, 2-diaryl-dihydrobenzofuran configuration. The additional NOEs of H-7b/H-8c and H-8b/H-7c supported the assignment of asymmetrically relative configuration of **4**. The relative configuration of **4** had an asymmetrical resveratrol dimer in its molecule, which was contrasted to those of resveratrol oligomers. The comparison of optical activity of reported resveratrol oligomers (ampelopsin H [$[\alpha]_D^{20}$ +105° (c 0.83, MeOH)], stenophyllol C [$[\alpha]_D^{20}$ -66° (c 0.1, MeOH)] and nepalensinol B [$[\alpha]_D^{20}$ +-24.4° (c 0.2, MeOH)]) strongly indicated that **4** ($[\alpha]_D^{20}$ +68.7° (c 0.1, MeOH)) was a diastereomer. All spectroscopic data allowed to assign the structure of **4** as dipterostilbene D.

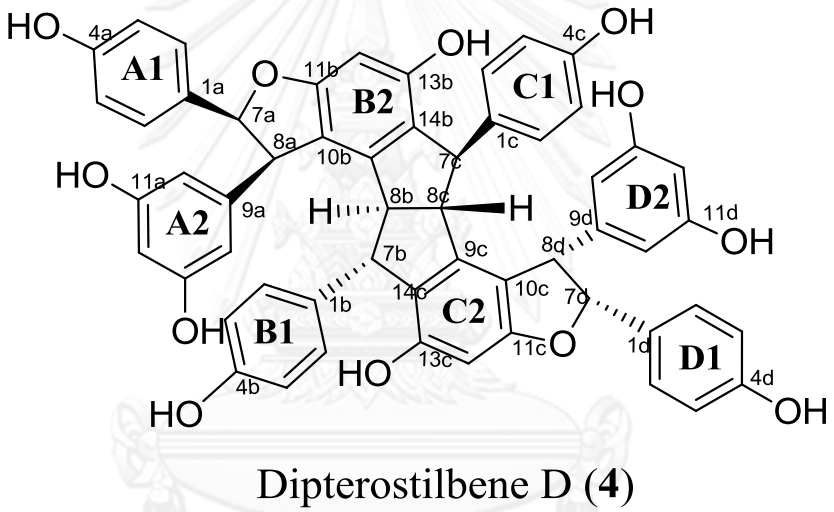

Figure **30** Position assignment of **4**.

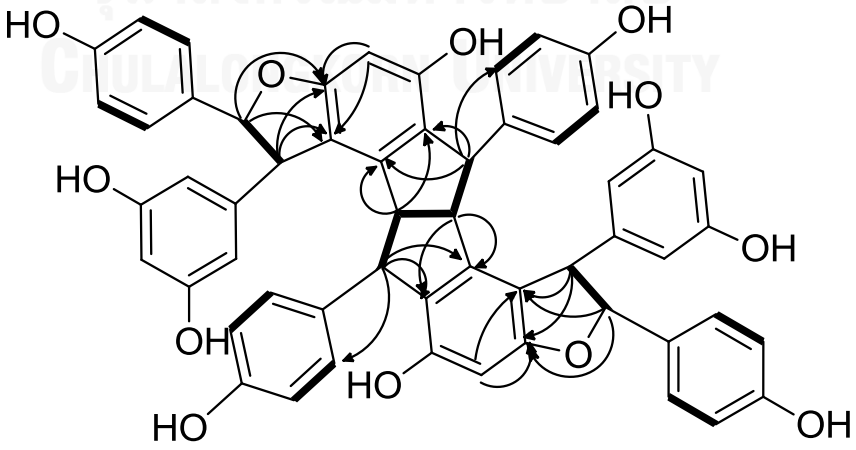

Figure **31** Selected HMBC (arrow curves) and COSY (bold lines) correlations of **4**.

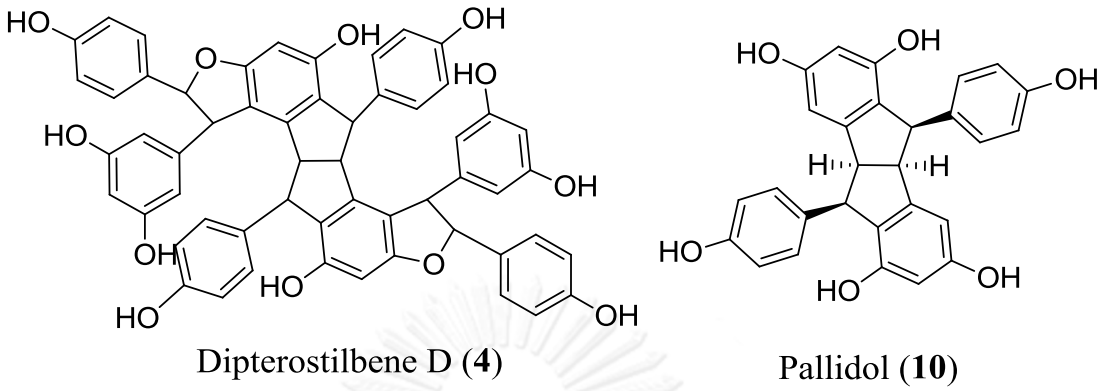

Figure **32** Comparison between Planar structure of **4** and pallidol (**10**).

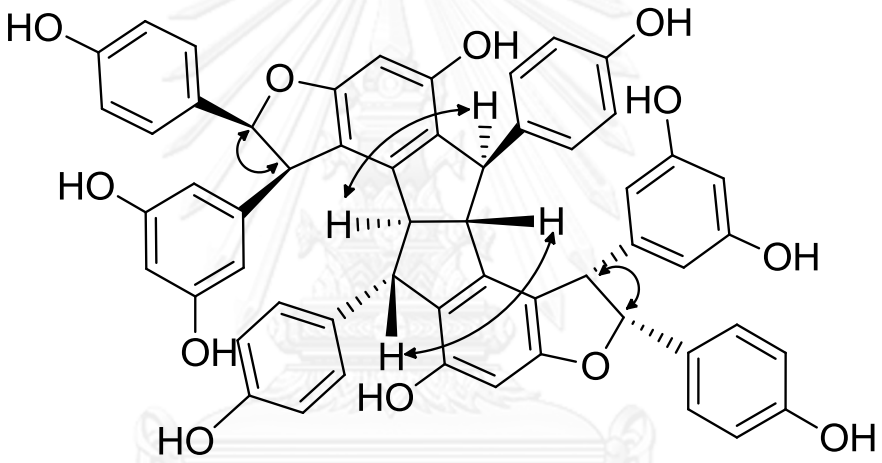

Figure **33** Selected NOESY correlations of **4**.

Table **4** ^{1}H and ^{13}C Spectroscopic data of compound **4**.

Position	δ_C, type	δ_H (*J* in Hz)	Position	δ_C, type	δ_H (*J* in Hz)
1a	132.5, C		14b	127.2, C	
2a (6a)	127.0, CH	7.24, d (8.5)	1c	133.3, C	
3a (5a)	114.6, CH	6.84, d (8.5)	2c (6c)	128.4, CH	6.66, d (8.5)
4a	157.1, C		3c (5c)	114.5, CH	6.46, d (8.5)
7a	93.2, CH	5.61, d (7.9)	4c	154.8, C	
8a	56.7, CH	4.55, d (7.9)	7c	46.5, CH	3.99, s
9a	144.7, C		8c	49.9, CH	3.10, s
10a	107.0, CH	6.55, d (2.1)	9c	143.0, C	
11a	158.9, C		10c	113.6, C	
12a	100.8, CH	6.33, t (2.1)	11c	156.7, C	
13a	158.9, C		12c	94.7, CH	6.16, s
14a	107.3, C		13c	158.6, C	
1b	137.2, C		14c	116.6, C	
2b (6b)	128.8, CH	7.01, d (8.5)	1d	132.5, C	
3b (5b)	115.0, CH	6.68, d (8.5)	2d (6d)	127.0, CH	7.23, d (8.5)
4b	154.9, C		3d (5d)	115.3, CH	6.85, d (8.5)
7b	44.5, CH	4.16, s	4d	157.1, C	
8b	48.5, CH	3.38, s	7d	93.2, CH	5.43, d (6.6)
9b	142.1, C		8d	55.6, CH	4.94, d (6.6)
10b	117.6, C		9d	147.2, C	
11b	159.8, C		10d (14d)	106.3, CH	6.40, d (2.1)
12b	94.8, CH	6.12, s	11d (13d)	158.8, C	
13b	152.4, C		12d	101.3, CH	6.36, t (2.1)

^{1}H and ^{13}C NMR spectra were recorded at 400 and 100 MHz in CD_3COCD_3. Chemical shifts (δ) are in ppm, and coupling constants (*J* in Hz) are given in parentheses. The assignments were based on COSY, HSQC, HMBC and NOESY experiments.

3.1.5. Dipterostilbenoside A (**14**)

Compound **14** was obtained as yellow amorphous solid with a molecular ion at 1091.3104 m/z [M+Na$^+$] (calculated for 1091.3102) in HRESIMS, corresponding to a molecular formula of $C_{62}H_{52}O_{17}Na$. The ^{1}H NMR spectrum indicated the presence of four sets of *ortho*-coupled protons in the A_2B_2 system on the *p*-substituted phenyl moieties [δ_H 7.14/6.73, 7.19/6.67, 6.53/6.47 and 7.17/6.78], one sets of A_2X-type *meta*-coupled aromatic proton signals [δ_H 6.19 and 6.48], two set of *meta*-coupled aromatic

proton signals [δ_H 6.18/6.44 and δ_H 6.52/6.13], one singlet aromatic proton signal [δ_H 6.04], a sequence of four aliphatic methine protons coupled successively in the COSY spectrum [δ_H 5.25, 4.10, 3.14 and 4.43] and two sets of mutually coupled aliphatic proton signals [δ_H 4.30, 5.68, 4.63 and 5.31]. The 2D NMR spectra of **14** including COSY, HSQC and HMBC allowed the assignment of all proton and carbon signals (Figure **34** and Table **5**). The significant HMBC correlations between H-7a/C-2a(6a), H-8a/C-14a, H-7b/C-2b(6b), H-8b/C-14b, H-7c/C-2c(6c), H-8c/C-14c, H-7d/C-2d(6d) and H-8d/C-10d(14d) support the respective C–C bonds C-1a/C-7a, C-8a/C-9a, C-1b/C-7b, C-8b/C-9b, C-1c/C-7c, C-8c/C-9c, C-1d/C-7d and C-8d/C-9d, which indicate the four resveratrol blocking units, resveratrols A-D (Figure **35**). The additional HMBC correlation for the connection of these units (H-8a/C-10b and C-11b, H-7b/C-10a, H-7c/C-9b and H-8c/C-14b, C-9c and C-14c, H-8d/C-14c, C-10d) confirmed the respective C-C bonds between the units C-8a/C-10b, C-7b/C-10a, C-8c/C-14b, C-7d/C-1d, C-8d/C-10c and C-9d. Therefore, the partial structure of **14** was similar to vaticanol B or vaticaphenol A which were isolated from *Vatica rassak* and *Vatica diospyroides* at the same time (Seo, Chai *et al*. 1999, Tanaka, Ito *et al*. 2000). The additional analysis of HSQC spectrum clearly showed one glucopyranosyl pattern and one correlation between the anomeric proton [δ_H 4.88 (1H, d, J = 7.7 Hz)] and the anomeric carbon (δ_C 102.0). Furthermore, a long-range correlation between the anomeric proton and an aromatic carbons (C-4c, δ_C 156.1) in the HMBC spectrum confirmed that the β-glucopyranosyl group was substituted at C-4c. The appearance of *O*-β-glucopyranosyl group was confirmed by the TLC analysis of the hydrolysis of **14** in 1% H_2SO_4. The relative configuration of **14** was determined by NOESY experiment (Figure **36**). The *trans*-1,2-diaryl-dihydrobenzofuran was confirmed by strong NOEs of H-7a/H-14a, H-8a/H2a(6a), H-7d/H-10d and H-8d/H-2d(6d). The strong NOEs of H-7b/H-7c and H-8b/H-8c additionally confirmed that aglycone **14** was diasteromer of vaticanol B and vatdiospyroidol. These spectroscopic data allowed us to assign **14** as dipterostilbenoside A.

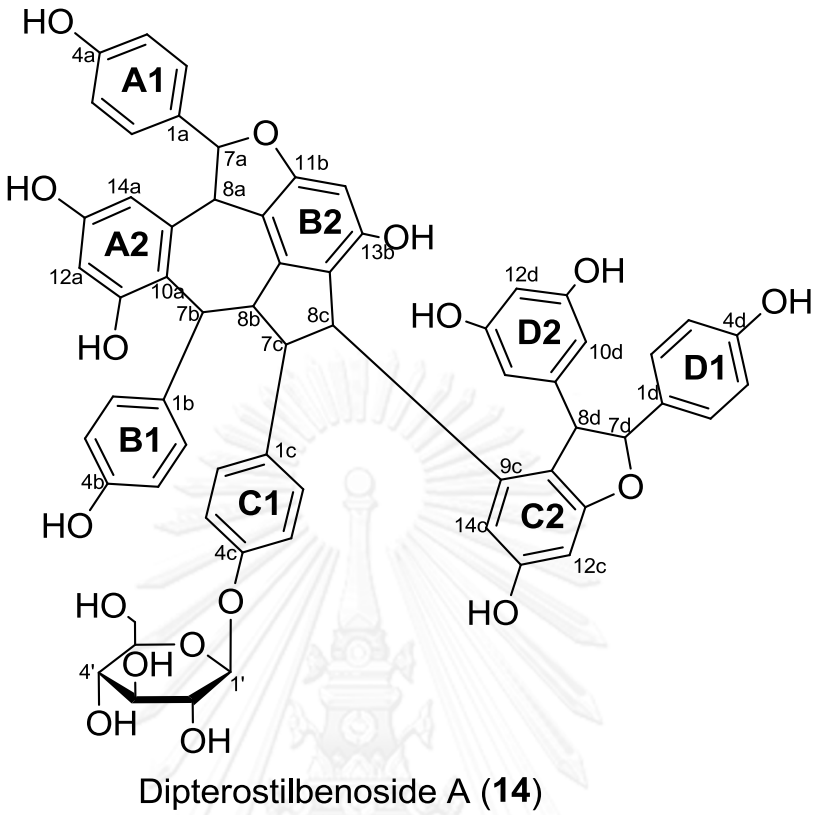

Dipterostilbenoside A (**14**)

Figure **34** Position assignment of **14**.

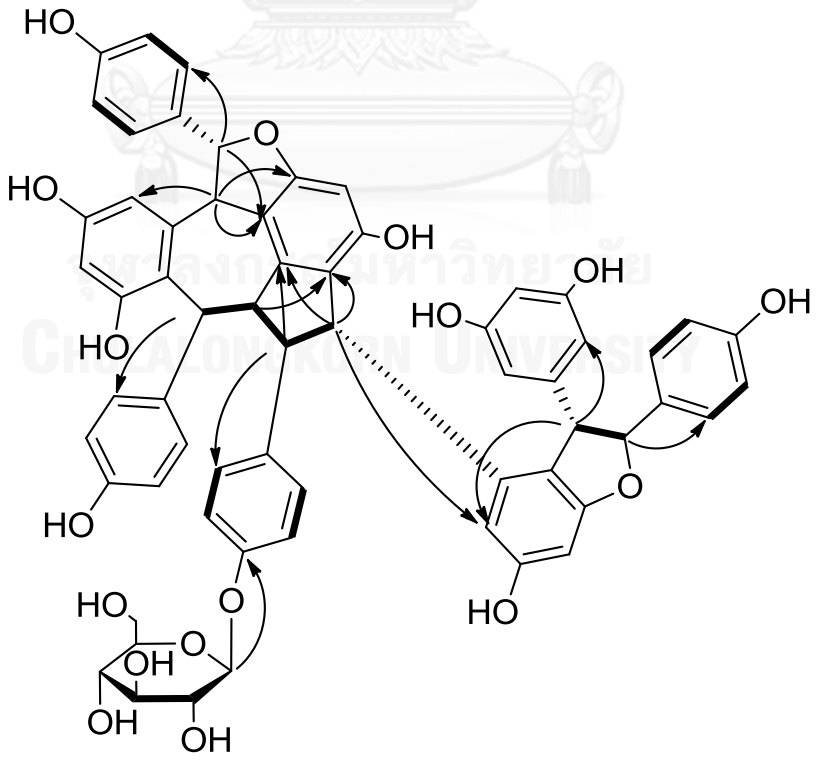

Figure **35** Selected HMBC (arrow curves) and COSY (bold lines) correlations of **14**.

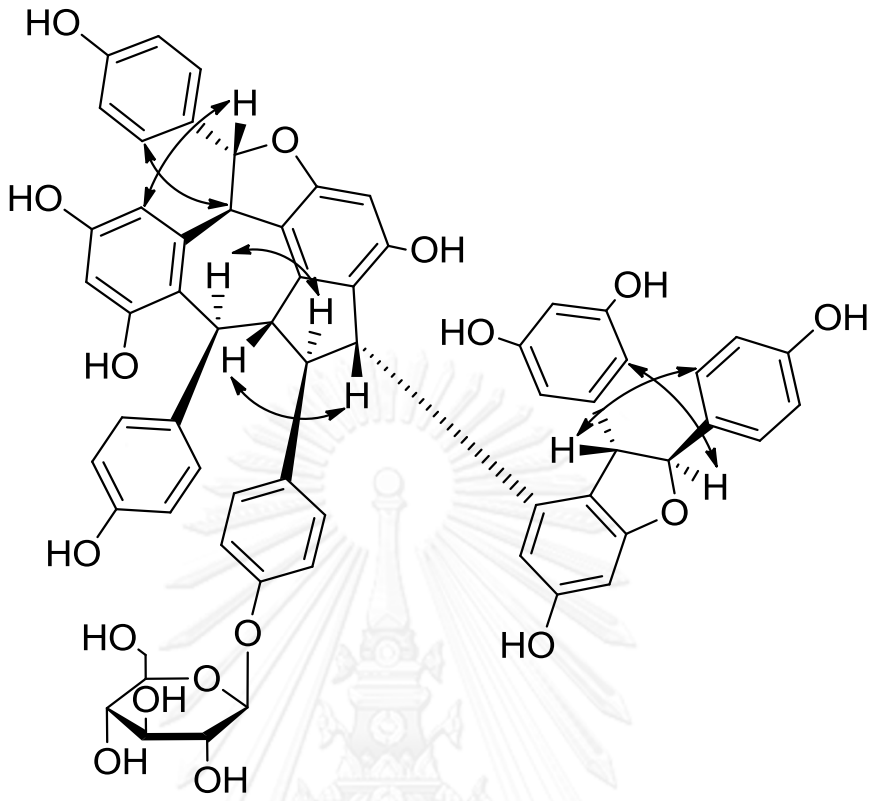

Figure **36** Key NOESY correlations for **14**.

Table **5** ^{1}H and ^{13}C Spectroscopic data of compound **14**.

Position	δ_H (*J* in Hz)	δ_C, type	Position	δ_H (*J* in Hz)	δ_C, type
1a	-	130.5, C	3c(5c)	6.47 (d, 8.6)	116.3,CH
2a(6a)	7.14 (d, 8.6)	130.4, CH	4c	-	156.1,C
3a(5a)	6.73 (d, 6.73)	116.3, CH	7c	3.14 (br d, 11.6)	52.7,CH
4a	-	159.0, C	8c	4.43 (d, 10.5)	50.1,CH
7a	5.68 (d, 11.8)	90.9, CH	9c	-	142.5,CH
8a	4.30 (d, 11.8)	49.9, CH	10c	6.44 (d, 1.9)	107.4,CH
9a	-	142.2, C	11c	-	159.3,C
10a	-	128.3, C	12c	6.18 (d, 1.9)	95.8CH
11a	-	154.6, C	13c	-	161.8,C
12a	6.52 (br s)	101.7, C	14c	-	123.9,C
13a	-	157.1, C	1d	-	134.9,C
14a	6.13 (d, 1.2)	108.3, CH	2d(6d)	7.17 (d, 8.6)	128.6,CH
1b	-	133.6, C	3d(5d)	6.78 (d, 8.6)	116.3,CH
2b(6b)	7.19 (d, 8.6)	131.4, CH	4d	-	158.3,C
3b(5b)	6.67 (d, 8.6)	116.2, CH	7d	5.31 (d, 5.1)	95.5,CH
4b	-	154.6, C	8d	4.63 (d, 5.1)	57.9,CH
7b	5.25 (d, 3.3)	37.5, CH	9d	-	148.5,C
8b	4.10 (d, 11.1)	58.1, CH	10d(14d)	6.48 (br s)	107.8,CH
9b	-	143.6, C	11d(13d)	-	158.9,C
10b	-	115.6, C	12d	6.19 (t, 2.2)	102.3,CH
11b	-	159.7, C	1'	4.88 (d, 7.7)	102.0,CH
12b	6.04 (s)	96.6, CH	2'	3.05 (dd, 7.9, 9.0)	74.8,CH
13b	-	155.6, CH	3'	3.39 (t, 9.0)	78.5,CH
14b	-	123.0, C	4'	3.26 (m)	71.5,CH
1c	-	132.4, C	5'	3.62 (dd, 5.8, 12.0)	78.2,CH
2c(6C)	6.53 (d, 8.6)	129.6, CH	6'	3.87 (dd, 2.0, 12.0)	62.9,CH

^{1}H and ^{13}C NMR spectra were recorded at 400 and 100 MHz in CD_3OD. Chemical shifts (δ) are in ppm, and coupling constants (*J* in Hz) are given in parentheses. The assignments were based on COSY, HSQC, HMBC and NOESY experiments.

3.1.6. Dipterostilbenoside B (**15**)

Compound **15** was obtained as yellow amorphous solid with a molecular ion at 639.1847 m/z [M+Na^+] (calculated for 639.1842) in HRESIMS, corresponding to a molecular formula of $C_{34}H_{32}O_{11}Na$. The ^1H NMR spectrum indicated the presence of two sets of *p*-hydroxyphenyl groups [δ_H 6.48/6.91 and 6.71/6.94], one sets of A_2X-type *meta*-coupled aromatic proton signals [δ_H 6.08, 6.16 and 6.38] and one set of *meta*-coupled aromatic proton signals [δ_H 6.23 and 6.25] and one set of mutually coupled aliphatic proton signals [δ_H 3.80, 5.18]. In addition, the ^1H NMR signals at δ_H 6.03 and 6.18 (d, *J* = 12.0 Hz) together with the UV (λ_{max} 324 nm) and IR (ν_{max} 988 cm^{-1}) spectra demonstrated the *cis*-olefinic protons present in the resveratrol unit. The 2D NMR spectra of **15** including COSY, HSQC and HMBC allowed the assignment of all proton and carbon signals (Figure **37** and Table **6**). The significant HMBC correlations between H-7a/C-2a(6a), C-10b and H-8a/C-9a, C-10b, C-11b support the respective C–C bonds C-1a/C-7a, C-8a/C-9a, C-8a/C-10b which indicate the two resveratrol blocking units, resveratrols A-B (Figure **38**). The additional cross correlation observed for H-7a/C-11b supported the presence of an ether linkage, C-7a-O-C-11b, which was a part of dihydrobenzofuran moiety. These spectroscopic data is a good agreement of *cis*-***ε***-viniferin (Langcake and Pryce 1977). The absolute stereochemistry of the **15** showed two negative Cotton effect near 236 and 336 nm as compared with authentic (-)-***ε***-viniferin (Figure **39**). ***ε***-viniferin is one of the common resveratrol dimer, which it mainly distribute in the family Dipterocarpaceae, Leguminosae, Cyperaceae, and Gnetaceae. However, each plant family has stereospecific biosynthesis of this resveratrol dimer. The positive optical activity resveratrol dimer, (+)-***ε***-viniferin, is predominant in the family Vitaceae, while the negative one, (-)-***ε***-viniferin, is dominant in the family Dipteracarpaceae and others (Takaya, Yan *et al*. 2002). Thus, the relative configuration of aglycone moiety was deduced according to the fact of ***ε***-viniferin biosynthesis in Dipterocarpaceous plants and CD spectroscopic evidence. The analysis of HSQC spectrum also showed one glucopyranosyl pattern and one correlation between the anomeric proton [δ_H 4.80 (1H, d, *J* = 7.3 Hz)] and the anomeric carbon (δ_C 101.9). Furthermore, HMBC correlations between the anomeric proton and an aromatic carbon (C-11a, δ_C 160.1) in the HMBC spectrum displayed the appearance of *O*-**β**-

glucopyranosyl linkage at C-11a. The appearance of β-glucopyranosyl group was confirmed by the TLC analysis of the acid hydrolysis of **15**. We found that compound **15** was a diastereomer of (-)-***ε***-viniferin glycoside which was reported from the stem bark of *Vitis vinifera* (Choi, Choi *et al*. 2010). These spectroscopic data allowed to assign **15** as dipterostilbenoside B.

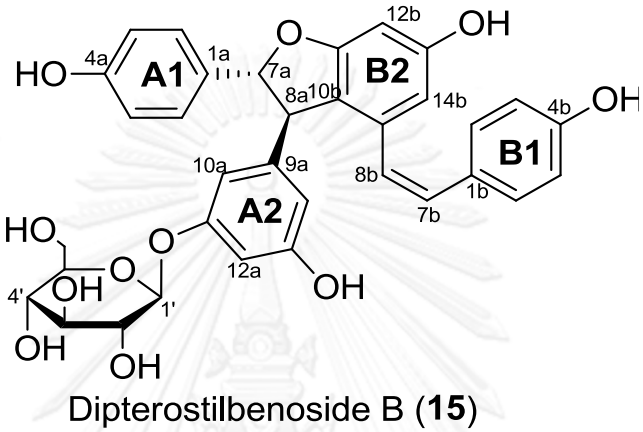

Figure **37** Position assignment of **15**.

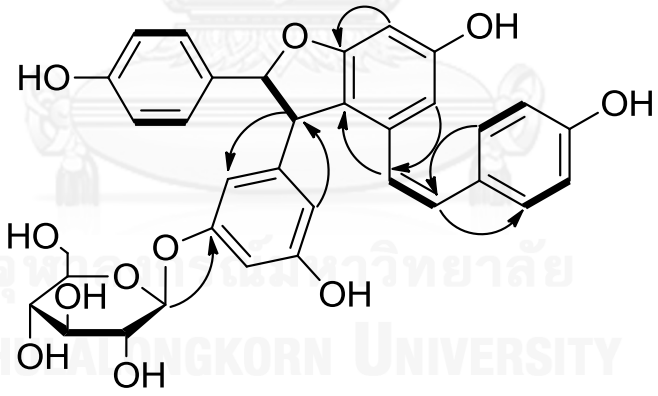

Figure **38** Selected HMBC (arrow curves) and COSY (bold lines) correlations of **15.**

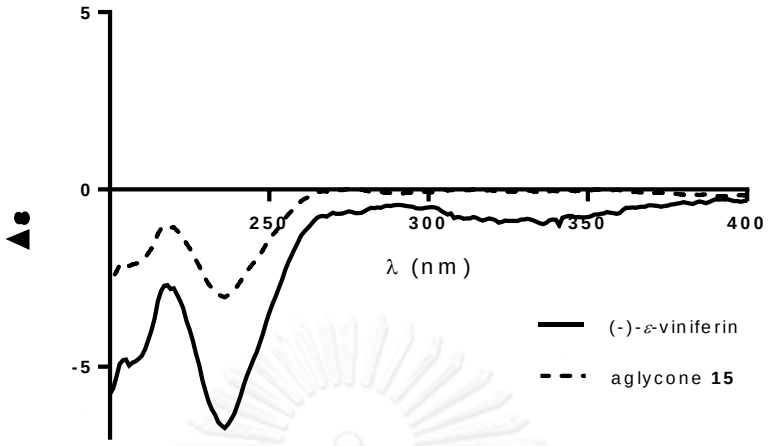

Figure **39** CD spectra of aglycone **15** and (-)-***ε***-viniferin in methanol.

Table **6** ^{1}H and ^{13}C Spectroscopic data of compound **15**.

Position	δ_H (*J* in Hz)	δ_C, type	Position	δ_H (*J* in Hz)	δ_C, type
1a	-	133.7,C	4b	-	157.9,C
2a(6a)	6.94 (d, 8.9)	128.5,CH	7b	6.18 (d, 12.0)	131.7,CH
3a(5a)	6.71 (d, 8.9)	116.3,CH	8b	6.03 (d, 12.0)	126.6,CH
4a	-	158.4,C	9b	-	137.8,C
7a	5.18 (d, 6.0)	94.8,CH	10b	-	120.2,C
8a	3.80 (d, 6.0)	57.7,CH	11b	-	162.8,C
9a	-	147.7,C	12b	6.23 (d, 2.0)	96.6,CH
10a	6.16 (t, 1.8)	108.3,CH	13b	-	159.5,C
11a	-	160.1,C	14b	6.25 (d, 2.0)	109,CH
12a	6.38 (t, 2.2)	103.2,CH	1'	4.80 (d, 7.3)	101.9,CH
13a	-	159.7,C	2'	3.33 (m)	74.8,CH
14a	6.08 (t, 1.8)	109.7,CH	3'	3.31 (m)	78.0,CH
1b	-	130.0,C	4'	3.19 (m)	71.0,CH
2b(6b)	6.91 (d, 8.9)	131.1,CH	5'	3.52 (m)	77.9,CH
3b(5b)	6.58 (d, 8.9)	115.9,CH	6'	3.74 (dd, 3.4, 10.8)	60.7,CH

^{1}H and ^{13}C NMR spectra were recorded at 400 and 100 MHz in CD_3OD. Chemical shifts (***δ***) are in ppm, and coupling constants (*J* in Hz) are given in parentheses. The assignments were based on COSY, HSQC, HMBC and NOESY experiments.

3.2. Chemical taxonomy significances

To date, a number of resveratrol oligomers were continuously reported from the family Dipterocarpaceae. Although *D. tuberculatus*, *D. hasseltii* and *D. grandiflorus* shared some common stilbenes (***α***- and ***ε***-viniferins, gnetin H, hopeaphenol and amurensin H), they also exhibited some genetic variations in the oligostilbene biosynthesis through the occurrence of minor stilbenes. Biphenyl-type resveratrol oligomers, compounds **1**-**3** and diptoindonesin E (**5**), were unique for *D. tuberculatus* and *D. hasseltii*, whereas they have not been reported from *D. grandiflorus*. However, no report on systemic molecular phylogeny has been demonstrated the differences in genetic background among these species. Therefore, both of extensively phytochemical taxonomy and molecular phylogeny are needed to determine the differences among those of dipterocarps. The structures of known compounds are shown in Figure **40**.

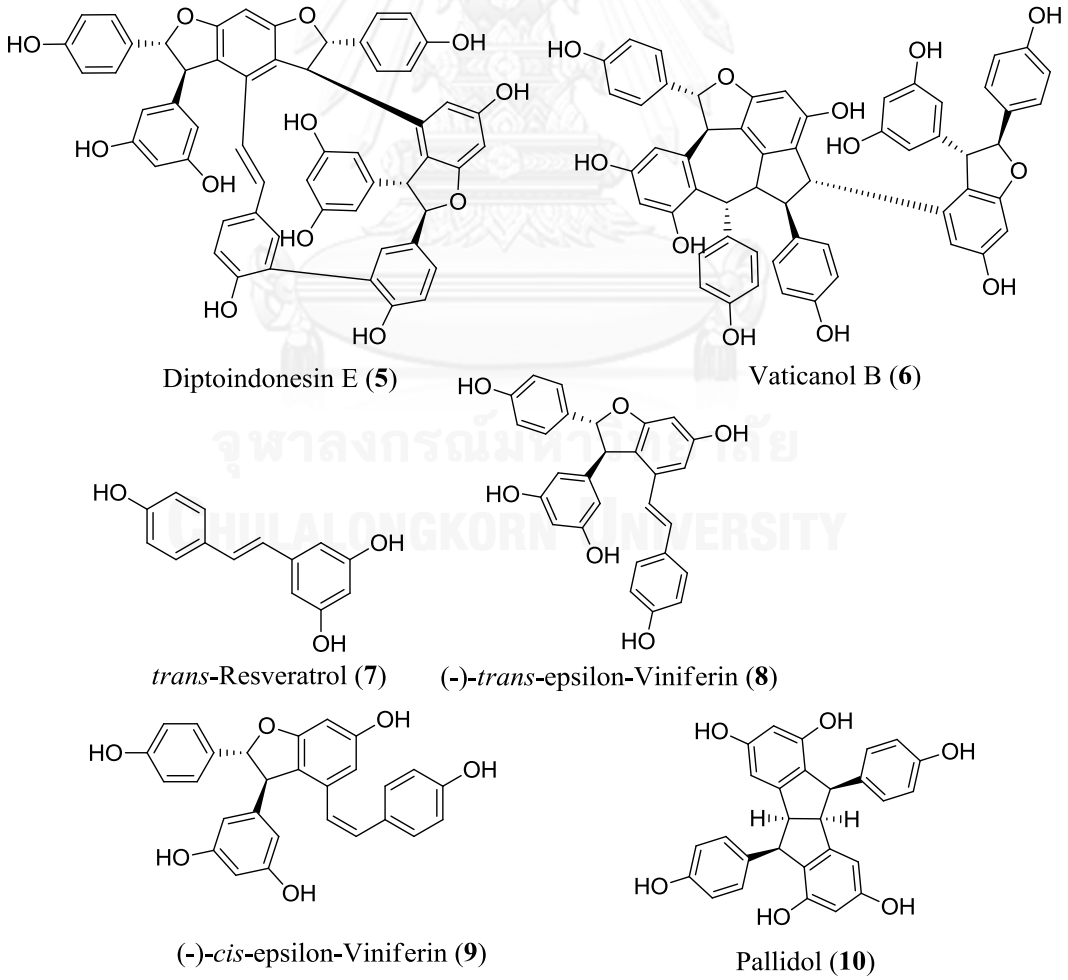

Figure **40** Structures of known stilbenoids from the roots of *D. tuberculatus*.

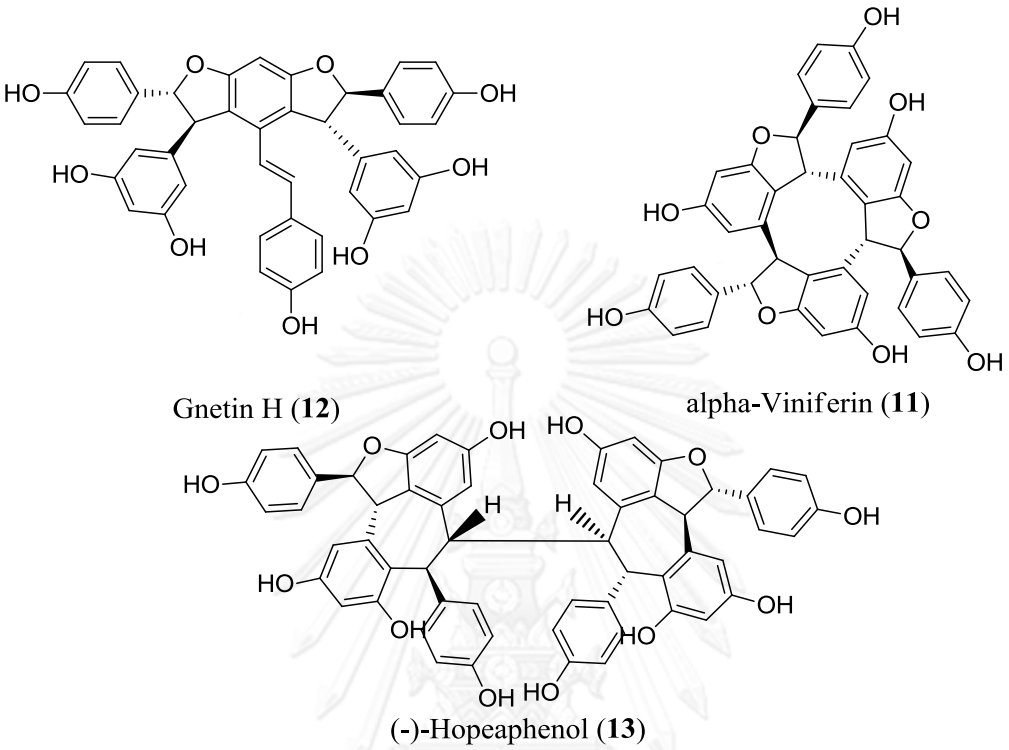

Figure **41** Structures of known stilbenoids from the roots of *D. tuberculatus* (Cont.).

3.3. Lipoxygenase inhibitory activity

For the study of structure-activity relationship, stilbenoids from *G. macrostachyum* and *S. roxburghii* were obtained to evaluate (Figure **42**-**44**). The colorimetric sbLOX-1 inhibitory assay showed that all monomeric stilbenes were inactive at the screening concentration (30μM) (Table **7**). Although *trans*-resveratrol (**7**) is a well-known lipoxygenase inhibitor, certain previous reports gave IC_{50} values for inhibition higher than under our defined conditions. We also found that monomeric stilbenes **16** and **17** were inactive for sbLOX-1 inhibitory activity. Compound **8** was more potent than **9** (P <0.05), which indicated that *trans* configuration exhibited more potent than the *cis* configuration. Compound **8** displayed less inhibitory activity as compared to **18** (P <0.05). It indicated that the position of 2-(4-hydroxyphenyl)ethenyl group affected the inhibitory activity. The inhibitory activity of **18** was significantly higher than **19** and **20** (P <0.05), indicating that an increase in number of methoxyl

groups in the inhibitor gave a reduced sbLOX-1 inhibitory activity. However, the additional methoxyl group substituent in **21** did not affect the inhibitory activity, with the IC_{50} value being comparable to that of **22**. The potency of **25** was significantly higher than its dimeric precursor **18** (P <0.05). Trimeric stilbene **24** was more potent than the dimeric stilbene **23** (P <0.05). Moreover, **26** was significantly more potent than **25** and **18** (P <0.05). The hexameric stilbenes, **1**, was more potent than the tetrameric **5** and **2** (P <0.05). We also found that tetrameric stilbene **6** was more potent than the trimeric stilbene **27** (P <0.05) and tetrameric **4** was more active than the dimeric **10** (P <0.05). However, the inhibitory activity of some oligostilbenes from *D. tuberculatus* did not depend on number of resveratrol monomer as observed for compounds **8** and **12** (P <0.05). Thus, these results allowed us to conclude that an increase in the number of stilbenoid monomers resulted in enhanced inhibitory activities of the Gnetum-type oligostilbenes. Compounds **2** and **5** were less potent than **3** (P <0.05), which the occurrence of biphenyl linkage probably reduced the inhibitory activity.

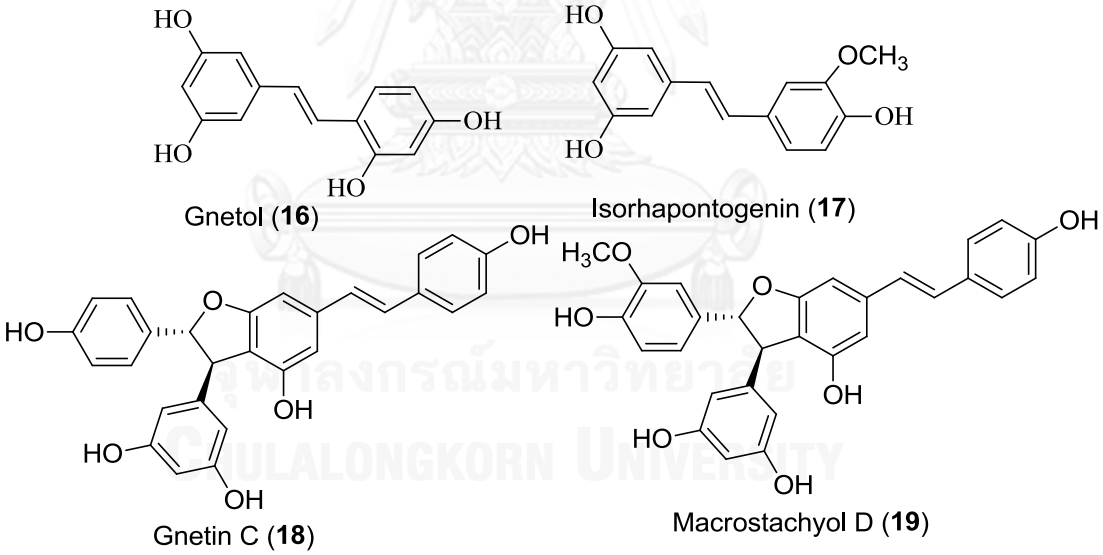

Figure **42** Structure of stilbenoids from *G. macrostachyum*.

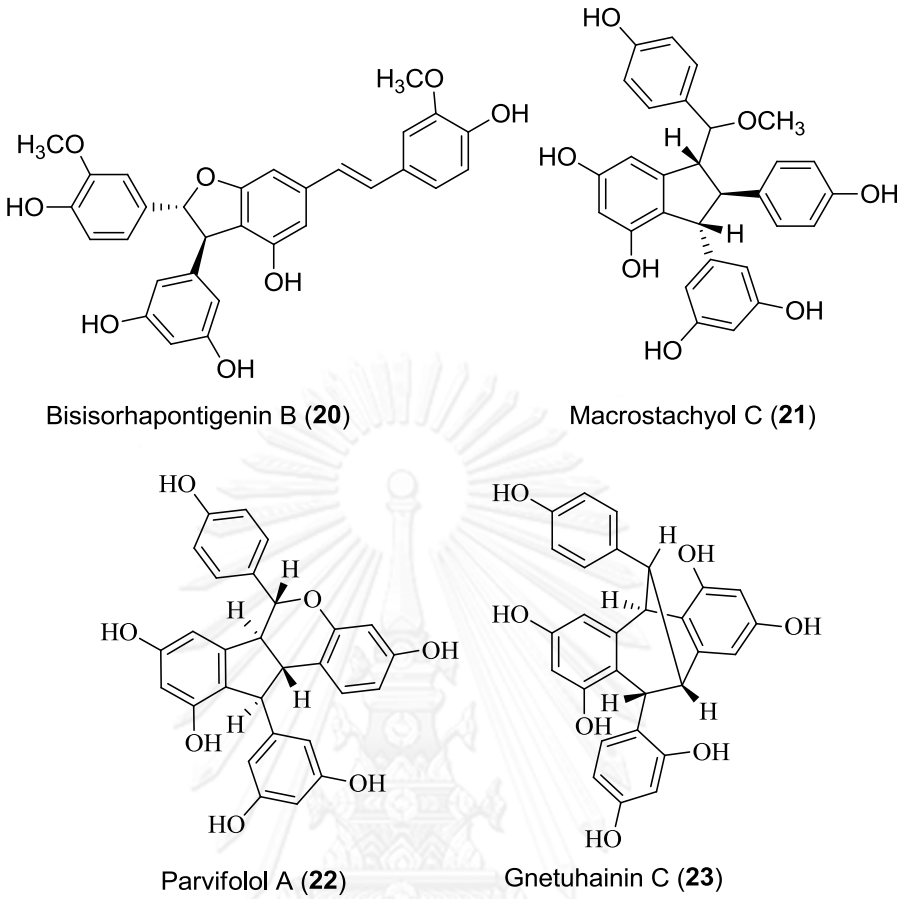

Figure 43 Structure of stilbenoids from *G. macrostachyum* (Cont.).

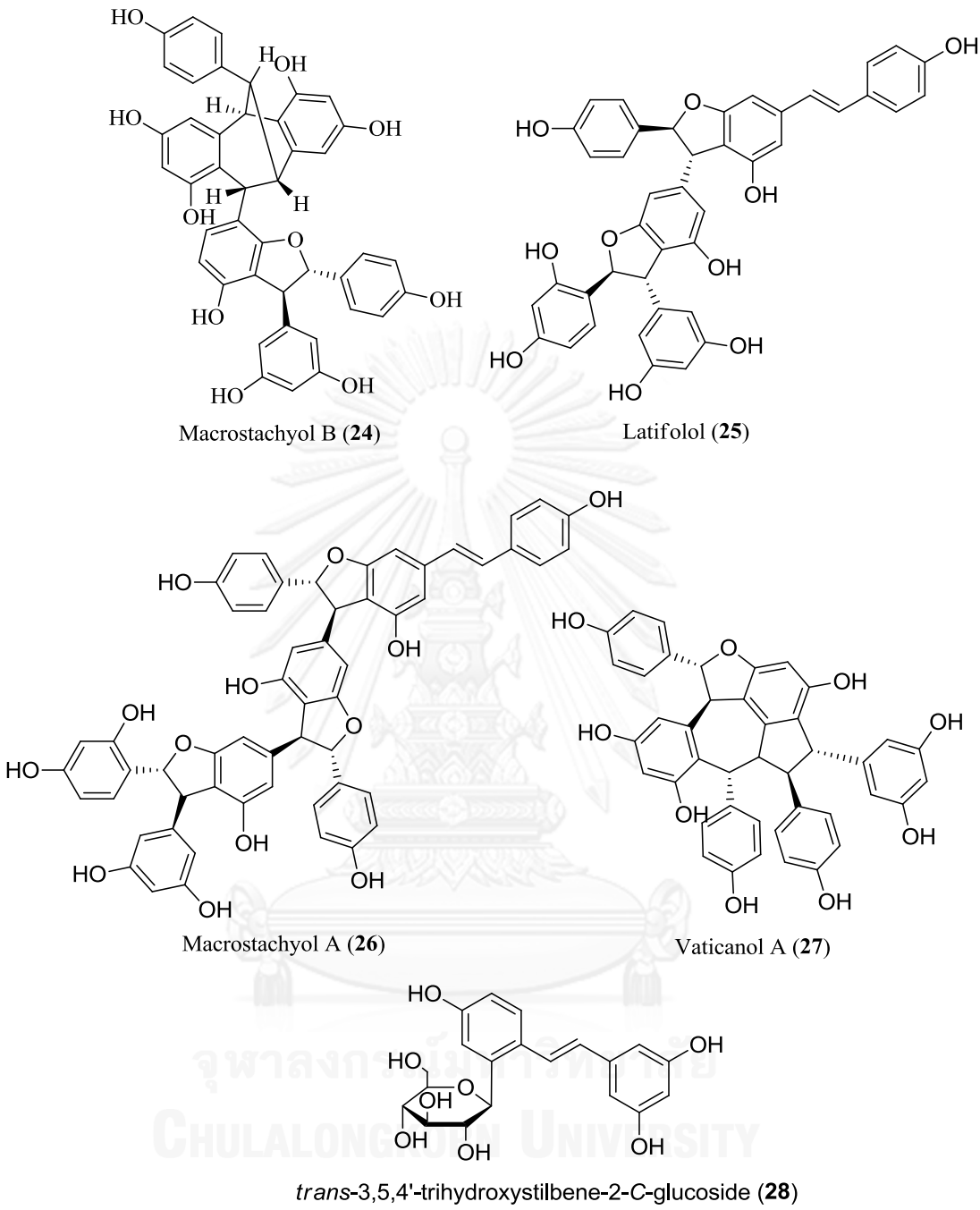

Figure **44** Structure of stilbenoids from *G. macrostachyum* and *S. roxburghii*.

3.4. Antioxidant activities of stilbenoids

Stilbenes are known as potent natural product-derived antioxidants which could possibly interfere with our defined colorimetric sbLOX-1 assays. The principle of the assay involves the quantitative formation of the sbLOX-1-generated hydroperoxide

product, 13(*S*)-hydroperoxy-9(*Z*),11(*E*)-octadecadienoic acid (13-HPOD), which could be retarded due to the antioxidant properties of the oligostilbenes. Therefore, as a more reliable indicator, DPPH and 13-HPOD scavenging assays were utilized to assess the antioxidant properties of the compounds. The results showed that all stilbenoids was inactive to scavenge either stable free radical DPPH, or 13-HPOD at a screening concentration of 30 μM (Table **7**). It was clearly illustrated that the sbLOX-1 inhibitory activity of the active oligostilbenes was not a result of their antioxidant properties.

Table **7** Lipoxygenase inhibitory activity of the oligostilbenes from *D. tuberculatus*, *G. macrostachyum* and *S. roxburghii*.

Cpds	Half Inhibition (IC_{50}; μM)			Cpds	Half Inhibition (IC_{50}; μM)		
	sbLOX-1[a]	13-HPOD[b]	DPPH[c]		sbLOX-1[a]	13-HPOD[b]	DPPH[c]
1	0.15 ± 0.01*	<30	<30	**16**	< 30	< 30	< 30
2	4.55 ± 0.35*	<30	<30	**17**	< 30	< 30	< 30
3	1.14 ± 0.20*	<30	<30	**18**	1.82 ± 0.21*	< 30	< 30
4	3.82 ± 0.56*	<30	<30	**19**	3.55 ± 0.28*	< 30	< 30
5	2.82 ± 0.09*	<30	<30	**20**	5.42 ± 0.60*	< 30	< 30
6	2.23 ± 0.34*	<30	<30	**21**	1.03 ± 0.43*	< 30	< 30
7	<30	<30	<30	**22**	1.07 ± 0.11*	< 30	< 30
8	7.42 ± 0.83*	<30	<30	**23**	11.91 ± 0.90	< 30	< 30
9	15.16 ± 1.96	<30	<30	**24**	0.33 ± 0.11*	< 30	< 30
10	2.92 ± 0.13*	<30	<30	**25**	0.49 ± 0.05*	< 30	< 30
11	3.48 ± 0.03*	<30	<30	**26**	0.14 ± 0.01*	< 30	< 30
12	13.94 ± 0.32	<30	<30	**27**	5.66 ± 0.29*	<30	<30
13	6.24 ± 0.65*	<30	<30	**28**	< 30	<30	<30
14	< 30	<30	<30	NDGA	12.19 ± 0.60	<30	<30
15	< 30	<30	<30				

* $P<0.05$ as compared to NDGA

[a] Data shown as mean±SEM of 7 independent experiments, each experiment was duplicate

[b] Data shown as mean of triplicate experiments

[c] Data shown as mean of duplicate experiments

3.5. Enzyme kinetic studies of selected active stilbenes

The mechanism of action on sbLOX-1 by the most active oligostilbenes, **1**, **3**, **21**, **24**, **25** and **26**, was evaluated. Compound **22** was excluded for enzyme kinetic study due to limit amount of sample. In this study, the Michealis-Menten constant (K_m) of sbLOX-1 was 22 μM, which is similar to that from the literature (Glickman and Klinman 1995).

The double reciprocal Lineweaver-Burk plot of 1/v versus 1/[S] of **1** (Figure **45**A) shows a family of parallel straight line. An increase in **1** concentration coincided with decreased K_m and V_{max} values but the ratio of K_m/V_{max} remained unchanged with concentration. These results indicated that **1** was an uncompetitive inhibitor with an inhibition constant (K_i) of 5.2 nM. The analysis of inhibitory mechanism of **26** (Figure **45**B) on sbLOX-1 showed the same mechanism to **1** except with the extremely low K_i value of 0.8 nM. Thus, **1** and **26** bound sbLOX-1 through an enzyme-substrate complex.

Analysis of the Lineweaver-Burk plots of **3** (Figure **46**A) and **21** (Figure **46**B) and **25** (Figure **46**C) revealed that the value of 1/V increased when concentration of the inhibitor increased, but K_m remained constant. These evidences indicated that the inhibitory mechanisms of **3** and **21** and **25** were noncompetitive, with K_i values of 113.2, 11.2 and 71.4 nM, respectively. Thus, **3** and **21** and **25** could bind either an enzyme or enzyme-substrate complex with equal affinity.

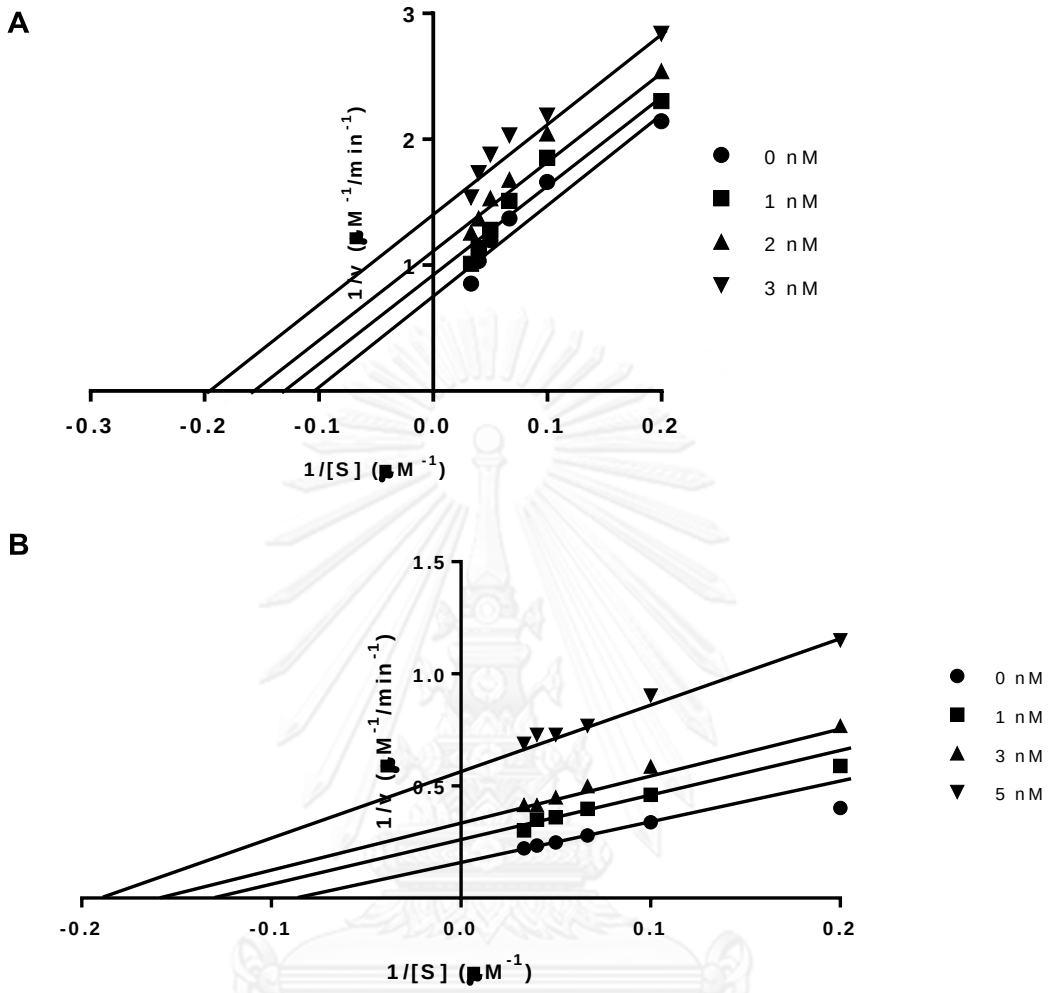

Figure 45 Lineweaver-Burk plot of 1 and 26.

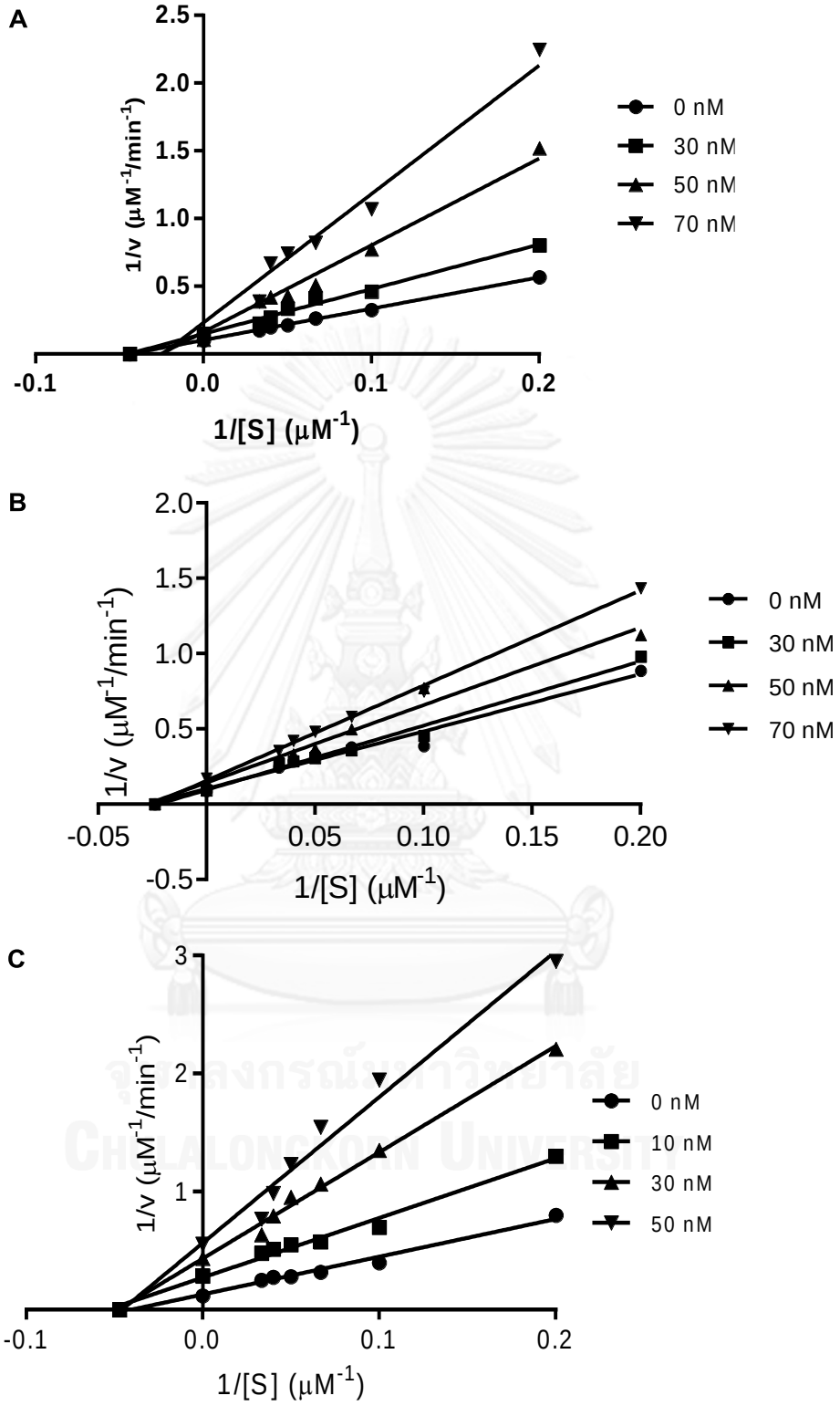

Figure 46 Lineweaver-Burk plot of 3, 21 and 25.

The double reciprocal plot of 1/v versus 1/[S] for **24** (Figure **47**) gave straight lines that did not intersect either X-axis or Y-axis. In addition, the value of 1/v increased when concentration of inhibitor increased, but the value of K_m was not affected. This behavior demonstrated that **24** was a mixed-competitive inhibitor with inhibition constants (K_i and K_i') of 13.8 and 56.7 nM. Compound **24** was thus able to bind at a site distinct from the active site, but it bound to either sbLOX-1 or the sbLOX-1-LA complex. However, the binding affinities of the inhibitor with each of the two separated sites are not equal.

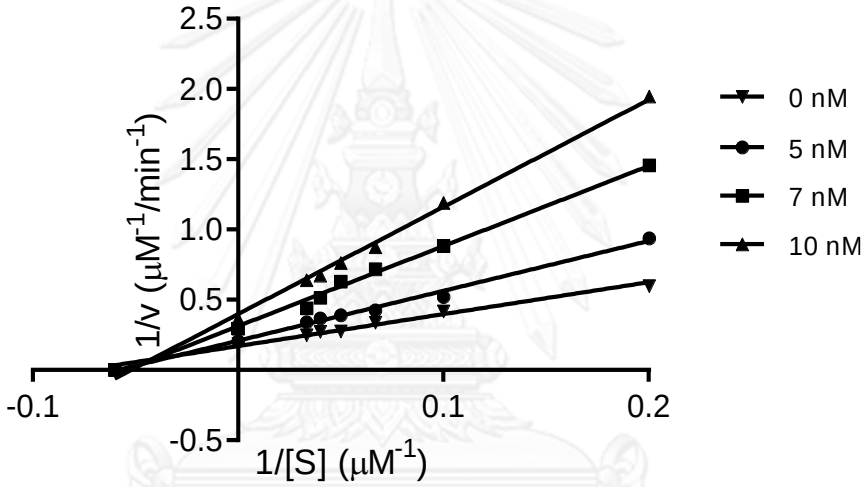

Figure **47** Lineweaver-Burk plot of **24**.

3.6. Iron redox interferences

Iron is an essential cofactor of LOX in dioxygenation, which is present in both the resting (Fe^{2+}-sbLOX-1) and active (Fe^{3+}-sbLOX-1) complexes. Thus, Fe^{3+} reduction at the active site is relevant to enzymatic inhibition. Compounds **1**, **3**, **21**, **24**, **25** and **26** were unable to oxidize Fe^{2+} in the ratio of 1:1 equivalent. By contrast, these compounds were able to reduce Fe^{3+}, with the percentages of reduction being 4.67, 2.63, 1.07, 2.56, 1.31 and 3.35% for **1**, **3**, **21**, **24**, **25** and **26**, respectively (Table **8**). The standard NDGA reduced Fe^{3+} completely at the ratio of 1:1 equivalents of NDGA to compound. It was found that the reducing property of the active oligostilbenes was

dependent on the number of hydroxyl groups; therefore, **1** showed stronger ferric ion reduction ability than **26**, **3**, **24**, **25** and **21**.

Spectroscopic studies of the Fe^{3+}-bound sbLOX-1 complex afforded different results. To clarify the effects of **1**, **3**, **21**, **24**, **25** and **26** on the yellow enzyme, active Fe^{3+}-sbLOX-1, the UV spectrophotometry and visible CD spectroscopy were utilized. The characteristics of both native and active sbLOX-1 was in agreement with a previous report (Spaapen, Veldink *et al*. 1979). Compounds **1**, **3**, **21**, **24**, **25** and **26** reduced only 1.65±0.51, 0.97±0.45, 0.51±0.05, 0.91±0.11, 0.73±0.31 and 1.17±0.23% of yellow enzyme levels, which is not statistically significant (Figure **48**). This result also agreed with the visible CD spectrum, with the positive Cotton Effect evident at 420 nm not being significantly perturbed by the incubation of Fe^{3+} sbLOX-1 with **1**, **3**, **21**, **24**, **25** and **26**. The result also illustrated that oligostilbenes did not alter the molecular structure of active Fe^{3+}-sbLOX-1, as observed in the visible CD spectra (Figure **49**). Although the active oligostilbenes were able to reduce Fe^{3+} in the free-Fe^{3+} model, the inhibitory effects of the active oligostilbenes did not result from the redox interference of Fe^{3+}-bound sbLOX-1 as indicated by UV spectrophotometry and visible CD spectroscopy. This indicated that the active oligostilbenes could not enter the enzyme catalytic site, and subsequently reduce Fe^{3+}. Several small molecule LOX inhibitors (3,4-dihydroxybenzonitrile, genistein, daidzein, and NDGA) deactivate lipoxygenases through penetration of the catalytic site and subsequent Fe^{3+} reduction (Nelson, Brennan *et al*. 1995, Mahesha, Singh *et al*. 2007). While the active oligostilbenes had relatively higher molecular weights than these inhibitors, they were ineffective at inhibiting LOX through Fe^{3+} reduction.

Table **8** Fe^{3+} and Fe^{3+}-sbLOX-1 reduction activity of the active oligostilbenes.

Compounds	Fe^{3+} Reduction (%)[a]	Fe^{3+}-sbLOX-1 reduction (Spectrophotometric assay; %)[b]
1	4.67	1.65±0.51
3	2.63	0.97±0.45
21	1.07	0.51±0.05
24	2.56	0.91±0.11
25	1.31	0.73±0.31
26	3.35	1.17±0.23
NDGA	100	ND[c]

[a] Data shown as mean of duplicate experiments

[b] Data shown as mean±SD of triplicate experiments

[c] ND not determine

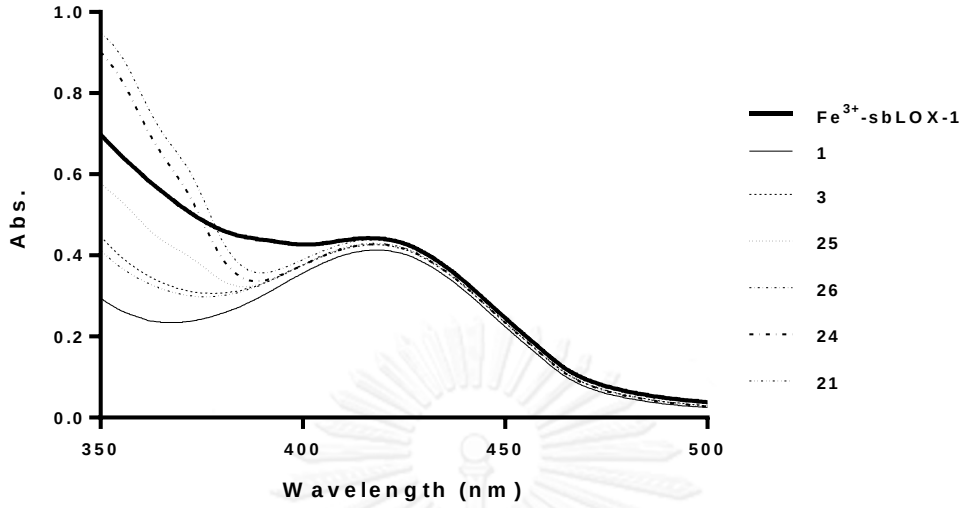

Figure 48 The UV-vis spectra of ferric reduction activities of oligostilbenes on Fe^{3+}-sbLOX-1.

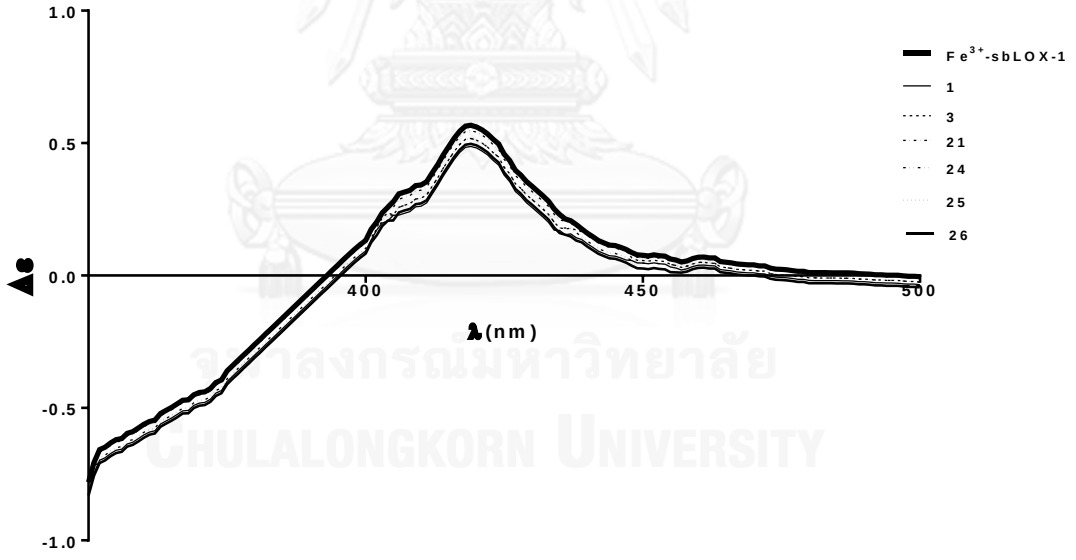

Figure 49 **Visible CD spectra of the effect of oligostilbenes on Fe^{3+}-sbLOX-1.**

Chapter IV

Conclusion

In conclusion, the isolation of the acetone crude extract from the roots of *Dipterocarpus tuberculatus* yielded fifteen stilbenoids. They were four new oligostilbenoids, dipterostilbenes A-D (**1**-**4**) and two stilbenoid glycosides, dipterostilbenosides A and B (**14**-**15**), were isolated together with nine known stilbenoids, diptoindonesin E (**5**), vaticanol B (**6**), trans-resveratrol (**7**), *trans*-***ε***-(-)-viniferin (**8**), *cis*-***ε***-(-)-viniferin (**9**), pallidol (**10**), ***α***-viniferin (**11**), gnetin H (**12**) and (-)-hopeaphenol (**13**). The chemical structures of all isolated compounds were characterized by means of NMR and MS experiments as well as comparison with the previous reports.

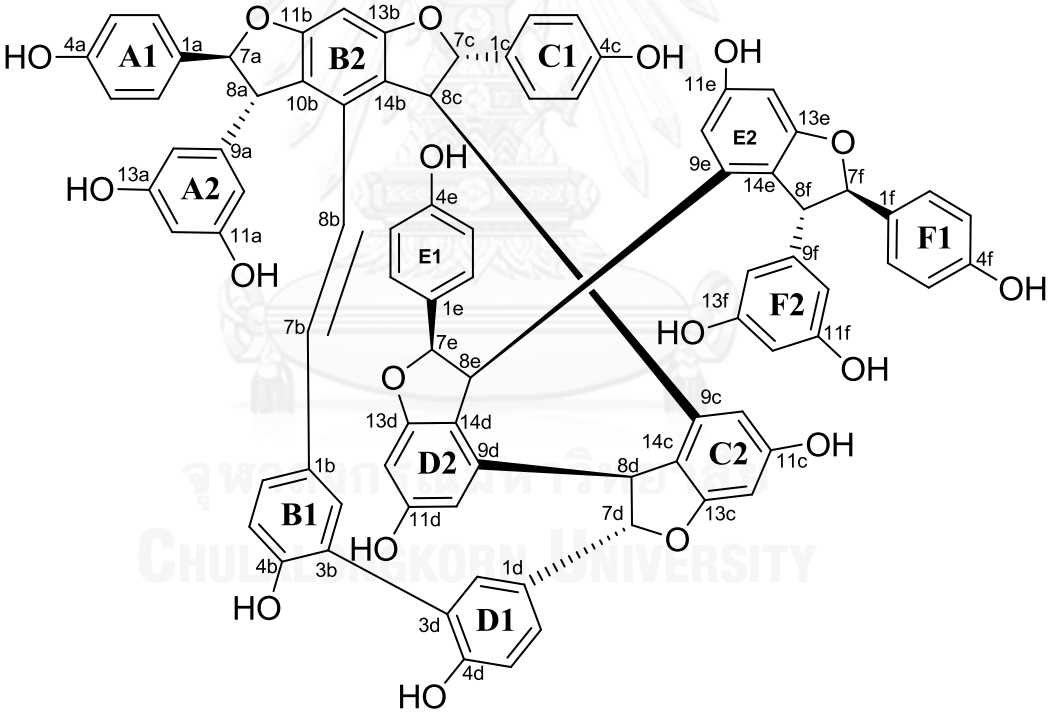

Dipterostilbene A (**1**, New Compound)

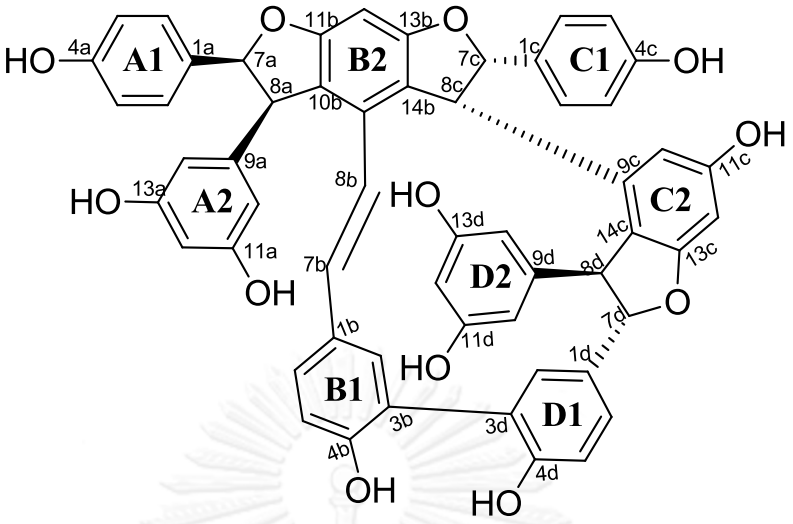

Dipterostilbene B (**2**, New Compound)

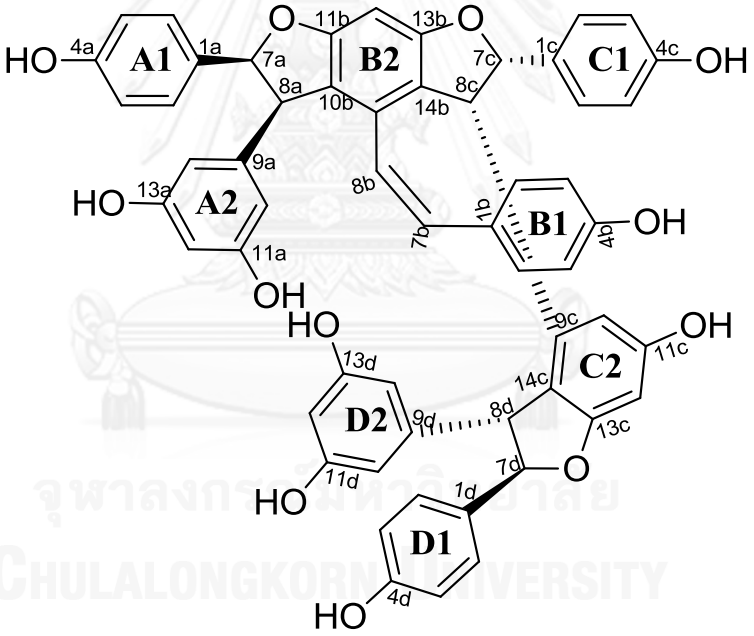

Dipterostilbene C (**3**, New Compound)

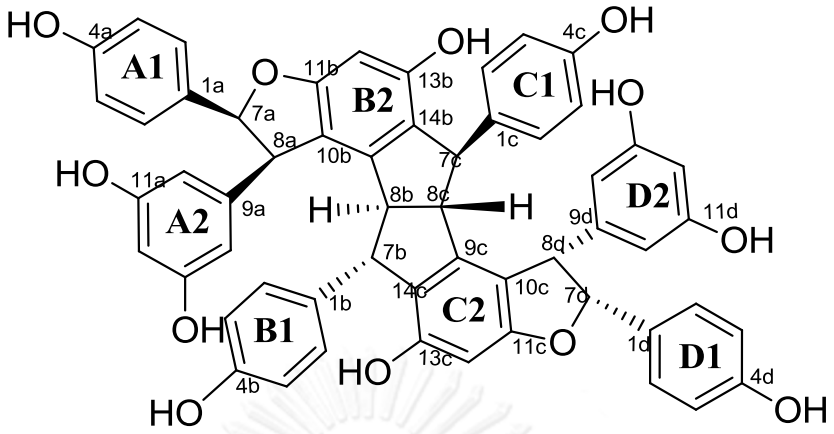

Dipterostilbene D (**4**, New Compound)

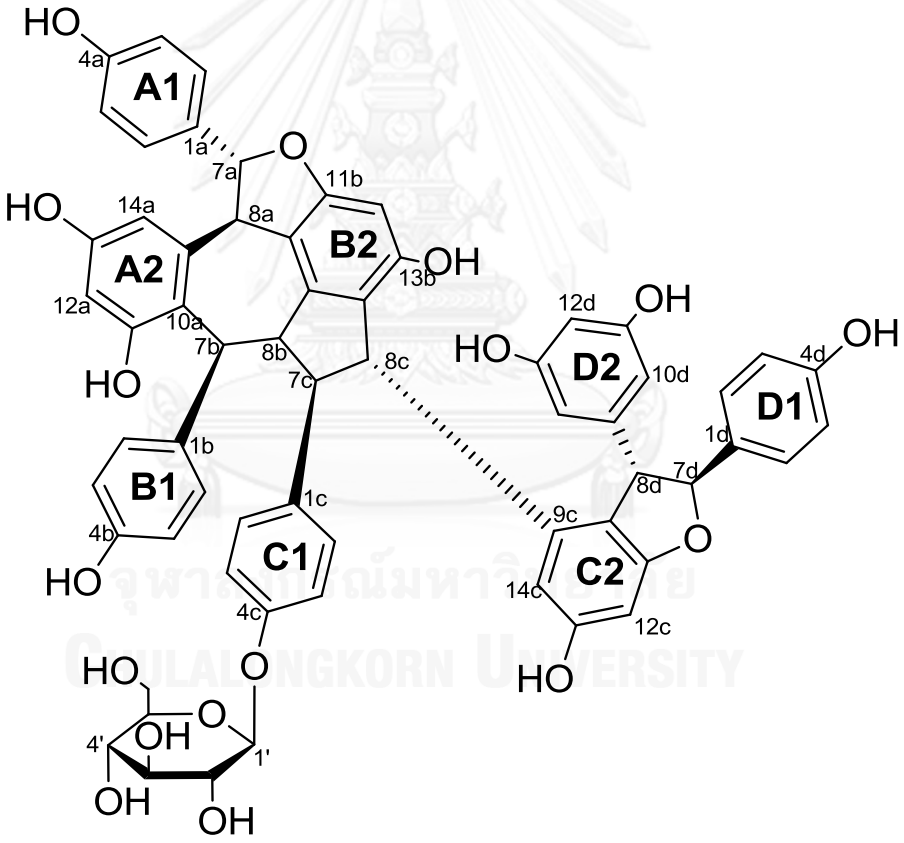

Dipterostilbenoside **A** (**14**, New Compound)

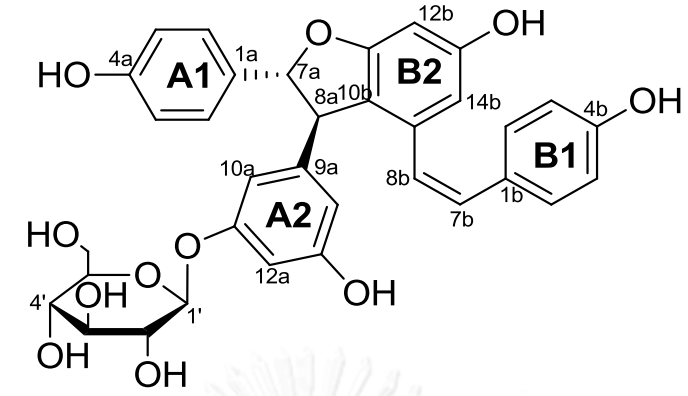

Dipterostilbenoside B (**15**, New Compound)

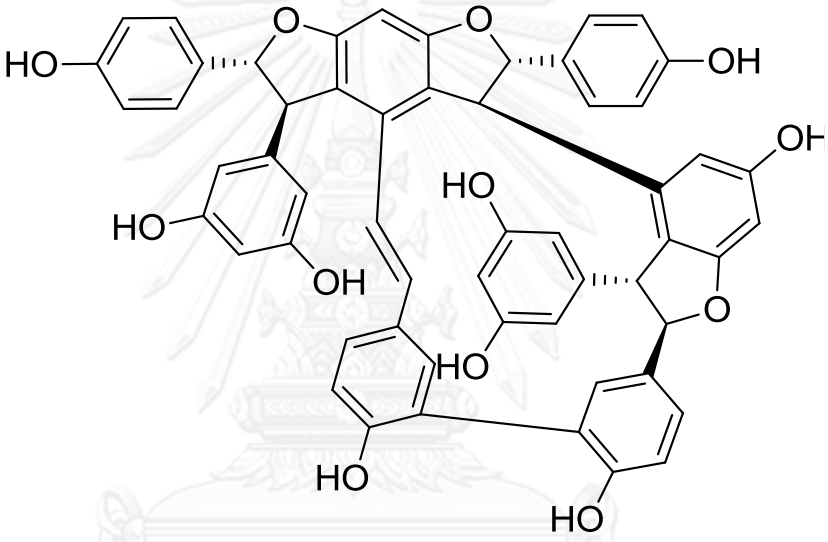

Diptoindonesin E (**5**)

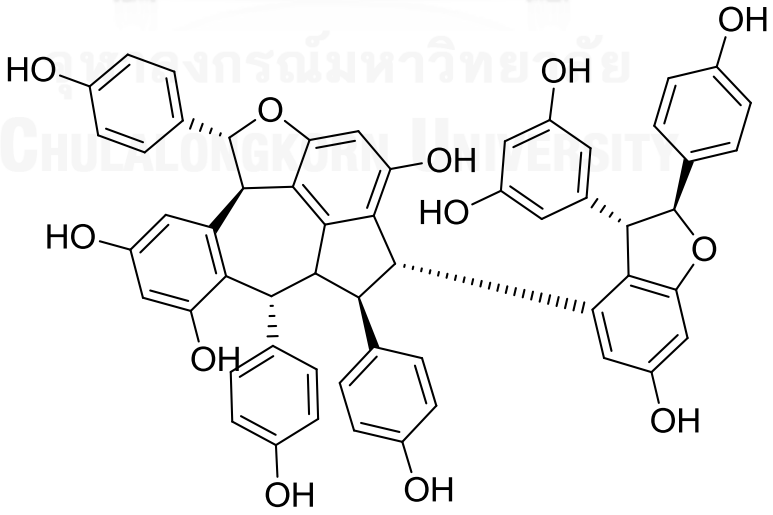

Vaticanl B (**6**)

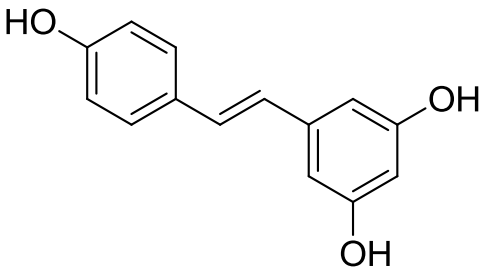

trans-Resveratrol (**7**)

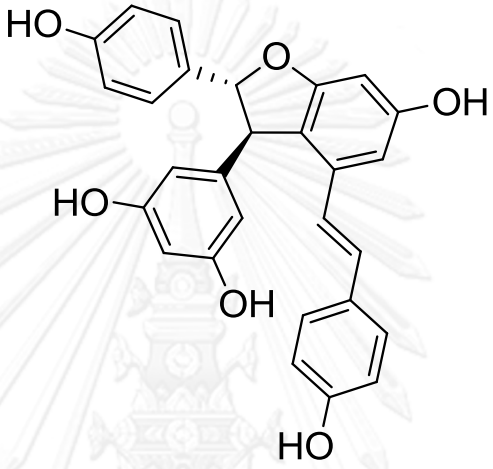

(-)-*trans*-epsilon-Viniferin (**8**)

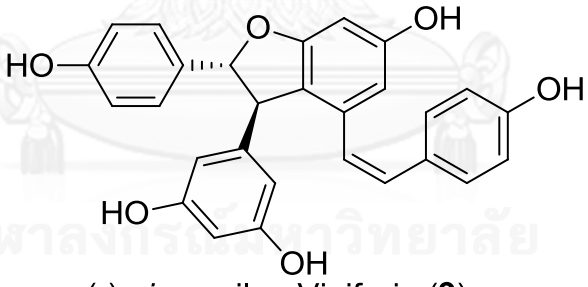

(-)-*cis*-epsilon-Viniferin (**9**)

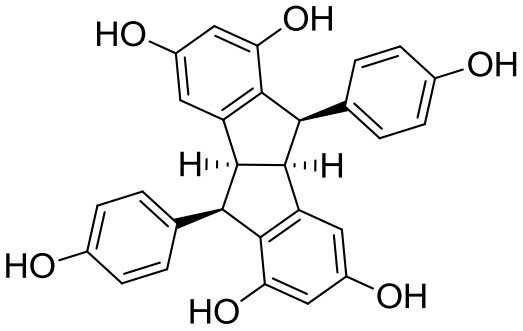

Pallidol (**10**)

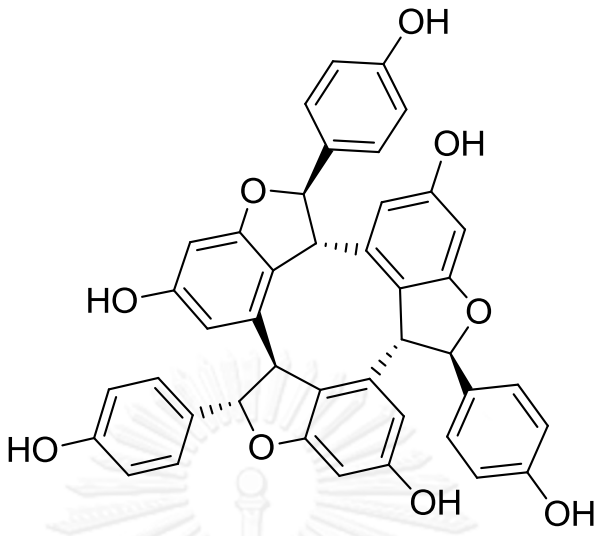

alpha-Viniferin (**11**)

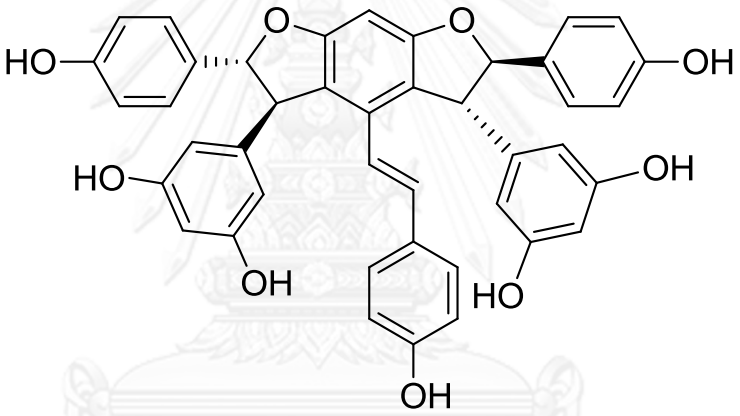

Gnetin H (**12**)

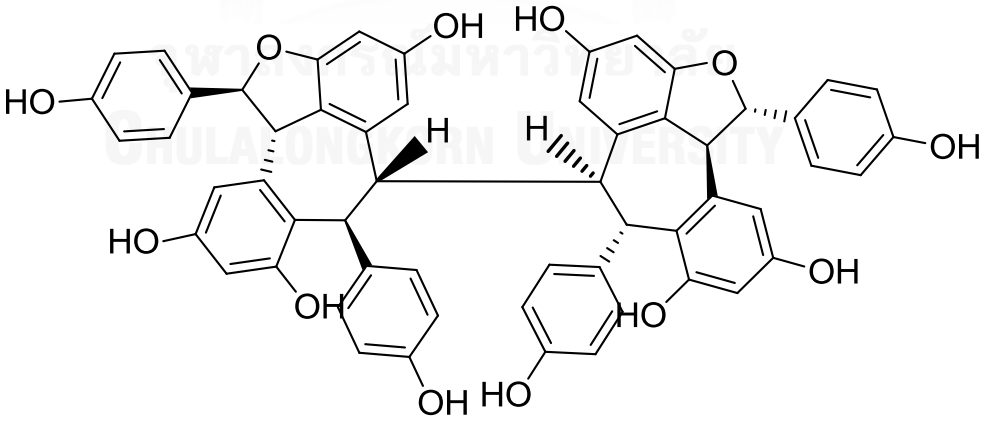

(-)-Hopeaphenol (**13**)

The isolated stilbenoids from *D. tuberculatus* were obtained to evaluate lipoxygenase inhibitory activity together with stilbenoids for the structure-activity relationship study, eleven stilbenes from *Gnetum macrostachyum* and two stilbenes from *Shorea roxburghii* were obtained evaluated sbLOX-1 inhibitory activity. Monomeric stilbenoids and stilbenoid glycosides were inactive to inhibit sbLOX-1. The inhibitory activities of stilbenoids from *G. macrostachyum* were enhanced with the increasing number of stilbenoid monomer. However, the potency of Shorea- and Dipterocarpus-type stilbenoids correlated with the type of oligostilbenes. The results of colorimetric sbLOX-1 screening assay showed that **1**, **3**, **21**, **24**, **25** and **26** were the most active oligostilbenes. Thus, these oligostilbenes were selected to study mode of inhibition. According to the enzyme kinetic study, compounds **1** and **26** were uncompetitive inhibitors with the extremely low inhibition constant of (K_i) 5.2 and 0.8 nM, respectively. Compounds **3**, **21** and **25** inhibited sbLOX-1 through non-competitive mechanism with the K_i values of 113.2, 11.3 and 71.4 nM, respectively. Compound **24** were mixed-competitive inhibitor with the K_i and K_i' values of 13.8 and 56.7 nM. The inhibition mechanisms of these active oligostilbenes did not correlate with type of oligostilbenes. Moreover, the inhibitory activity of **1**, **3, 21**, **24**, **25** and **26** was not resulted from the antioxidant property as demonstrated by DPPH and 13-HPOD scavenging assays. Although these compounds exhibited Fe^{3+} reducing property, they had no effect in Fe^{3+}-bound sbLOX-1 model as indicated by UV spectrophotometric and CD spectroscopic studies. Thus, the inhibitory mechanisms of these active oligostilbenoids were resulted from the enzyme inhibition without iron redox interferences or alteration of the active enzyme structure.

REFERENCES

Adams, M., et al. (2005). "Inhibition of leukotriene biosynthesis by stilbenoids from Stemona species." J Nat Prod **68**(1): 83-85.

Avis, I. M., et al. (1996). "Growth control of lung cancer by interruption of 5-lipoxygenase-mediated growth factor signaling." The Journal of Clinical Investigation **97**(3): 806-813.

Berliner, J. A. and A. D. Watson (2005). "A role for oxidized phospholipids in atherosclerosis." New England Journal of Medicine **353**(1): 9-11.

Berry, H., et al. (1998). "Oxygen concentration determines regiospecificity in soybean lipoxygenase-1 reaction via a branched kinetic scheme." Journal of Biological Chemistry **273**(5): 2769-2776.

Braunschweig, J., et al. (2012). "Reevaluation of colorimetric iron determination methods commonly used in geomicrobiology." Journal of Microbiological Methods **89**(1): 41-48.

Buczynski, M. W., et al. (2009). "Thematic review series: Proteomics. An integrated omics analysis of eicosanoid biology." Journal of Lipid Research **50**(6): 1015-1038.

Burrall, B. A., et al. (1988). "Enzymatic properties of the 15-lipoxygenase of human cultured keratinocytes." Journal of Investigative Dermatology **91**(4): 294-297.

Catalano, A. and A. Procopio (2005). "New aspects on the role of lipoxygenases in cancer progression." Histol Histopathol **20**(3): 969-975.

Choi, C. W., et al. (2010). "A new glycoside of resveratrol dimer from stem bark of *Vitis vinifera*." Bulletin of the Korean Chemical Society **31**(11): 3448-3450.

Choi, O., et al. (2011). "Biosynthesis of plant-specific phenylpropanoids by construction of an artificial biosynthetic pathway in *Escherichia coli*." Journal of Industrial Microbiology and Biotechnology **38**(10): 1657-1665.

Chong, J., et al. (2009). "Metabolism and roles of stilbenes in plants." Plant Science **177**(3): 143-155.

Cipollone, F., et al. (2005). "Association between 5-lipoxygenase expression and plaque instability in humans." Arteriosclerosis, Thrombosis, and Vascular Biology **25**(8): 1665-1670.

De Caterina, R. and A. Zampolli (2004). "From asthma to atherosclerosis — 5-lipoxygenase, leukotrienes, and inflammation." New England Journal of Medicine **350**(1): 4-7.

Deschamps, J. D., et al. (2006). "Baicalein is a potent in vitro inhibitor against both reticulocyte 15-human and platelet 12-human lipoxygenases." Bioorg Med Chem **14**(12): 4295-4301.

Drazen, J. M., et al. (1999). "Treatment of asthma with drugs modifying the leukotriene pathway." New England Journal of Medicine **340**(3): 197-206.

Eliel, E. L., et al. (1994). Stereochemistry of organic compounds. New York, Wiley.

Fang, L., et al. (2007). "Three new bibenzyl derivatives from the chinese liverwort *Marchantia polymorpha*." Helvetica Chimica Acta **90**(4): 748-752.

Funk, C. D., et al. (2002). "Lipoxygenase genes and their targeted disruption." Prostaglandins & Other Lipid Mediators **68–69**(0): 303-312.

Gao, X., et al. (1995). "Elevated 12-lipoxygenase mRNA expression correlates with advanced stage and poor differentiation of human prostate cancer." Urology **46**(2): 227-237.

Gay, C., et al. (1999). "Hydroperoxide assay with the ferric-xylenol orange complex." Anal Biochem **273**(2): 149-155.

Ghosh, J. and C. E. Myers (1997). "Arachidonic acid stimulates prostate cancer cell growth: Critical role of 5-lipoxygenase." Biochemical and Biophysical Research Communications **235**(2): 418-423.

Ghosh, J. and C. E. Myers (1998). "Inhibition of arachidonate 5-lipoxygenase triggers massive apoptosis in human prostate cancer cells." Proceedings of the National Academy of Sciences **95**(22): 13182-13187.

Gilbert, N. C., et al. (2011). "The structure of human 5-lipoxygenase." Science **331**(6014): 217-219.

Glickman, M. H. and J. P. Klinman (1995). "Nature of rate-limiting steps in the soybean lipoxygenase-1 reaction." Biochemistry **34**(43): 14077-14092.

Ha do, T., et al. (2009). "Antioxidant and lipoxygenase inhibitory activity of oligostilbenes from the leaf and stem of *Vitis amurensis*." J Ethnopharmacol **125**(2): 304-309.

Hayes, W. A., et al. (2011). "Determination of the molar extinction coefficient for the ferric reducing/antioxidant power assay." Anal Biochem **416**(2): 202-205.

Huang, K.-S., et al. (2001). "Anti-inflammatory tetramers of resveratrol from the roots of *Vitis amurensis* and the conformations of the seven-membered ring in some oligostilbenes." Phytochemistry **58**(2): 357-362.

Ito, T., et al. (2009). "Two novel resveratrol trimers from *Dipterocarpus grandiflorus*." Helvetica Chimica Acta **92**(6): 1203-1216.

Ito, T., et al. (2004). "Two new resveratrol (=5-[(1e)-2-(4-hydroxyphenyl)ethenyl]benzene-1,3-diol) tetramers with a tetrahydrofuran ring from *Dipterocarpus grandiflorus*." Helvetica Chimica Acta **87**(2): 479-495.

Ito, T., et al. (2001). "A novel bridged stilbenoid trimer and four highly condensed stilbenoid oligomers in *Vatica rassak*." Tetrahedron **57**(34): 7309-7321.

Ivanov, I., et al. (2010). "Molecular enzymology of lipoxygenases." Archives of Biochemistry and Biophysics **503**(2): 161-174.

Kuhn, H. and B. J. Thiele (1999). "The diversity of the lipoxygenase family. Many sequence data but little information on biological significance." FEBS Lett **449**(1): 7-11.

Kunz, S. and H. Becker (1994). "Bibenzyl derivatives from the liverwort *Ricciocarpos natans*." Phytochemistry **36**(3): 675-677.

Landa, P., et al. (2013). "Inhibition of in vitro leukotriene B4 biosynthesis in human neutrophil granulocytes and docking studies of natural quinones." Nat Prod Commun **8**(1): 105-108.

Langcake, P. and R. J. Pryce (1977). "A new class of phytoalexins from grapevines." Experientia **33**(2): 151-152.

Lehninger, A. L., et al. (2013). Lehninger principles of biochemistry. New York, W.H. Freeman.

Li, W., et al. (1998). "Flexuosol A, a new tetrastilbene from *Vitis flexuosa*." J Nat Prod **61**(5): 646-647.

Lin, M. and C.-S. Yao (2006). Natural oligostilbenes. Studies in Natural Products Chemistry. R. Atta-ur, Elsevier. **Volume 33, Part M:** 601-644.

Maccarrone, M., et al. (2001). "Lipoxygenases and their involvement in programmed cell death." Cell Death Differ **8**(8): 776-784.

Mahesha, H. G., et al. (2007). "Inhibition of lipoxygenase by soy isoflavones: Evidence of isoflavones as redox inhibitors." Archives of Biochemistry and Biophysics **461**(2): 176-185.

Morikawa, T., et al. (2012). "Antidiabetogenic oligostilbenoids and 3-ethyl-4-phenyl-3,4-dihydroisocoumarins from the bark of *Shorea roxburghii*." Bioorganic and Medicinal Chemistry **20**(2): 832-840.

Muhtadi, et al. (2006). "Cytotoxic resveratrol oligomers from the tree bark of *Dipterocarpus hasseltii*." Fitoterapia **77**(7–8): 550-555.

Nelson, M. J., et al. (1995). "Structure and kinetics of formation of catechol complexes of ferric soybean lipoxygenase-1." Biochemistry **34**(46): 15219-15229.

Nelson, M. J., et al. (1990). "Enzyme-bound pentadienyl and peroxyl radicals in purple lipoxygenase." Biochemistry **29**(29): 6897-6903.

Odukoya, O. A., et al. (1999). "Lipoxygenase inhibitors in the seeds of *Aframomum danielli* K. Schum (Zingiberaceae)." Phytomedicine **6**(4): 251-256.

Ohyama, M., et al. (1998). "Phenolic compounds isolated from the roots of *Sophora stenophylla*." CHEMICAL & PHARMACEUTICAL BULLETIN **46**(4): 663-668.

Oshima, Y. and Y. Ueno (1993). "Ampelopsins E, F, H and *cis*-ampelopsin E, oligostilbenes from *Ampelopsis brevipedunculata* var. Hancei roots." Phytochemistry **33**(1): 179-182.

Sadeghian, H., et al. (2008). "Design and synthesis of eugenol derivatives, as potent 15-lipoxygenase inhibitors." Bioorg Med Chem **16**(2): 890-901.

Sala, A., et al. (2010). "Transcellular biosynthesis of eicosanoids." Pharmacological Reports **62**(3): 503-510.

Seo, E.-K., et al. (1999). "Resveratrol tetramers from *Vatica diospyroides*." The Journal of Organic Chemistry **64**(19): 6976-6983.

Shureiqi, I. and S. M. Lippman (2001). "Lipoxygenase modulation to reverse carcinogenesis." Cancer Res **61**(17): 6307-6312.

Sircar, J. C., et al. (1983). "Soybean lipoxygenase inhibition by nonsteroidal antiinflammatory drugs." Prostaglandins **25**(3): 393-396.

Sotheeswaran, S. and V. Pasupathy (1993). "Distribution of resveratrol oligomers in plants." Phytochemistry **32**(5): 1083-1092.

Spaapen, L. J. M., et al. (1979). "Circular dichroism of lipoxygenase-1 from soybeans." Biochimica et Biophysica Acta (BBA) - Lipids and Lipid Metabolism **574**(2): 301-311.

Sparrow, C. P., et al. (1989). "A macrophage receptor that recognizes oxidized low density lipoprotein but not acetylated low density lipoprotein." Journal of Biological Chemistry **264**(5): 2599-2604.

Takaya, Y., et al. (2002). "Biogenetic reactions on stilbenetetramers from Vitaceaeous plants." Tetrahedron **58**(45): 9265-9271.

Tanaka, T., et al. (2000). "Stilbenoids in the stem bark of *Hopea parviflora*." Phytochemistry **53**(8): 1015-1019.

Tanaka, T., et al. (2000). "Oligostilbenoids in stem bark of *Vatica rassak*." Phytochemistry **54**(1): 63-69.

Timar, J., et al. (2000). "Expression, subcellular localization and putative function of platelet-type 12-lipoxygenase in human prostate cancer cell lines of different metastatic potential." International Journal of Cancer **87**(1): 37-43.

Tome-Carneiro, J., et al. (2013). "Resveratrol and clinical trials: The crossroad from in vitro studies to human evidence." Curr Pharm Des **19**(34): 6064-6093.

Toyota, M., et al. (1994). "Bibenzyl cannabinoid and bisbibenzyl derivative from the liverwort *Radula perrottetii*." Phytochemistry **37**(3): 859-862.

Udomchotphruet, S., et al. (2012). "Xanthones from the stems of *Cratoxylum cochinchinense*." Phytochemistry **73**(1): 148-151.

Waslidge, N. B. and D. J. Hayes (1995). "A colorimetric method for the determination of lipoxygenase activity suitable for use in a high throughput assay format." Anal Biochem **231**(2): 354-358.

Woody, R. W. (1995). "Circular dichroism." Methods Enzymol **246**: 34-71.

Wu, J. M. and T.-c. Hsieh (2011). "Resveratrol: A cardioprotective substance." Annals of the New York Academy of Sciences **1215**(1): 16-21.

Yamada, M., et al. (2006). "Stilbenoids of *Kobresia nepalensis* (Cyperaceae) exhibiting DNA topoisomerase II inhibition." Phytochemistry **67**(3): 307-313.

ผู้พัฒนพงศ์, ล. and ธ. วงศ์ประเสริฐ์ (2530). สมุนไพรไทยตอนที่ 5. กรุงเทพฯ, ฝ่ายพฤกษศาสตร์ป่าไม้ กองบำรุง กรมป่าไม้.

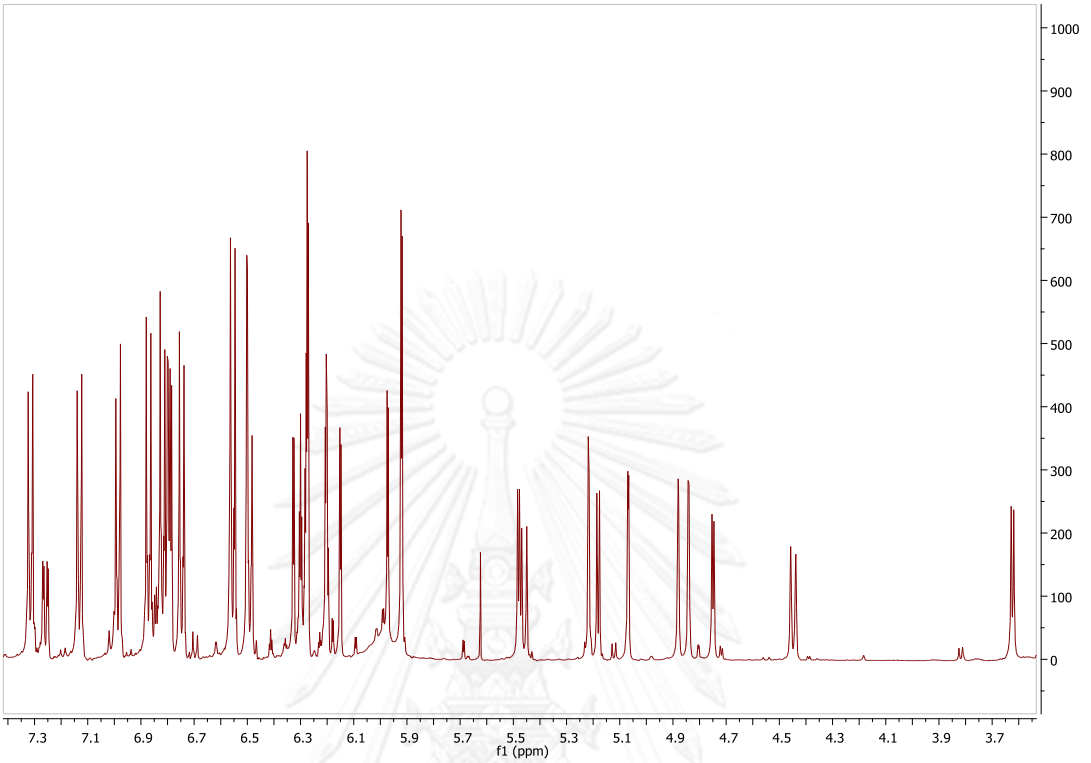

Figure **50** ^{1}H-NMR spectrum of **1** in CD_3COCD_3.

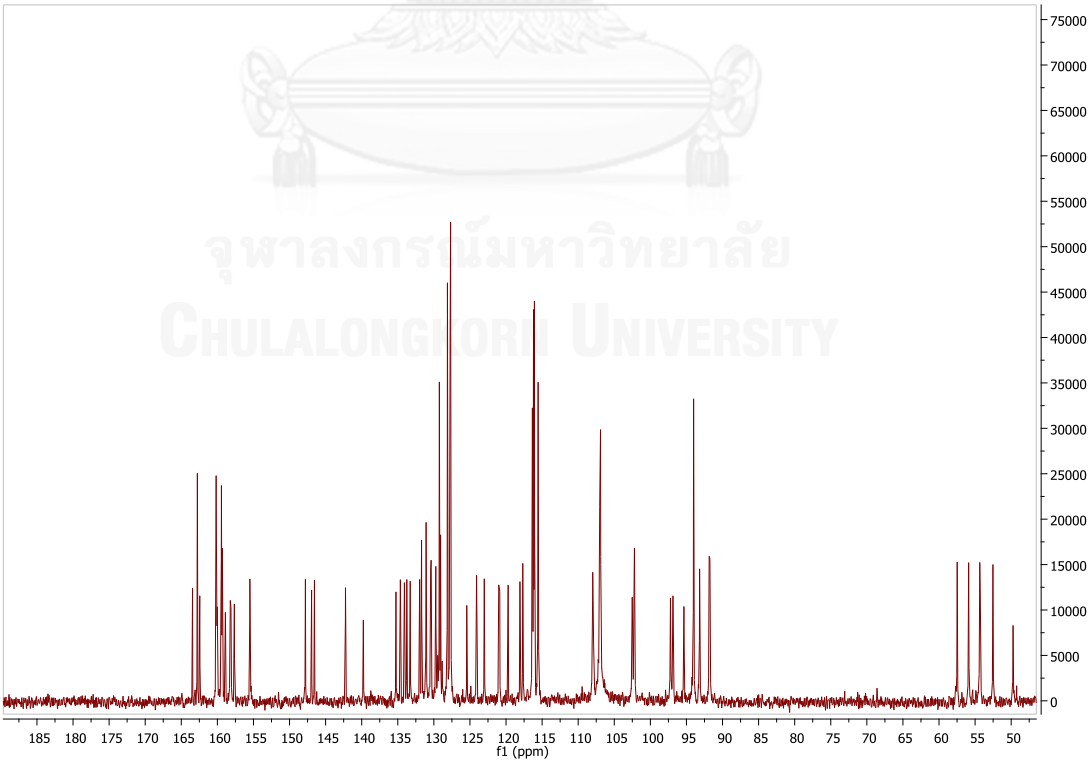

Figure **51** ^{13}C-NMR spectrum of **1** in CD_3COCD_3.

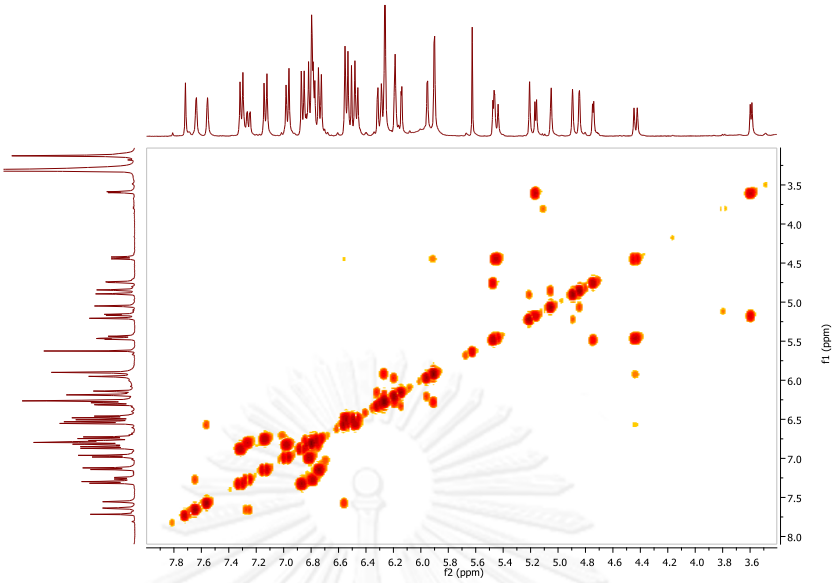

Figure **52** COSY spectrum of **1** in CD_3COCD_3.

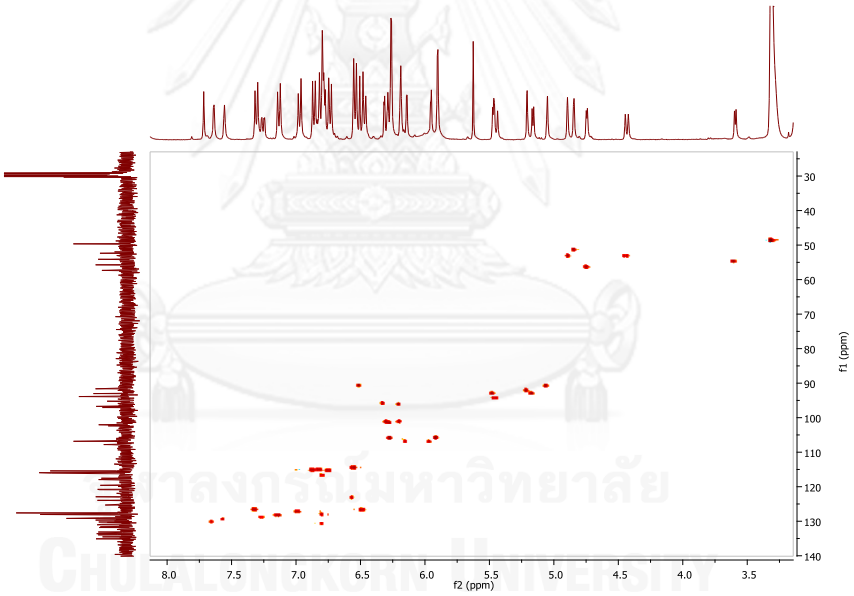

Figure **53** HSQC spectrum of **1** in CD_3COCD_3.

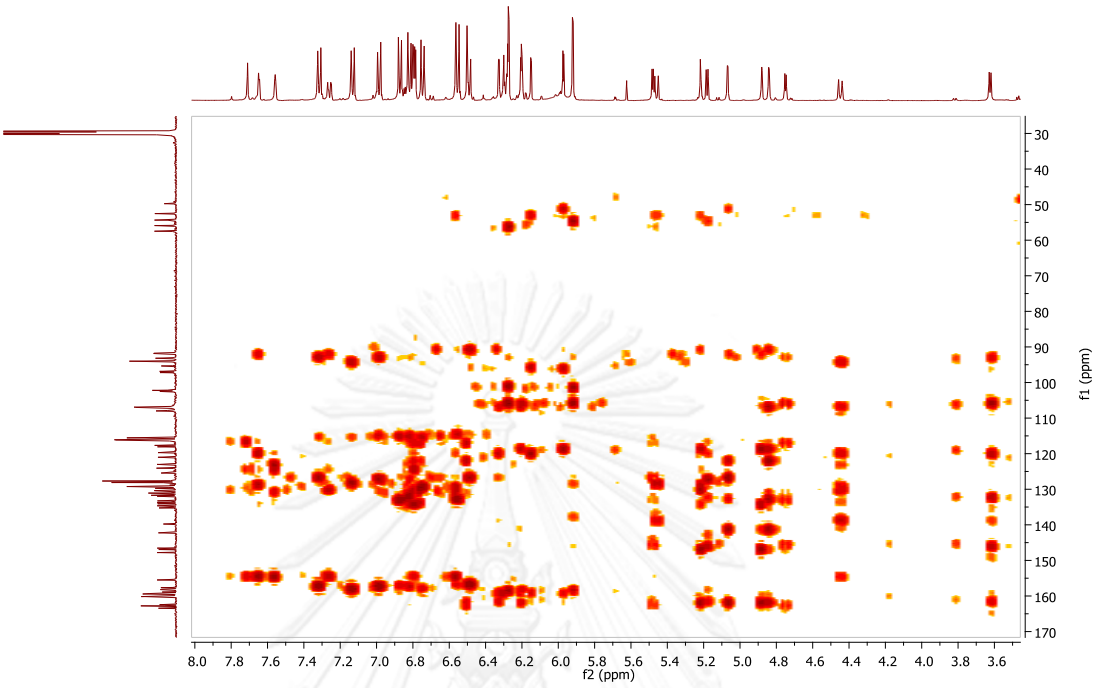

Figure **54** MHBC spectrum of **1** in CD_3COCD_3.

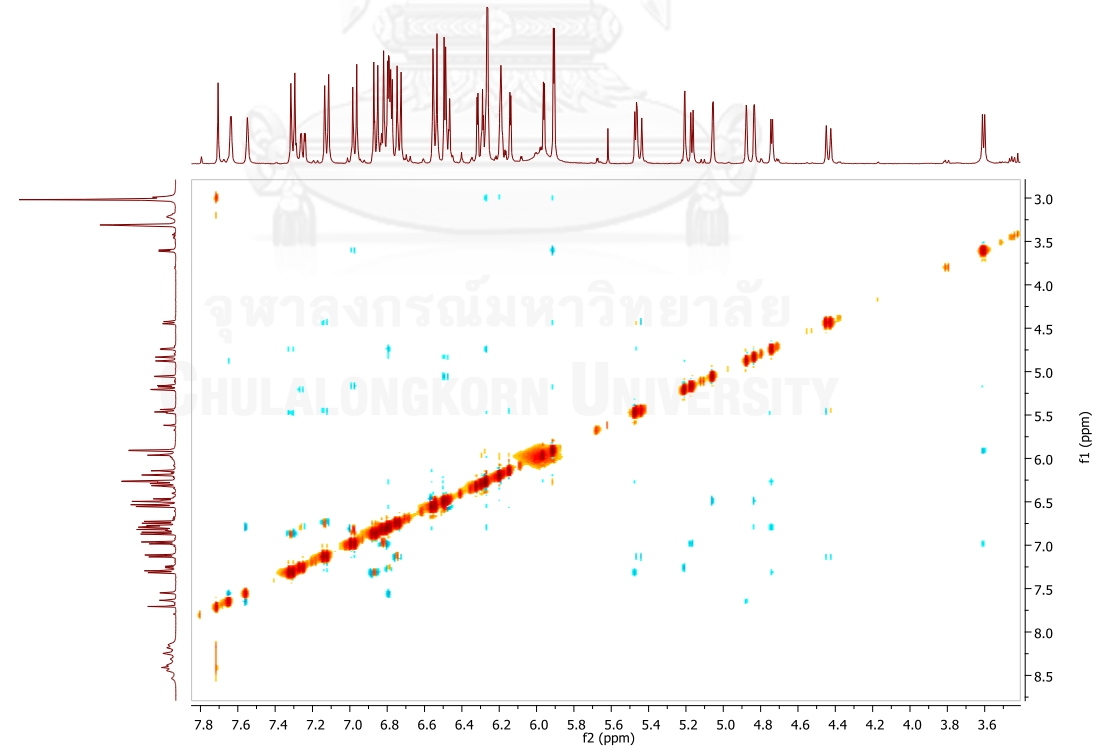

Figure **55** NOESY spectrum of **1** in CD_3COCD_3.

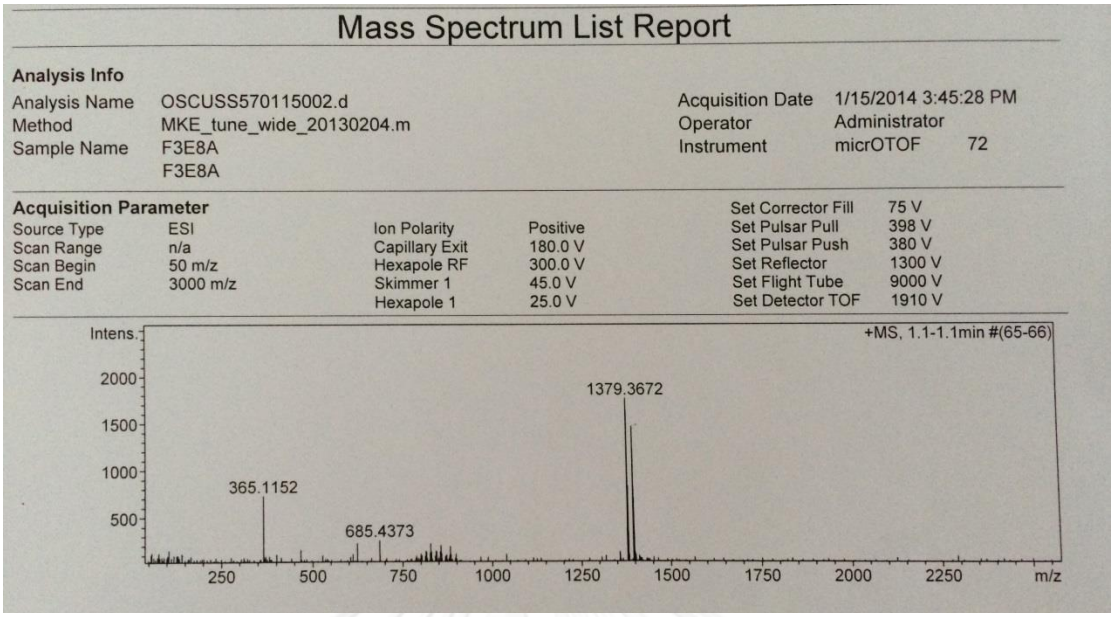

Figure **56** HRESIMS spectrum of **1**.

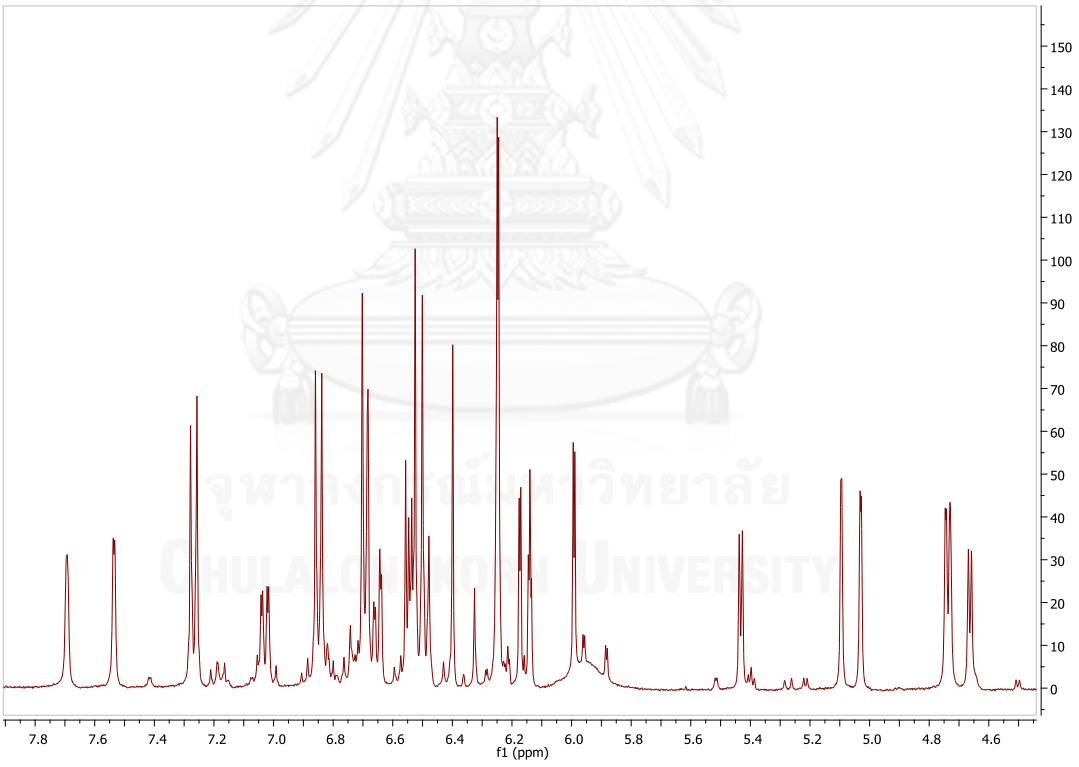

Figure **57** ^{1}H-NMR spectrum of **2** in CD_3COCD_3.

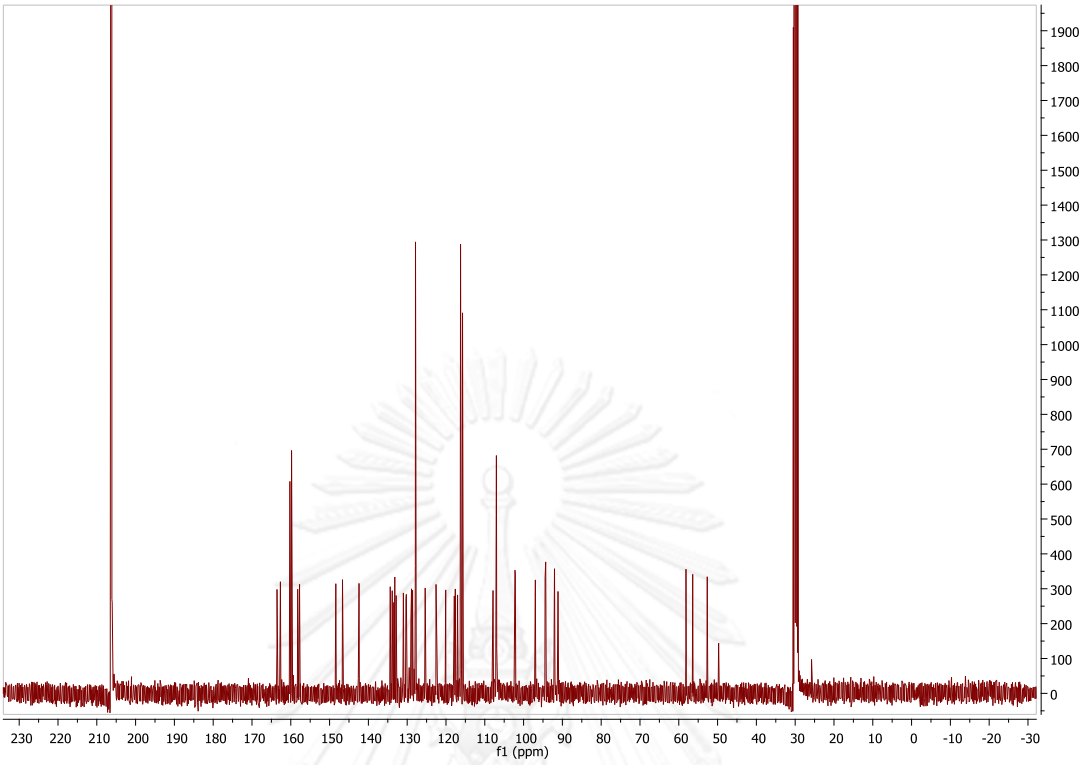

Figure **58** ^{13}C-NMR spectrum of **2** in CD_3COCD_3.

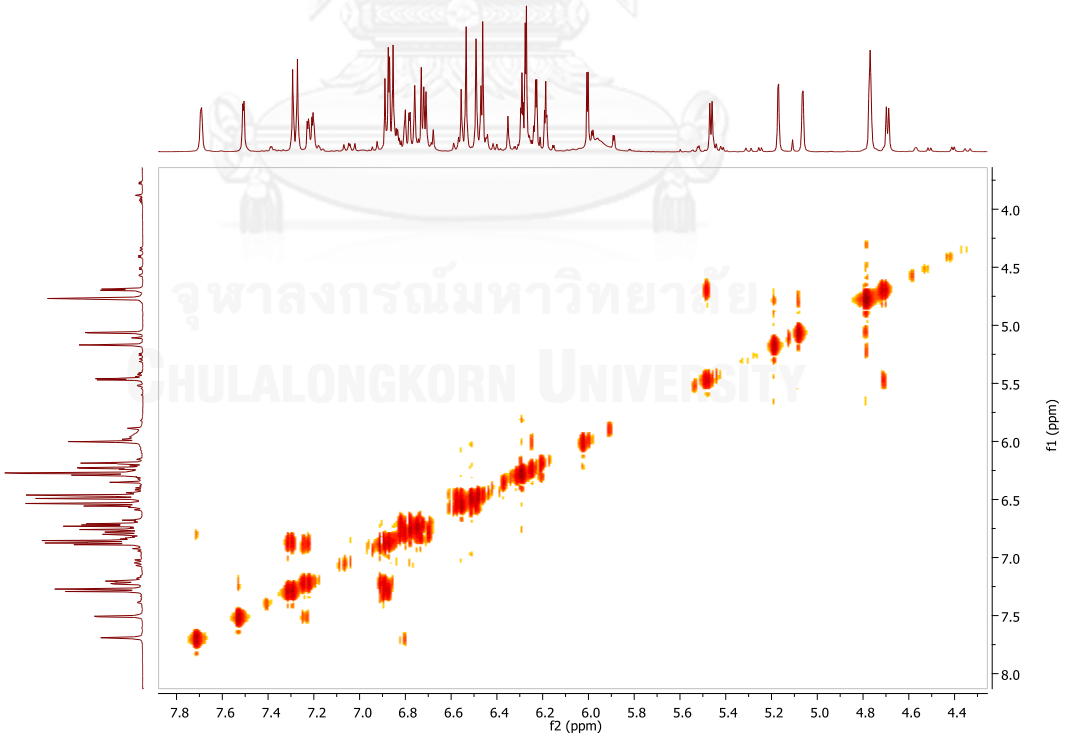

Figure **59** COSY spectrum of **2** in CD_3COCD_3.

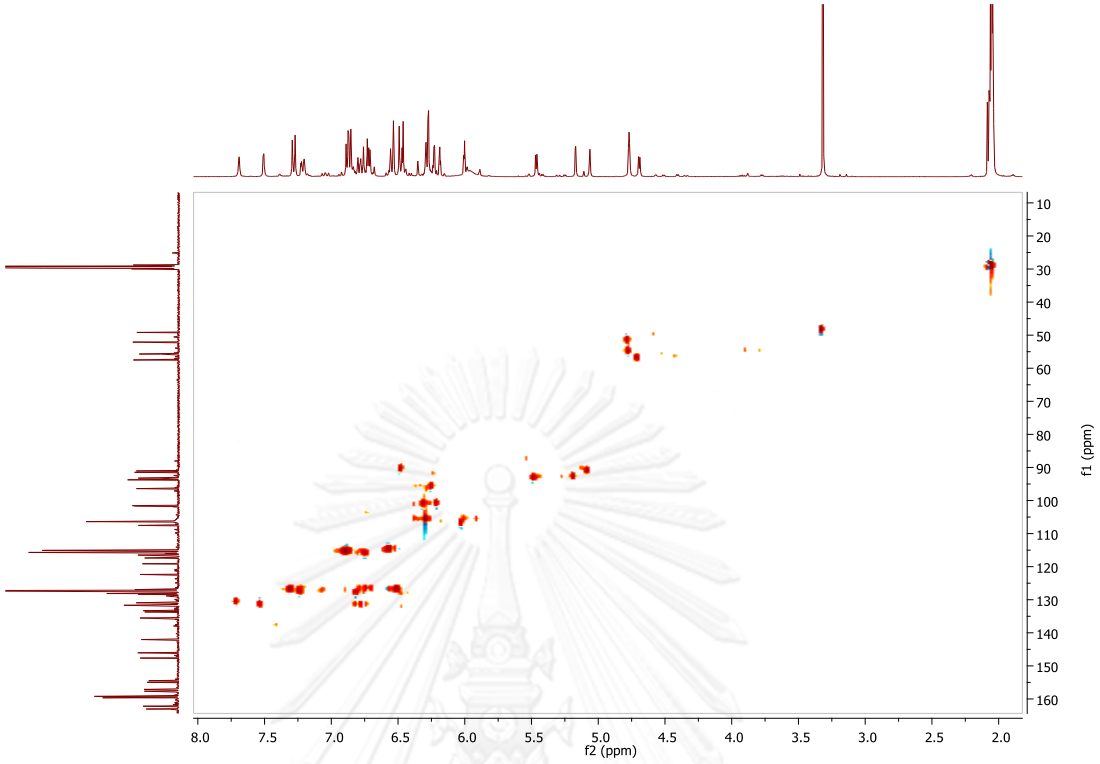

Figure **60** MHBC spectrum of **2** in CD_3COCD_3.

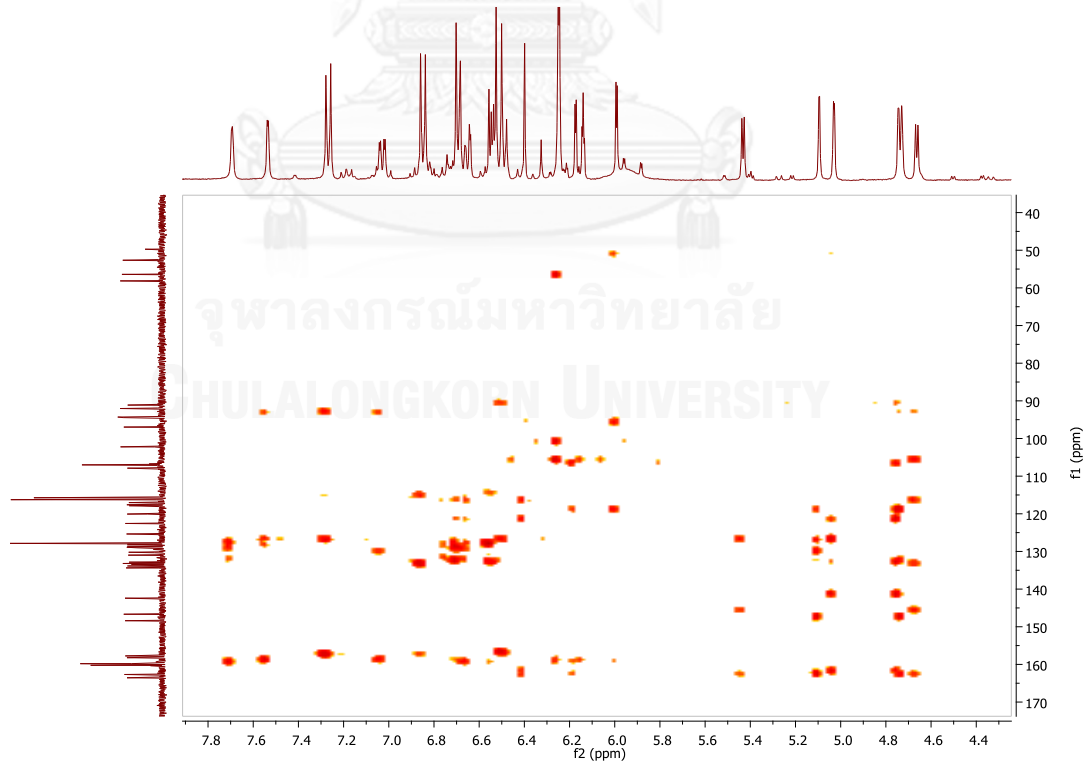

Figure **61** MHBC spectrum of **2** in CD_3COCD_3.

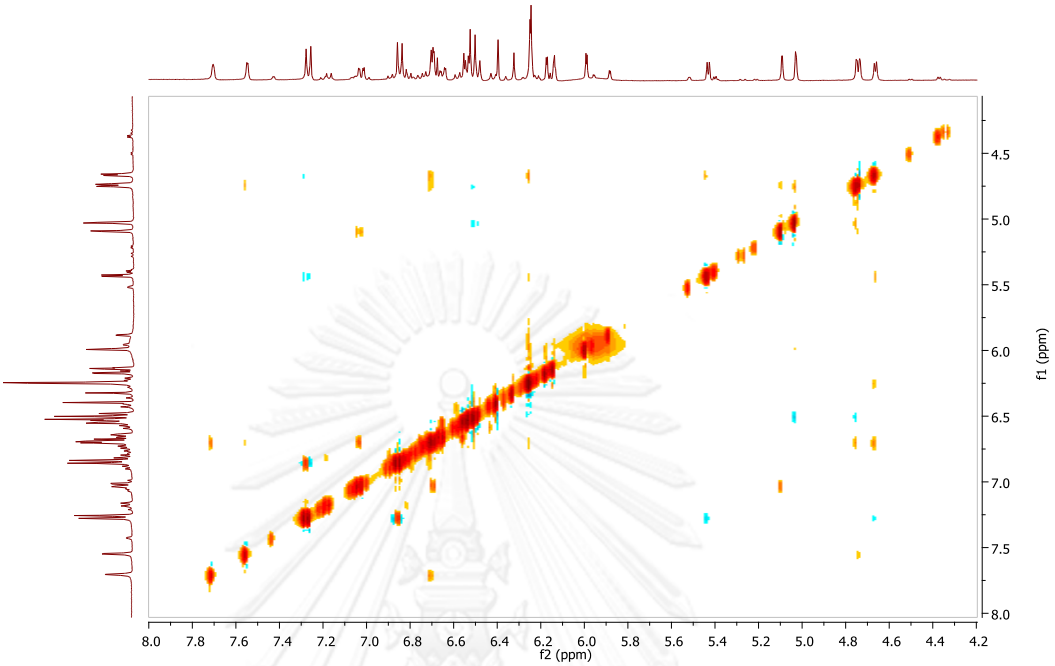

Figure **62** NOESY spectrum of **2** in CD_3COCD_3.

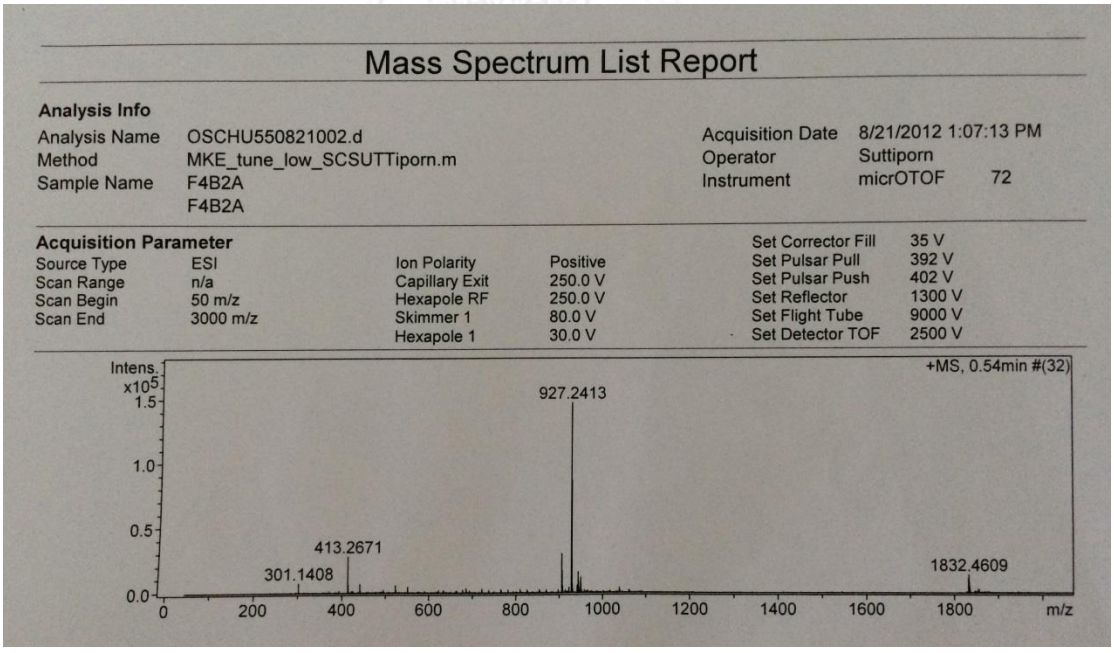

Figure **63** HRESIMS spectrum of **2.**

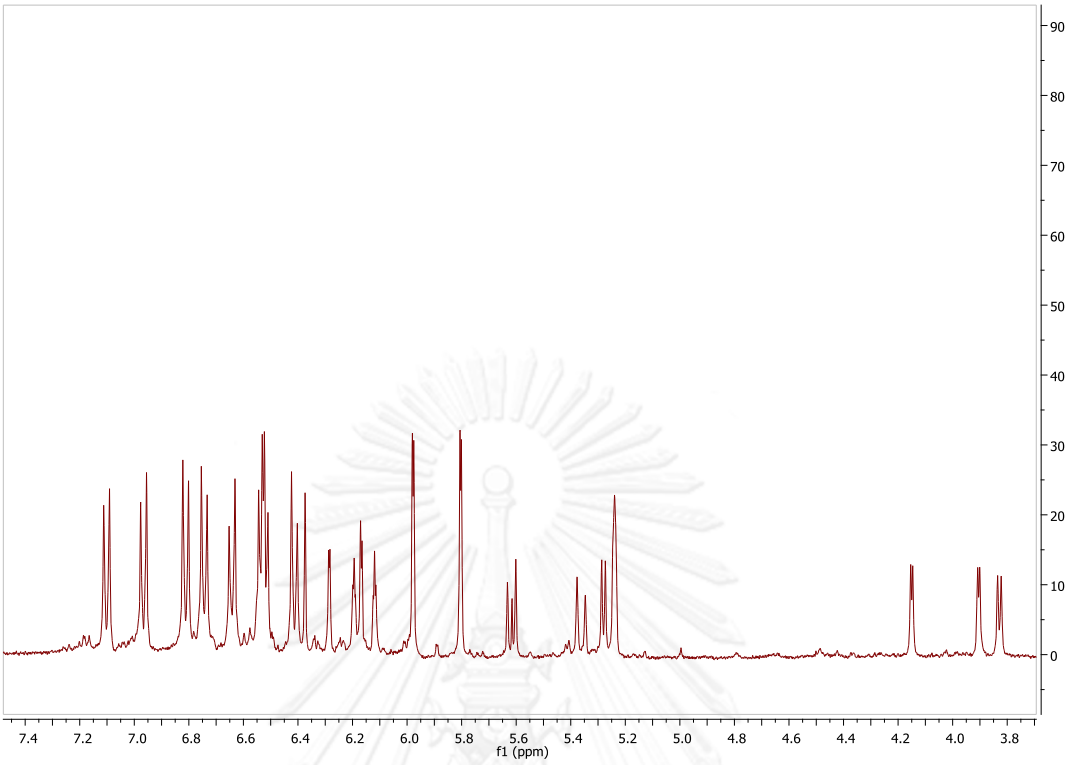

Figure **64** ^{1}H-NMR spectrum of **3** in CD_3COCD_3.

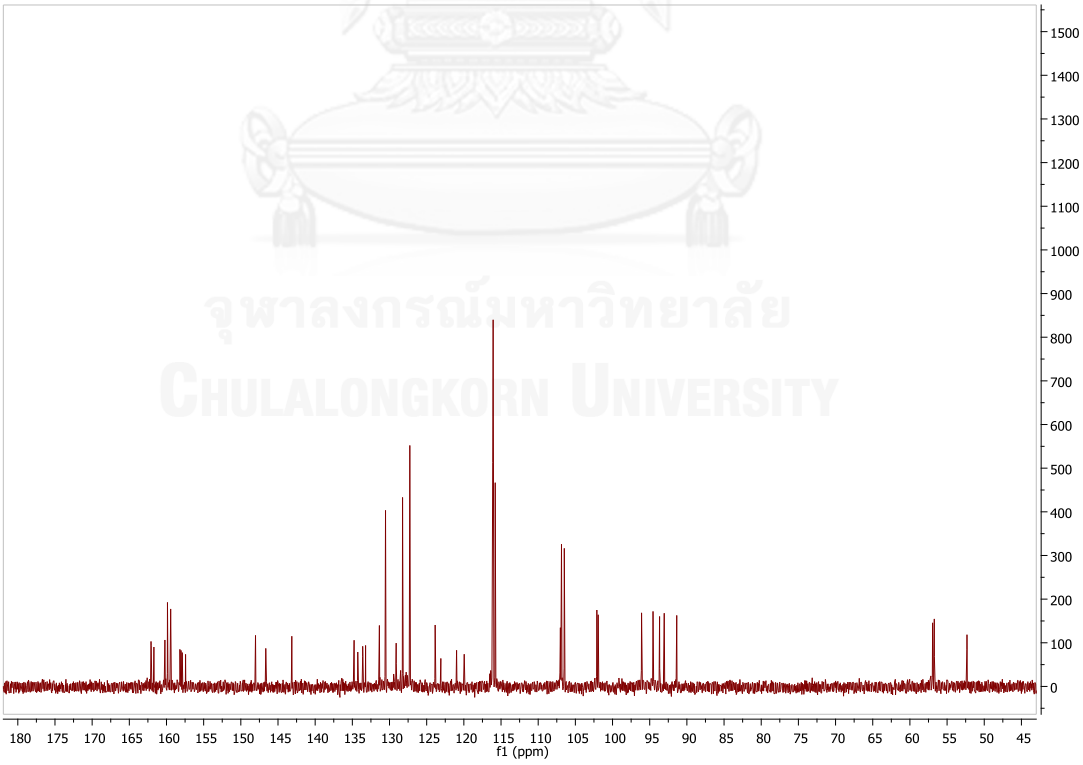

Figure **65** ^{13}C-NMR spectrum of **3** in CD_3COCD_3.

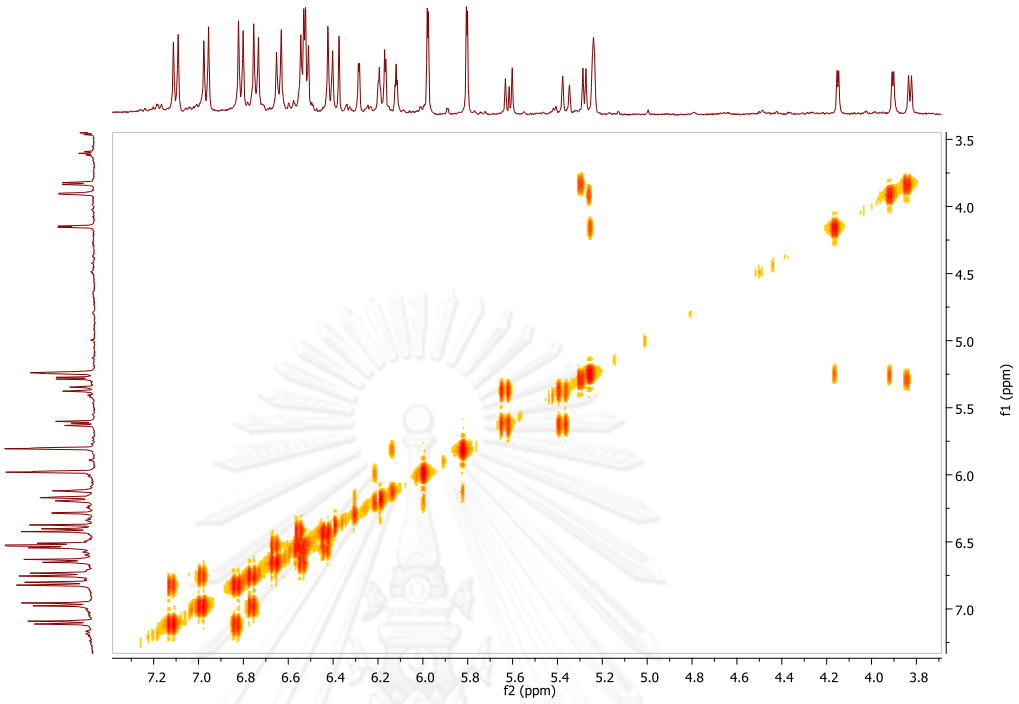

Figure **66** COSY spectrum of **3** in CD_3COCD_3.

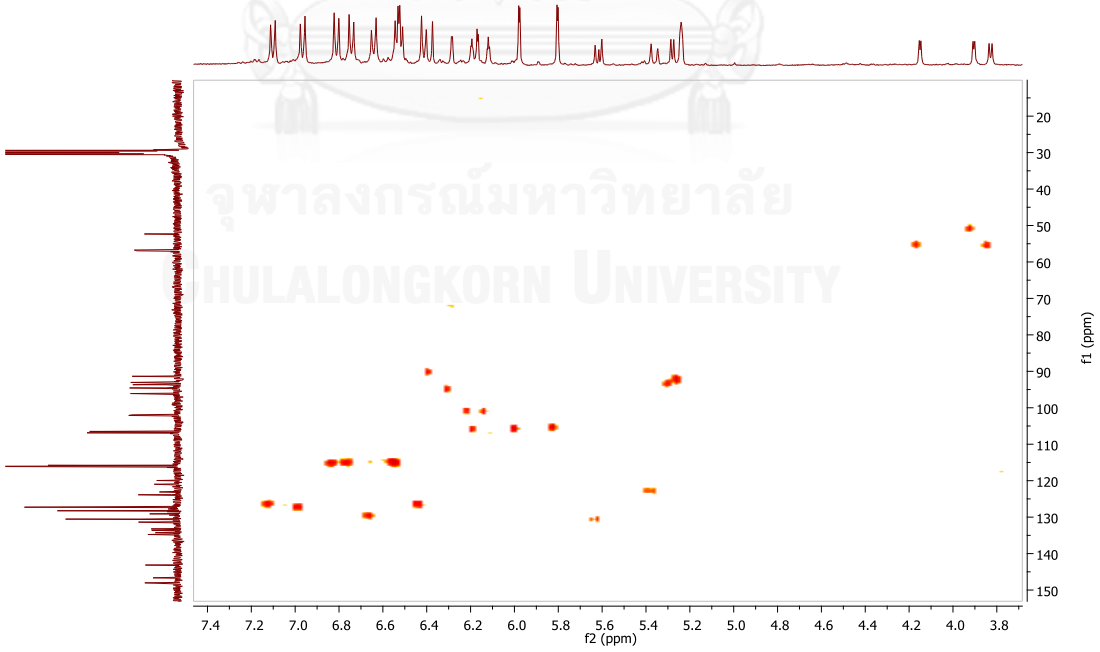

Figure **67** HSQC spectrum of **3** in CD_3COCD_3.

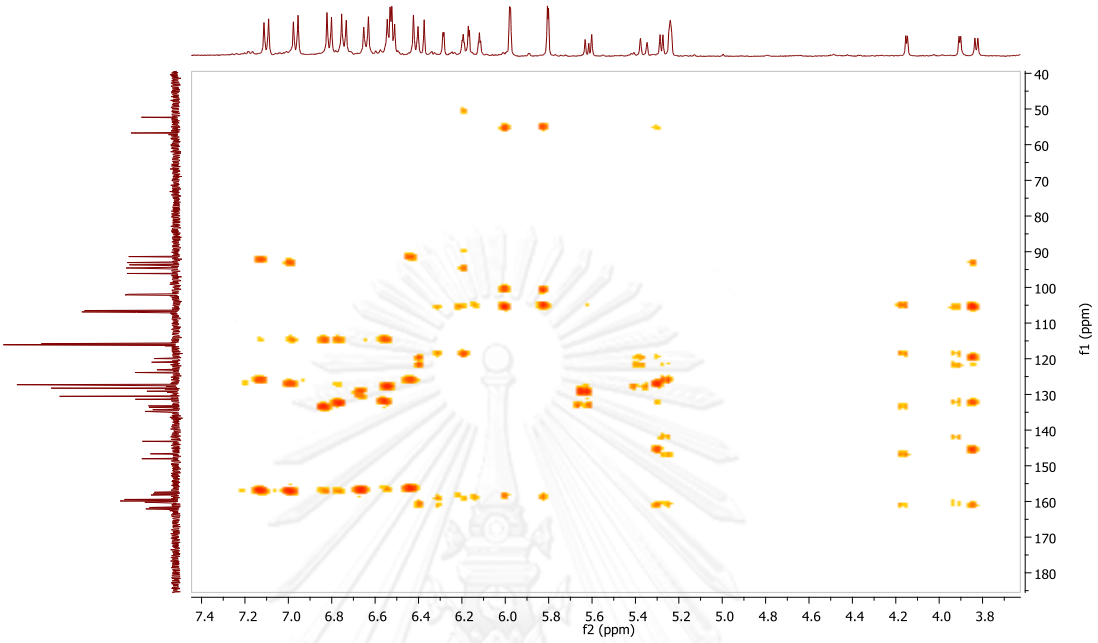

Figure **68** HMBC spectrum of **3** in CD_3COCD_3.

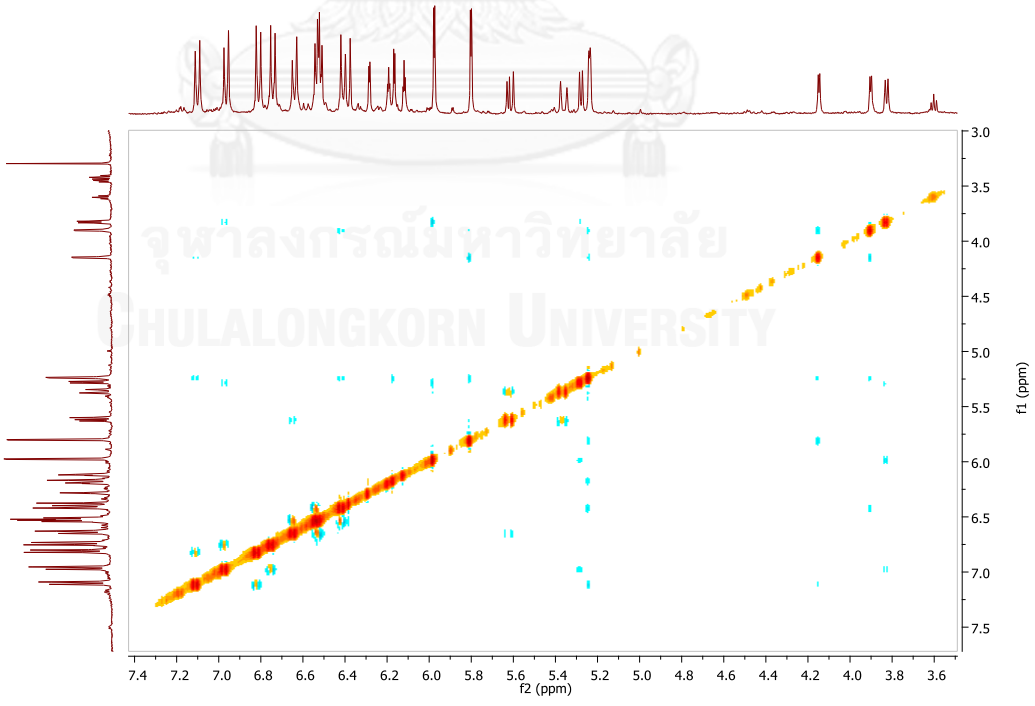

Figure **69** NOESY spectrum of **3** in CD_3COCD_3.

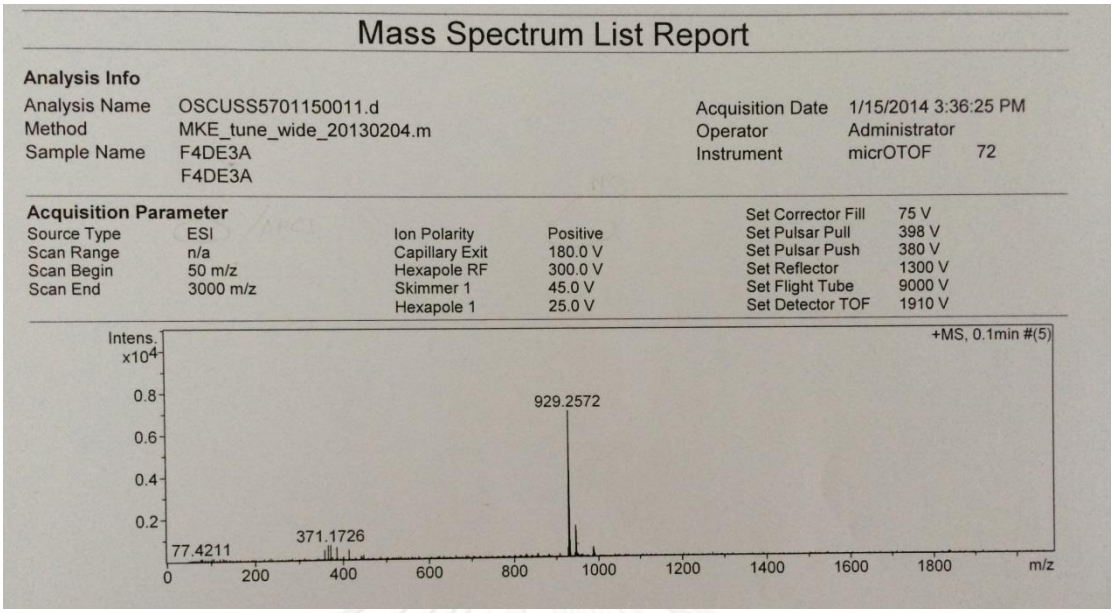

Figure **70** HRESIMS spectrum of **3**.

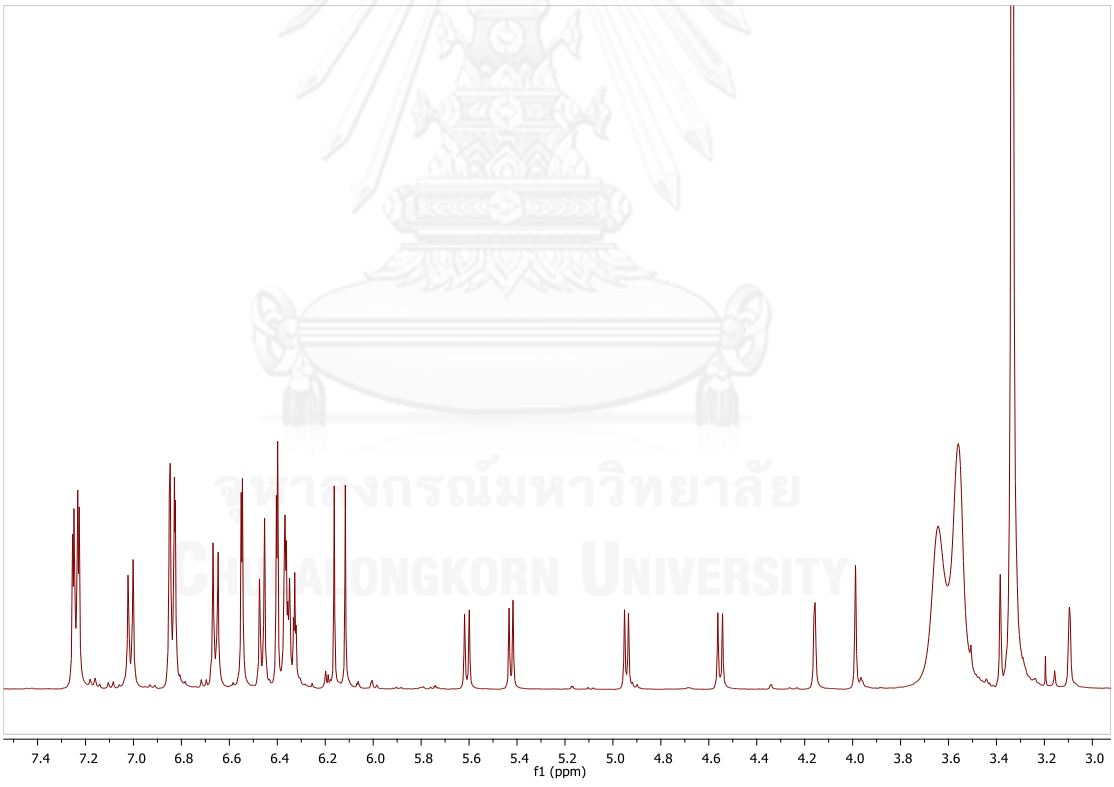

Figure **71** ^{1}H-NMR spectrum of **4** in CD_3COCD_3.

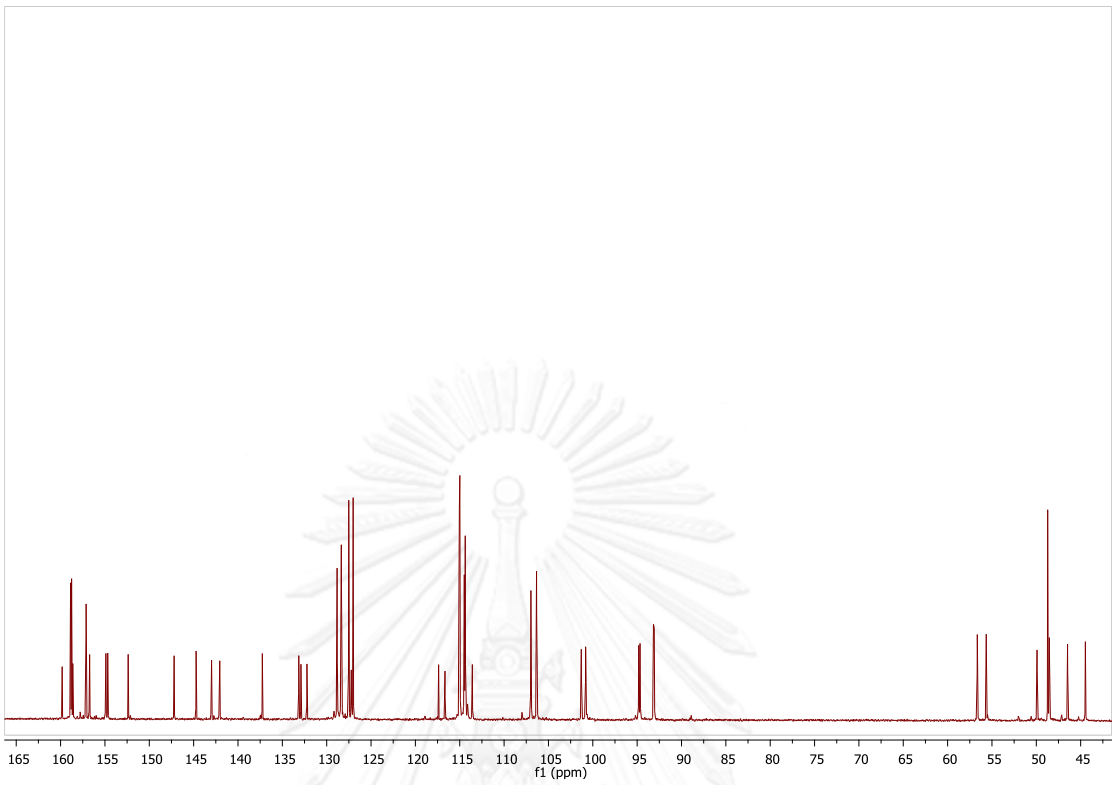

Figure **72** ^{13}C-NMR spectrum of **4** in CD_3COCD_3.

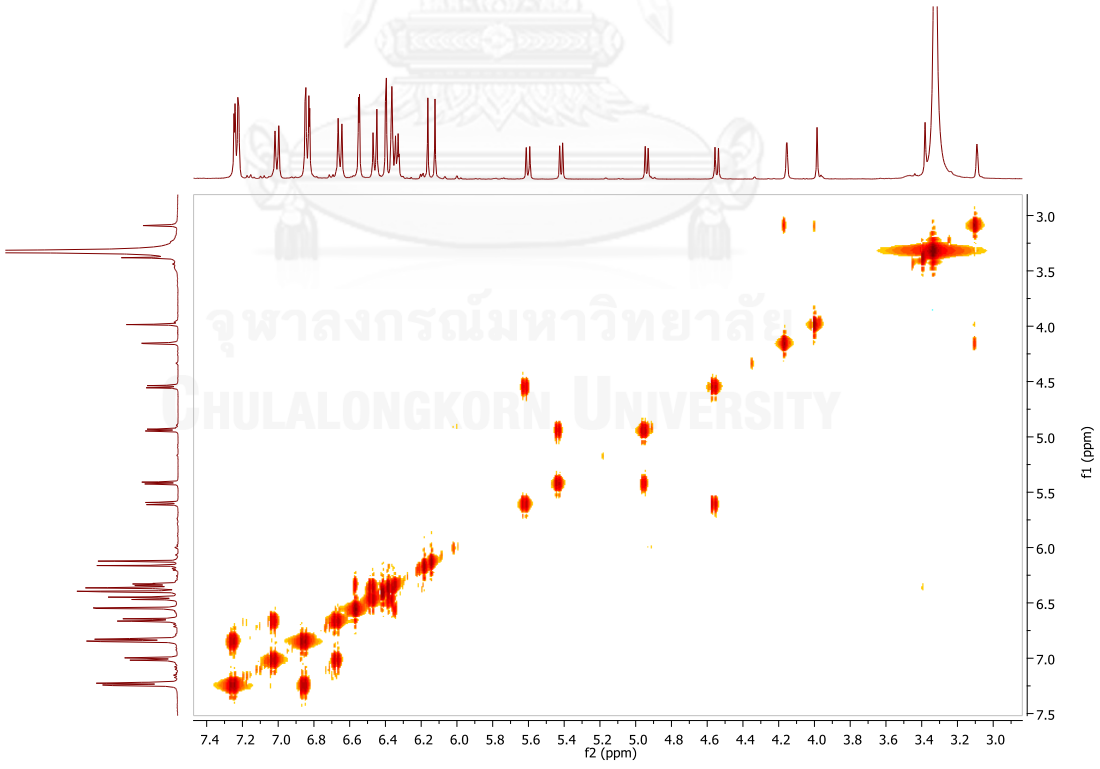

Figure **73** COSY spectrum of **4** in CD_3COCD_3.

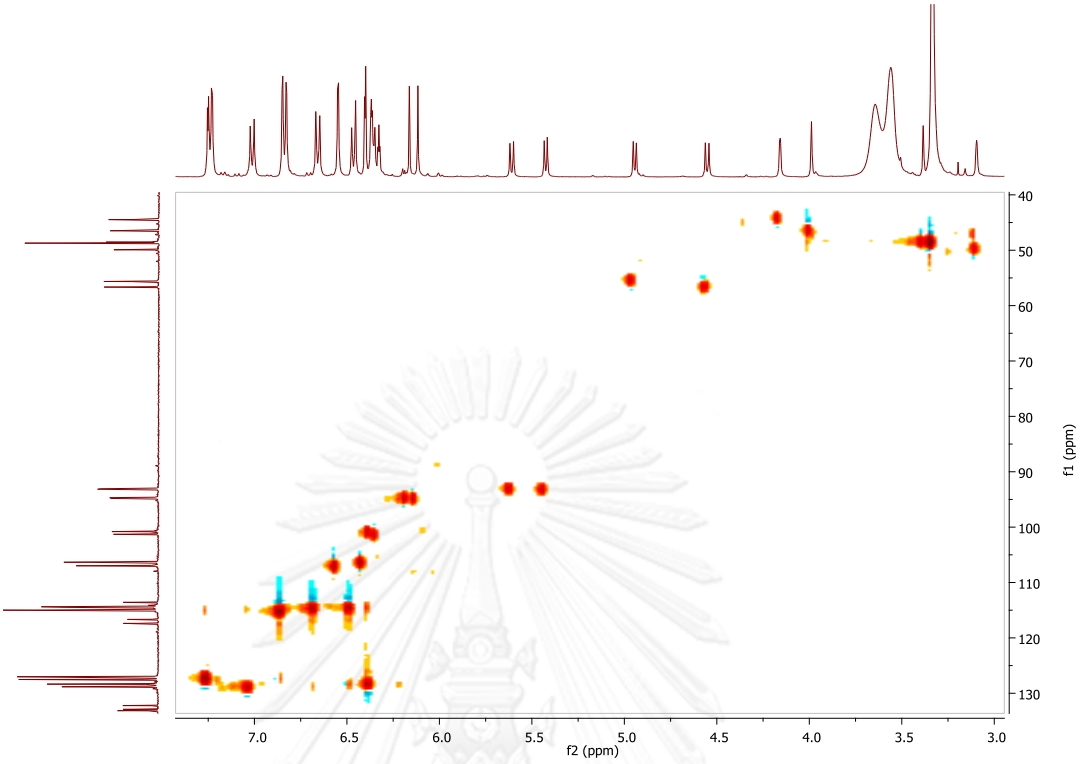

Figure **74** HSQC spectrum of **4** in CD_3COCD_3.

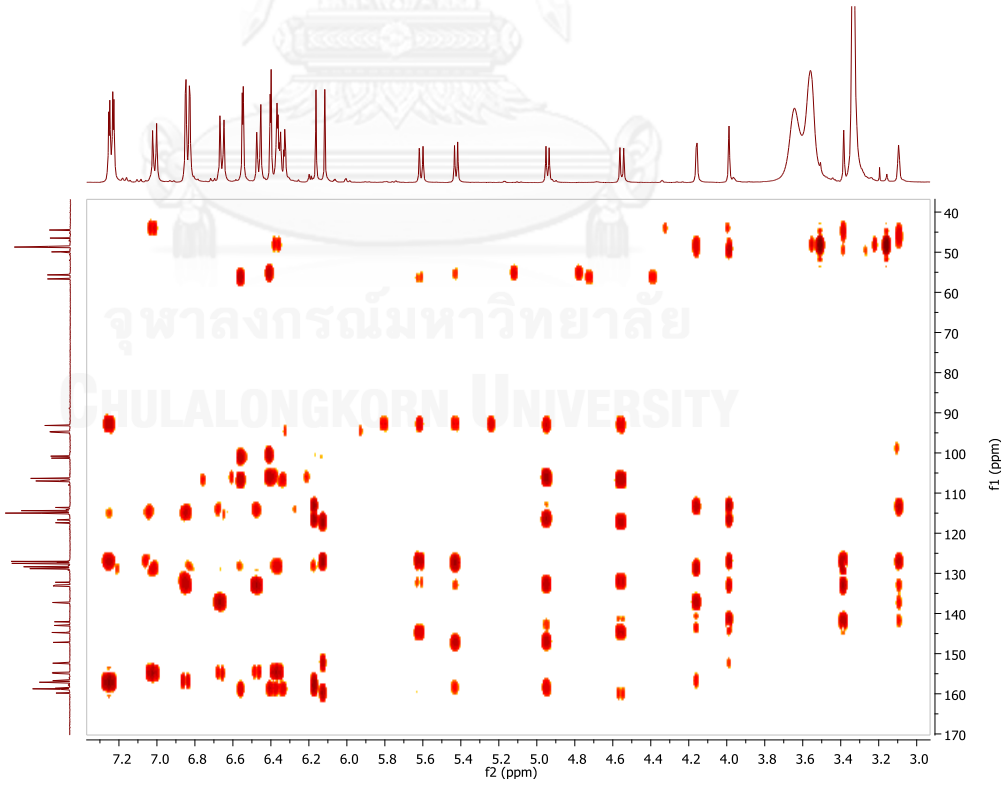

Figure **75** HMBC spectrum of **4** in CD_3COCD_3.

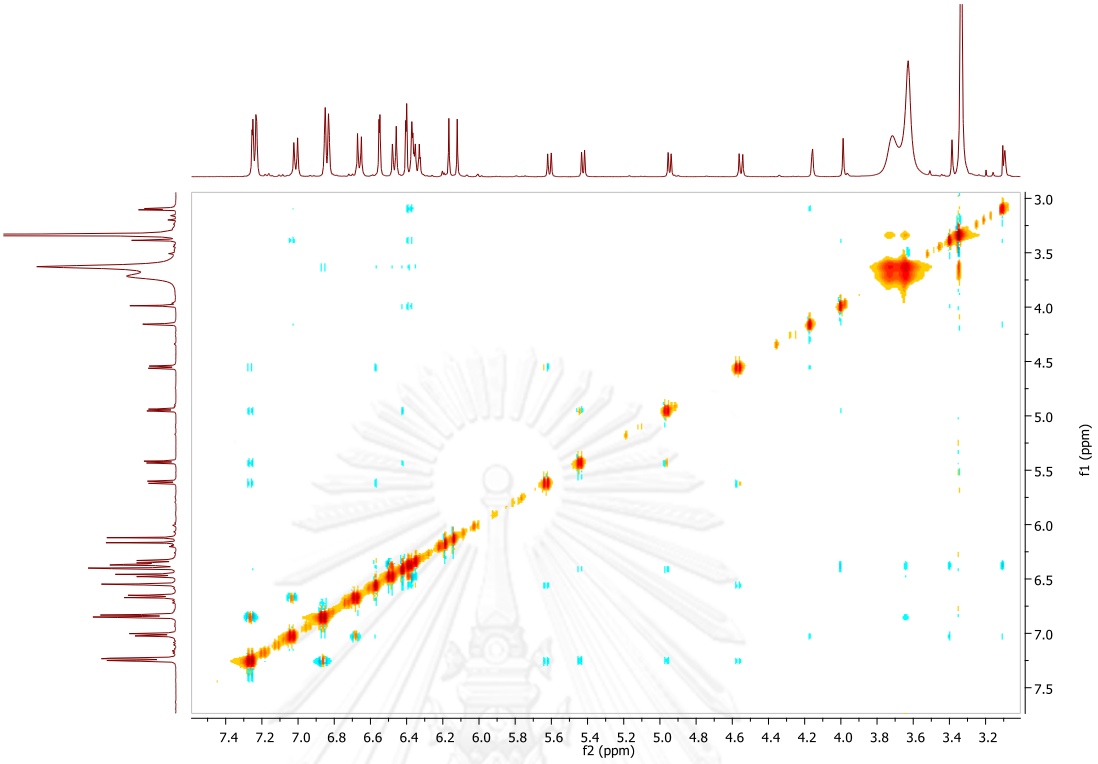

Figure **76** NOESY spectrum of **4** in CD_3COCD_3.

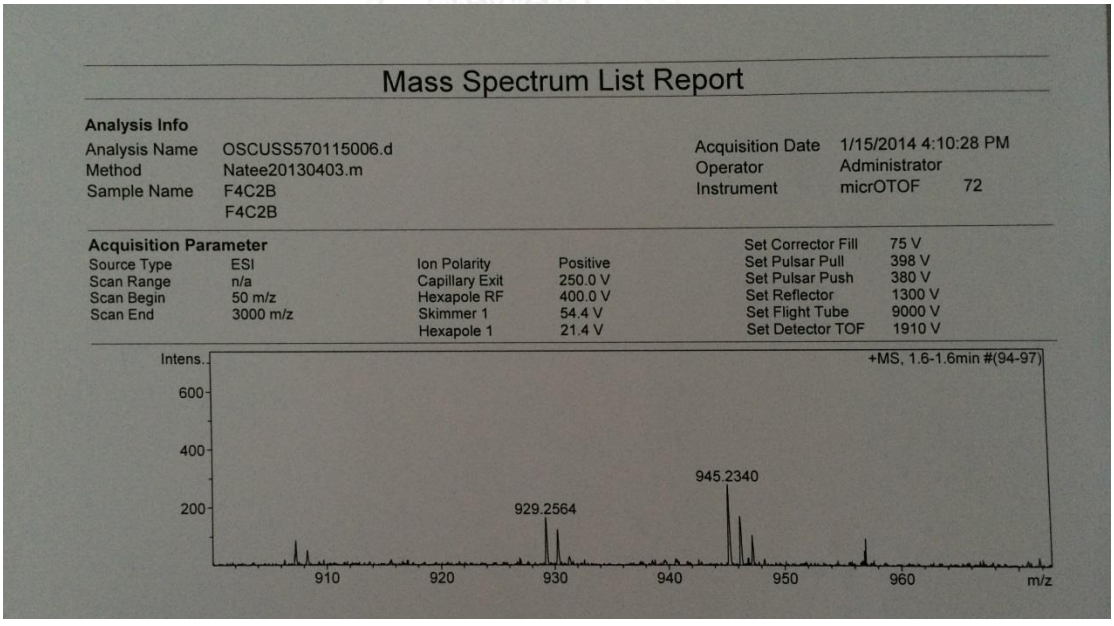

Figure **77** HRESIMS spectrum of **4**.

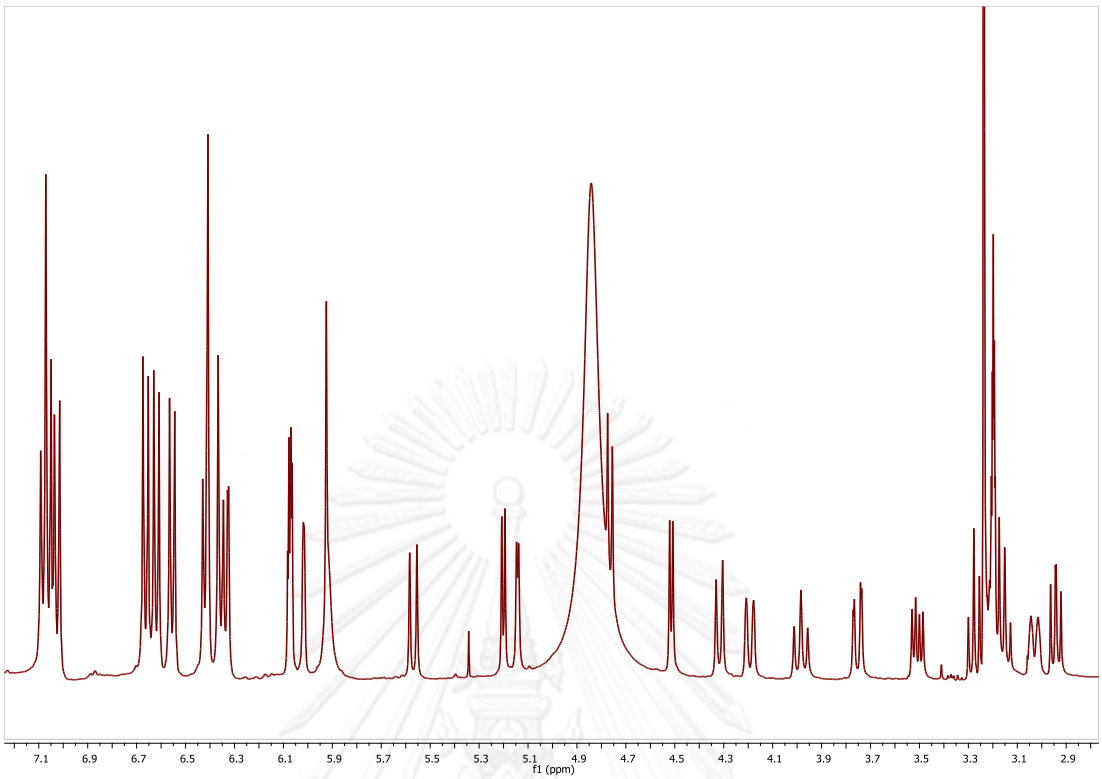

Figure **78** ^{1}H-NMR spectrum of **14** in CD_3OD.

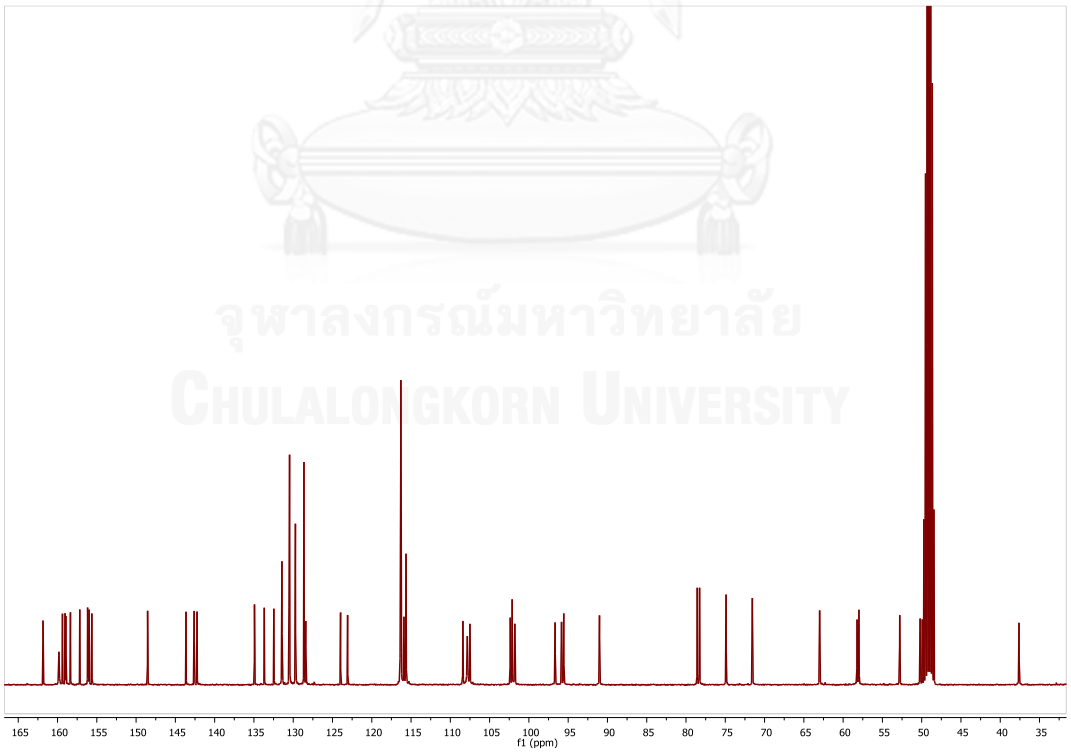

Figure **79** ^{13}C-NMR spectrum of **14** in CD_3OD.

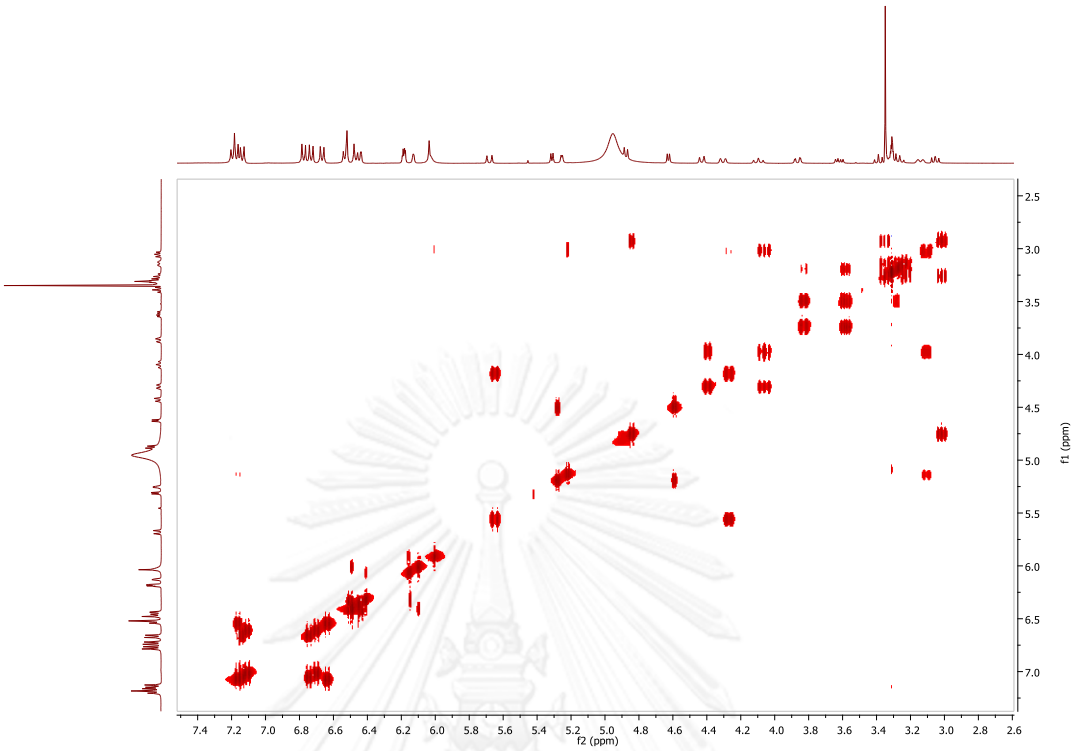

Figure **80** COSY spectrum of **14** in CD_3OD.

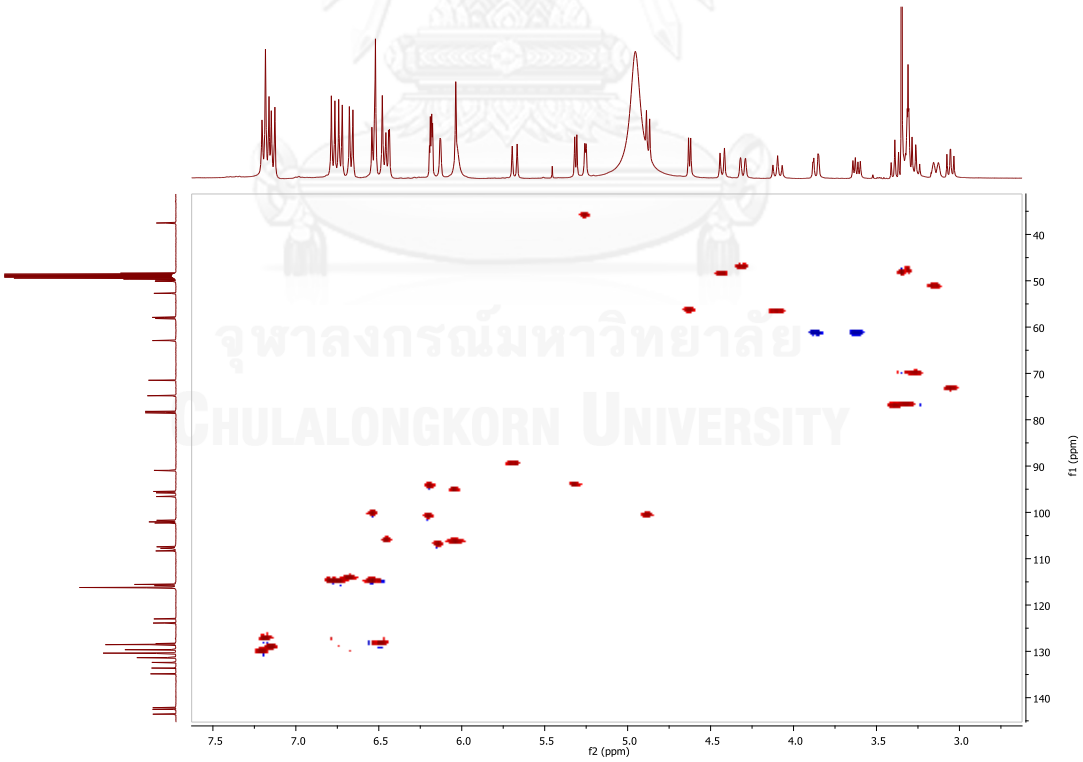

Figure **81** HSQC spectrum of **14** in CD_3OD.

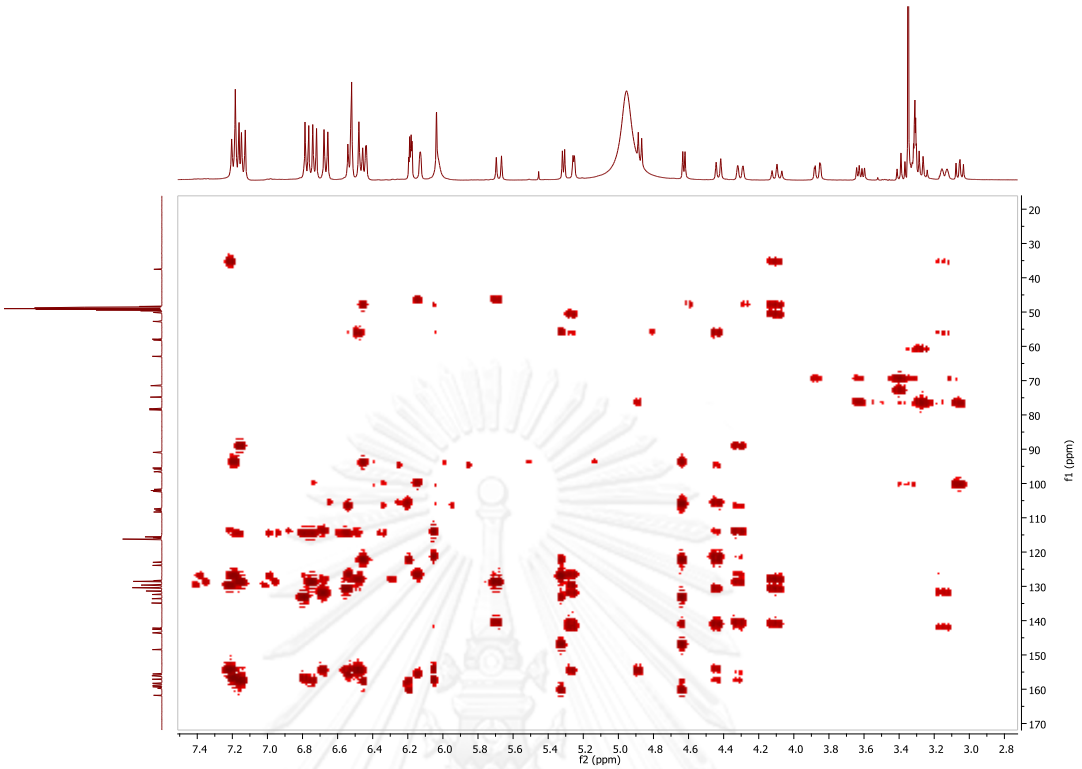

Figure **82** HMBC spectrum of **14** in CD_3OD.

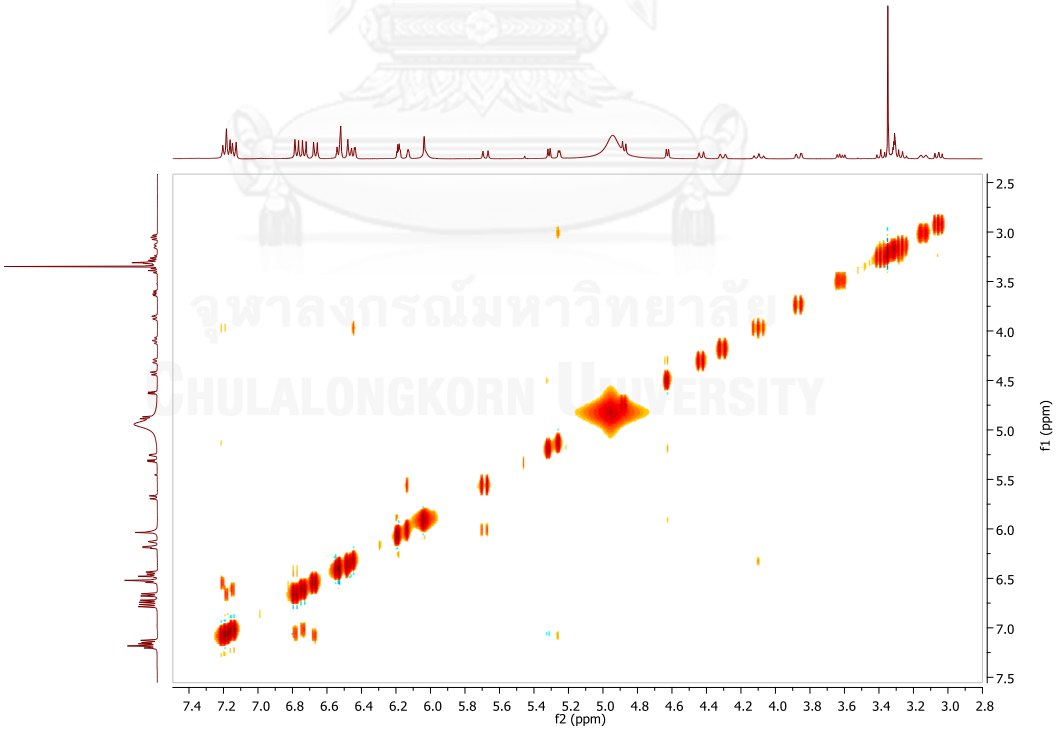

Figure **83** NOESY spectrum of **14** in CD_3OD.

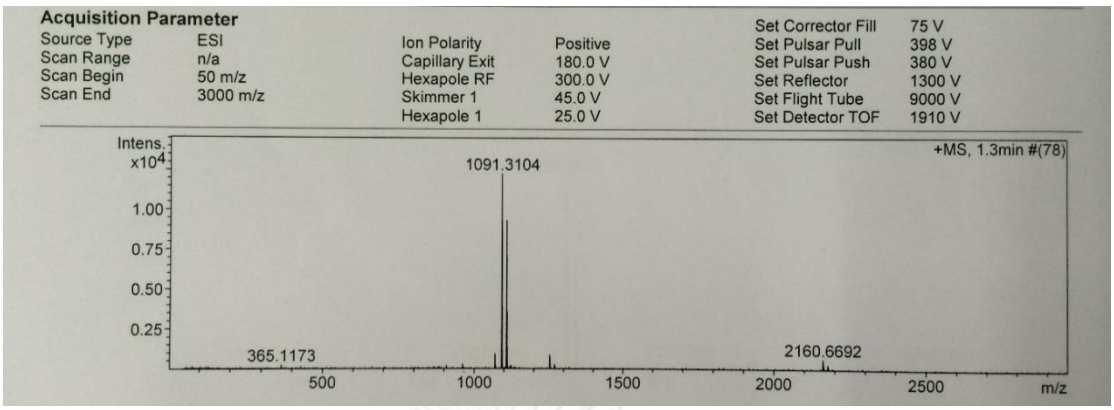

Figure **84** HRESIMS spectrum of **14.**

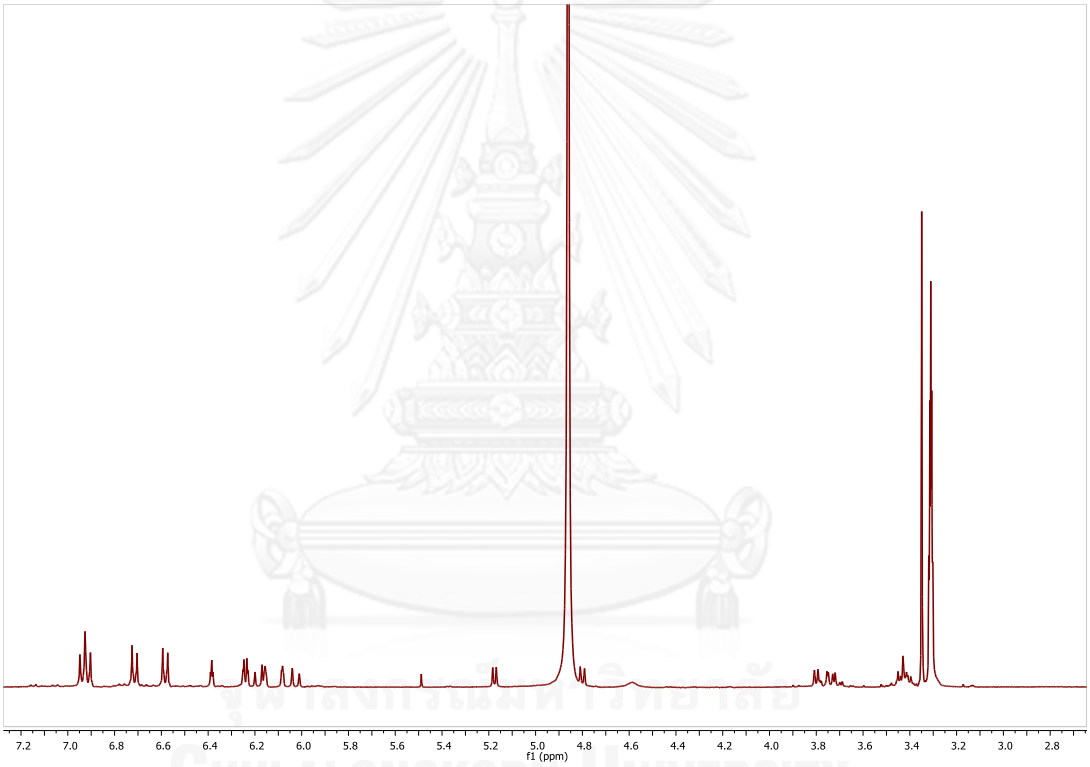

Figure **85** ^{1}H-NMR spectrum of **15** in CD_3OD.

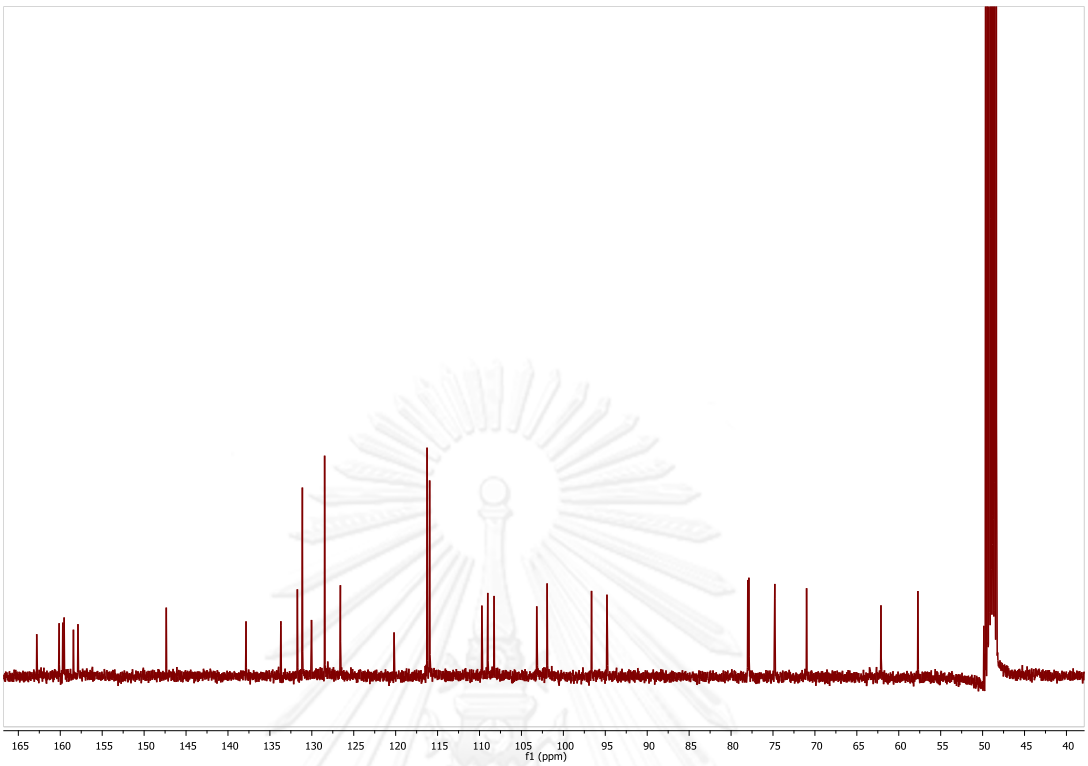

Figure **86** ^{13}C-NMR spectrum of **15** in CD_3OD.

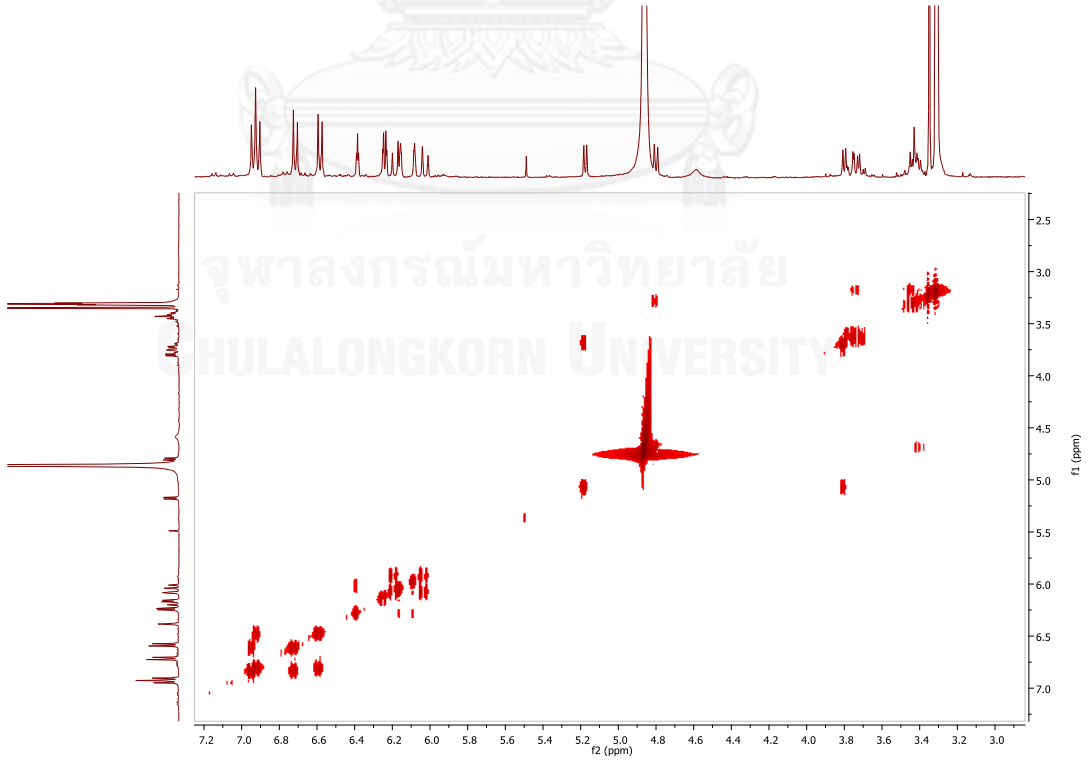

Figure **87** COSY spectrum of **15** in CD_3OD.

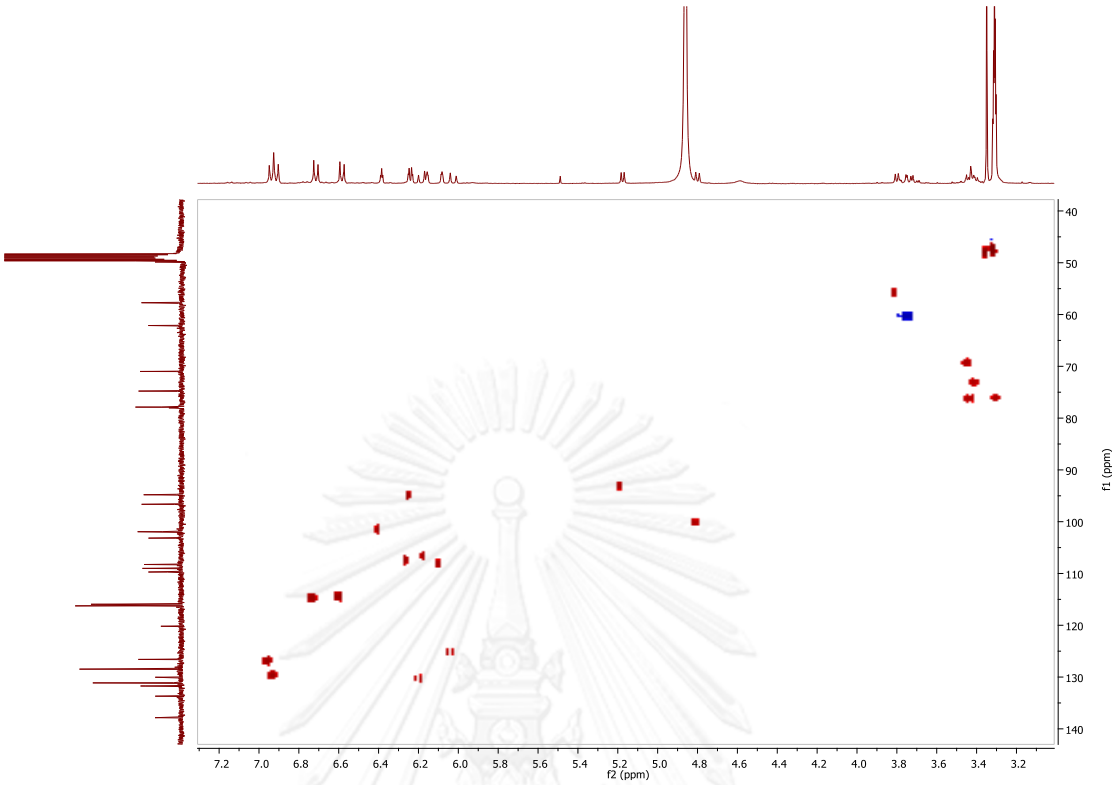

Figure **88** HSQC spectrum of **15** in CD_3OD.

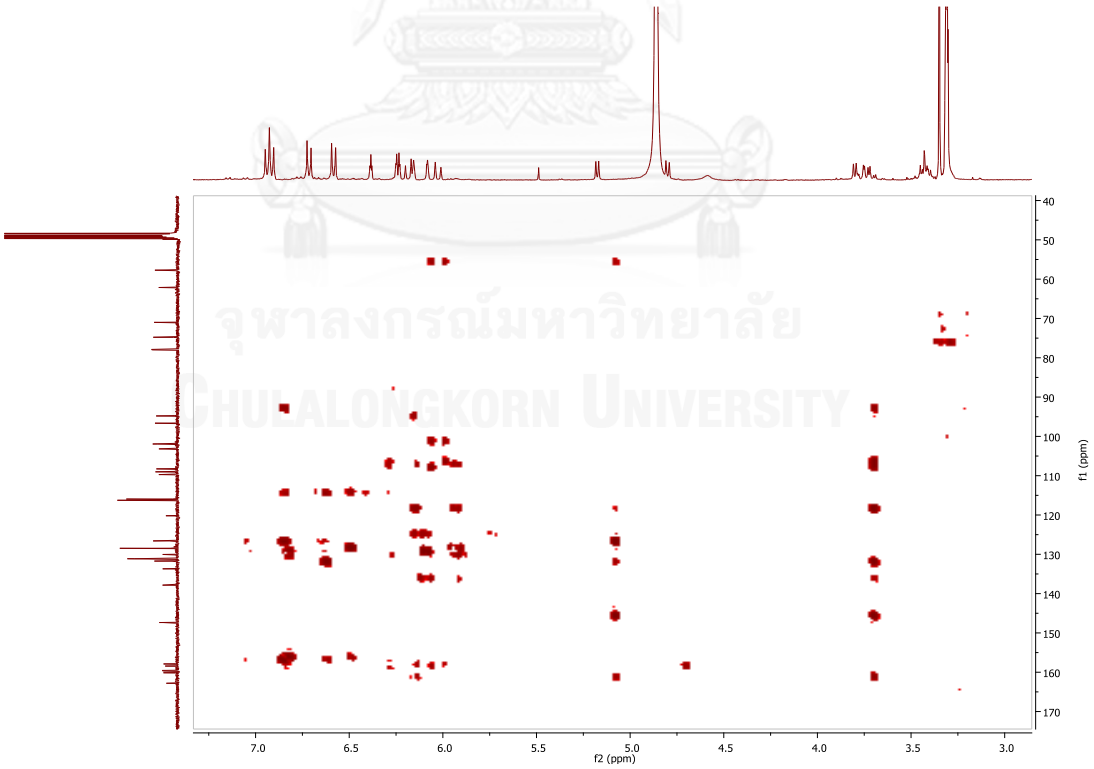

Figure **89** HMBC spectrum of **15** in CD_3OD.

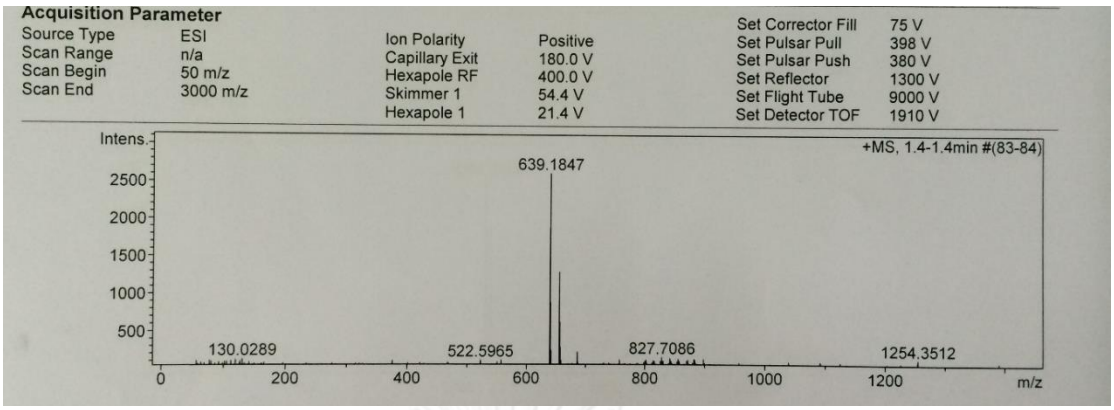

Figure **90** HRESIMS spectrum of **15.**

VITA

Mr. Serm Surapint was born on January5, 1981 in, Roi-Et, Thailand. He graduated with Bachelor Degree of Science in Medical Technology from Allied Health Sciences, in 2004 and Master Degree of Science in Biotechnology from Faculty of Sciences, in 2007 from Chulalongkorn University.

His present address is 133 Moo 16, Tambon Mae-kha, Amphoe Muang, Phayao, Thailand, 56000.